Jyrki Tuominen
Hyperspectral Remote Sensing of Coastal Environment

Jyrki Tuominen

Hyperspectral Remote Sensing of Coastal Environment

Thesis for the degree of Doctor of Science in Technology to be presented with due permission for public examination and criticism in Auditorium 125, at Tampere University of Technology - Pori, on the 18th of November 2016, at 1 pm.

Thesis advisor   Author

Tarmo Lipping   **Jyrki Tuominen**

Hyperspectral Remote Sensing of Coastal Environment

Abstract

Remotely sensed earth observation (EO) has revolutionized our understanding of our dynamic environment. Hyperspectral remote sensing is, in many ways, the ultimate optical remote sensing technology. Hyperspectral remote sensing is suited especially well for environmental studies due to it's capability to discriminate between species and quantify the abundance of different materials and chemicals. In this thesis remote sensing methods for hyperspectral data, applicable in environmental monitoring of coastal environment are developed and tested.

The planning of hyperspectral flight campaign HYPE08 in South-West Finland raised the need to validate and develop data processing methods for HYPE08 as well as for future hyperspectral flight campaigns. The research presented in this thesis can be largely considered as a response to this need. The study concentrates on four main topics: wetlands mapping, benthic mapping, water quality and atmospheric correction. The study was done using airborne hyperspectral data and field spectroscopy measurements.

The results of this study emphasize the importance of local calibration and validation of methods used. Water quality retrieval algorithms developed in local environmental conditions outperformed those validated elsewhere. The results also show that hyperspectral remote sensing of benthic cover types is limited to rather shallow areas, indicating the need to use state of the art methodology in order to increase operational depth range. The proposed atmospheric correction algorithm produced very good results. The accuracy of model-based algorithm increases when Empirical-Line (EL) correction using spectral field measurements was applied to spectra generated by the model.

Keywords: Hyperspectral, wetlands mapping, benthic mapping, water quality, atmospheric correction

Contents

Acknowledgments

Pori, September 14, 2016,

Jyrki Tuominen

Abbreviations

AIS	Airborne Imaging Spectrometer
AISA	Airborne Imaging Spectrometer for Applications
ATREM	Atmosphere Removal Algorithm
AVIRIS	Airborne Visible/Infrared Imaging Spectrometer
CASI	Compact Airborne Spectrographic Imager
CDOM	Colored Dissolved Organic Matter
DAIS	Digital Airborne Imaging Spectrometer
DOM	Dissolved Organic Matter
ED	Euclidean Distance
EFFORT	Empirical Flat Field Optimal Reflectance Transformation
EL	Empirical Line
FLM	Functional Linear Model
GCP	Ground Control Point
GTK	Geological Survey of Finland
HATCH	High-accuracy Atmospheric Correction for Hyperspectral Data
HVI	Hyperspectral Vegetation Indices
IOP	Inherent Optical Property
LiDAR	Light Detection and Ranging
ML	Maximum Likelihood
MLC	Maximum Likelihood Classifier
MODIS	Moderate Resolution Imaging Spectrometer
MODTRAN	Moderate Resolution Transmittance
NIR	Near Infrared
PIF	Pseudo Invariant Feature
RMSE	Root Mean Square Error
RT	Radiative Transfer

SAM	Spectral Angle Mapper
SCM	Spectral Correlation Mapper
SID	Spectral Information Divergence
SVC	Supervised Vicarious Calibration
SVM	Support Vector Machine
SWIR	Short Wave Infrared
TSM	Total Suspended Matter
TSS	Total Suspended Solids
UAV	Unmanned Aerial Vehicle
VELMU	Finnish Inventory Program for the Underwater Marine Environment
VNIR	Visible Near Infrared
VTT	Technical Research Center of Finland

List of Original Publications

This thesis is based on the following original publications that will be referred to as publications [**P1**] to [**P5**]:

[**P1**] Tuominen, J. Lipping, T., Kuosmanen, V. and Repka, S. (2010). Hyperspectral detection of marine clay in coastal waters using the spectral angle method. *EARSeL eProceedings*, 9(2): 31-41.

[**P2**] Tuominen, J. and Lipping, T. (2014). Feasibility of Benthic Cover-Type Mapping in Turbid Waters near Estuaries Using Hyperspectral Remote Sensing. *Journal of Coastal Research*, 30(6):1131-1139.

[**P3**] Tuominen, J. and Lipping, T. (2016). Spectral Characteristics of Common Reed Beds: Studies on Spatial and Temporal Variability. *Remote Sensing*, 8(3):181.

[**P4**] Tuominen, J. and Lipping, T. (2012). Assessment of hyperspectral classification methods for benthic cover type mapping. In *Proceedings of IEEE International Geoscience and Remote Sensing Symposium*, Munich, Germany.

[**P5**] Tuominen, J. and Lipping, T. (2011). Atmospheric correction of hyperspectral data using combined empirical and model based method. In *Proceedings of 7th EARSeL Imaging Spectroscopy Workshop*, Edinburgh, Scotland.

Author's contribution

Publication P1: Jyrki Tuominen was the principal author of the paper. Viljo Kuosmanen designed and supervised the field measurements. He also designed and carried out the correction algorithm for spectral measurements. Tarmo Lipping contributed to the preparation of manuscript. Sari Repka was involved in the birth of the original idea of the study and helped with her expertise on coastal studies.

Publication P2: Jyrki Tuominen was the principal author of the paper. Tarmo Lipping contributed to the study design and the preparation of the manuscript.

Publication P3: Jyrki Tuominen was the principal author of the paper. Tarmo Lipping contributed to the study design and the preparation of the manuscript.

Publication P4: Jyrki Tuominen was the principal author of the paper. Tarmo

Lipping contributed to the study design and the preparation of the manuscript

Publication P5: Jyrki Tuominen was the principal author of the paper. Tarmo Lipping contributed to the study design and the preparation of the manuscript

Chapter 1

Introduction

Broadly defined, remote sensing is any technology employed to study the characteristics of objects from a distance. The term is usually used in a more restricted sense in which the observation is made from above the phenomena of interest, from a sensor carried on an airborne or spaceborne platform, and the information is carried by electromagnetic radiation (Rees, 2001). The apparatus currently used for remote sensing can be divided into two groups: active and passive systems. The active sensors generate and transmit a signal toward the target, and receive and record the returned signal after its interaction with the target. The use of remote sensing in environmental applications has certain advantages and disadvantages compared to conventional in situ measurements (Tuominen and Lipping, 2011). It should be pointed out that remote sensing studies almost always involve some use of ground truth measurements or observations. Thus remote sensing is not replacing conventional field studies; on the contrary, it is extrapolating from them.

Remotely sensed earth observation (EO) has revolutionized our understanding of our dynamic environment (de Leeuw et al., 2010). The employment of remotely sensed EO techniques expanded in the 1970s when digital satellite borne imagery became available. Remote sensing has provided major advances in understanding the climate system and its changes, by quantifying the processes and states of the atmosphere, land and oceans. A variety of ecological applications such as the prediction of the distribution of species, studying the spatial variability in species richness and

detecting natural and human-caused changes at scales ranging from individual land-scapes up to that of the entire Earth, require data from broad spatial extents that cannot be collected using field studies. Remote sensing methodology addresses these needs (Kerr and Ostrovsky, 2003).

Hyperspectral imaging is a rather young scientific discipline. The first airborne imaging spectrometer was flown in 1982, more than three decades ago (Vane et al., 1984). Hyperspectral remote sensing is suited especially well for environmental studies due to it's capability to discriminate between species and quantify the abundance of different materials and chemicals. In Finland the vast majority of the environment is either forest of water areas, both of which can be studied using hyperspectral imaging. The beginning of hyperspectral imaging in Finland is closely related to the development of Airborne Imaging Spectrometer for Applications (AISA), built in 1992 (Mäkisara et al., 1993). AISA was developed by the Technical Research Center of Finland (VTT) and later matured into a commercial product manufactured by Specim Ltd.

As a result of the geological studies, whose aim was to assist in geospatial municipal planning, the need for hyperspectral studies in Satakunta was raised. In 2004 a large regional hyperspectral flight campaign HyperGeos was planned. This campaign, planned to cover the whole Satakunta province, was coordinated by the Geological Survey of Finland. Unfortunately the plan was not realized. However, the careful planning of HyperGeos laid ground to a new flight campaign: in June 2008the hyperspectral flight campaign HYPE08 was conducted. The planning and implementation of HYPE08 flight campaign in Satakunta raised the need to validate and develop data processing methods for HYPE08 as well as for future hyperspectral flight campaigns. The research presented in this thesis can be largely considered as a response to this need. Hyperspectral remote sensing in coastal regions is more complex than in inland. There are several issues that have to be considered. Due to the high absorption and transmission of water bodies the reflected radiation level is much lower in water areas compared to terrestrial (Gao et al., 2009). The interface between the atmosphere and water (i.e. the water surface) has two effects on the radiation detected by a sensor aimed at it; sun glints and refraction causing changes in radiation. Due to these

reasons, atmospheric correction of coastal areas is challenging, especially at water areas. Benthic mapping near estuaries is a difficult task. The attenuation of light in turbid waters is high. The water quality parameters such as chlorophyl content and turbidity can change rapidly.

This doctoral study is closely related to two environmental programs, the Finnish Inventory Programme for the Underwater Marine Environment (VELMU) and Posiva Ltd's Environmental Research Programme. The marine environment in Finland is threatened by various human-induced processes and activities, e.g., eutrophication, harmful discharge of substances and climate change. In the VELMU programme, both abiotic and biotic characteristics of the marine environment are inventoried. Inventories are conducted particularly to map the distribution of benthic habitats, and the vascular plants, macro-algae, and fish species living in these habitats (Kallasvuo, 2010). Hyperspectral remote sensing has a potential to provide such potential. The aim of the Posiva's environmental research programme is to record as extensively as possible the current state of the surface environment and, at the same time, to produce material that can assist in predicting the development of the environment over a period spanning thousands of years (Pere et al., 2015). The research programme focuses, among others, on the fauna, flora and water system of the Olkiluoto island and surrounding area. Hyperspectral remote sensing can provide cost efficiency and widen the spatial coverage of such research by supplementing conventional field studies.

1.1 Objectives

The objectives of this thesis were largely influenced by the needs of collaborative partners of the data analytics research group of the Pori Department of TUT. The atmospheric correction of HYPE08 hyperspectral data is important to Posiva Ltd. The data can be used as a baseline for future hyperspectral missions. Change detection can not be implemented without state of the art atmospheric correction. Posiva also had another interest related to hyperspectral imaging, namely, reed bed inventories using remote sensing. Information revealing the environmental effects of the non-organic turbidity in coastal areas is needed by the environmental adminis-

tration for the Environmental Impact Analysis of projects that will increase the clay induced turbidity. Centre for Maritime Studies of Turku University was looking for new methods for providing such information. The Finnish Inventory Programme for the Underwater Marine Environment (VELMU), designed to provide information for the protection of the Baltic Sea, collects data on the diversity of underwater marine biotopes and species. Finnish Environment Institute and South-Bothnia ELY Centre were interested in the feasibility of remote sensing as a tool in VELMU.

The general objectives of this thesis were to validate and develop methods for hyperspectral monitoring of coastal environment. One of the major disadvantages related to remote sensing algorithms is that they tend to be site specific. This is especially true when water areas are considered. Algorithm that works at oceans fails at the coastal waters of the Baltic Sea. The specific objectives of this study are:

1. to develop algorithms for water quality parameter retrieval applicable in turbid optically complex coastal waters of the Baltic Sea

2. to evaluate the applicability of hyperspectral imaging for benthic cover mapping in turbid coastal waters and determine the most efficient methods to be used

3. to develop an atmospheric correction method that can produce reliable results in challenging conditions of coastal regions, i.e, high amount of water vapor in the lower atmosphere.

4. study the temporal and spatial spectral variability of reed beds and test the discrimination between reed beds and other vegetation.

Chapter 2

Background and literature overview

2.1 Hyperspectral imaging and sensors

Hyperspectral remote sensing is, in many ways, the ultimate optical remote sensing technology. It allows to uniquely identify and map planetary surface materials through the measurement of continuous, relatively high resolution spectrum of each pixel in spatially high resolution images of the surface (MacDonald et al., 2009). The advances in hyperspectral imaging in the past few decades have been remarkable, but it is clear that the technology is not yet anywhere near complete. In the literature the terms hyperspectral imaging, imaging spectroscopy, and imaging spectrometry are often used interchangeably. Even though some differences might exist, a common framework for such definitions is the simultaneous acquisition of spatially co-registered images in many narrow, spectrally contiguous bands, which are expressed in calibrated radiance units (Schaepman, 2007). The original definition for imaging spectrometry proposed by Goetz et al. (1985) is: "the acquisition of images in hundreds of contiguous, registered, spectral bands such that for each pixel a radiance spectrum can be derived". Although Goetz et al. (1985) defined the prerequisite of hundreds of spectral bands, it can be argued that it is not the number of the measured wavelength bands that qualifies a sensor as hyperspectral but rather the narrowness

and contiguous nature of the measurements (Shippert, 2004). There is not a specific number of bands required to qualify a sensor as hyperspectral, it largely depends on the spectral characteristics of the materials under study.

The absorption features of natural materials in reflectance spectra are due to specific chemical bonds in a solid, liquid, or gas. The variations in material composition often causes shifts in the position and shape of the absorption features in the spectrum (Clark, 1999). The concept of spectral signatures is fundamental in hyperspectral imaging. If the reflectance values for a given material are plotted across a range of wavelengths, the resulting curve is referred to as the spectral signature of that material. Because the spectral signature is different, for each material, it is possible to discriminate between materials based on the differences in their spectral signatures (Pabich, 2002). Hyperspectral data can be analyzed with respect to spectral signatures obtained from spectral libraries available or collected in the field. As an example, the spectral signature of muscovite (mineral) is shown in Figure 2.1. In order to demonstrate the difference between hyperspectral and multispectral imaging, the bands of multispectral Landsat TM sensor are also indicated in the figure. It can be seen that multispectral sensor is not able to record the strong absorption features of the muscovite spectra. Some features are missed because of the gaps in spectral coverage and some due to poor spectral resolution.

Hyperspectral imagery is acquired by the instruments called imaging spectrometers. The most common operation principles of hyperspectral sensors are the pushbroom scanning (electronical) and the whiskbroom scanning (electro-mechanical) (Ortenberg, 2011). Pushbroom scanners use an array of line detectors located at the focal plane of the image formed by sensor optics, which are moved along in the flight track direction. Whiskbroom scanners use mirrors in order to scan a sweep from one edge of the swath to the other.

There are several ways to acquire hyperspectral data. They can be categorized into three groups according to where the sensor is located with respect to the Earth's surface: ground, airborne or spaceborne imaging. Field spectroscopy is the technique used to measure reflectance properties of rocks, soils, vegetation and water bodies in the natural environment, generally under solar illumination (Milton, 1987). It is
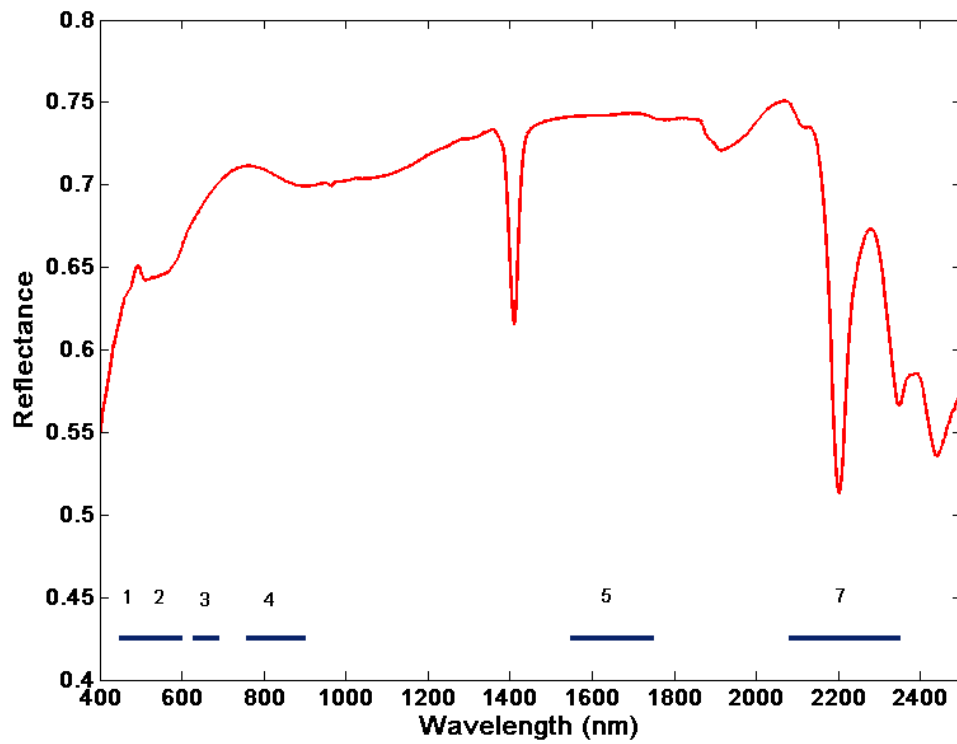
Figure 2.1: The spectral signature of muscovite and the bands of the Landsat TM sensor

essential to measure the reflectance spectra of intact materials in the field, because removal of the sample can easily destroy the sample's surface properties. Furthermore, the laboratory measurements are impractical for many large natural surfaces. The validation radiometric and atmospheric correction of remotely sensed data is an important application where the data acquired using field spectrometers are essential (Brook and Ben-Dor, 2011). Field spectroscopy is technically less challenging than airborne imaging spectrometry, as the sensing instrument can remain fixed over the target of interest for much longer, and the distance between the instrument and the target is short (Milton et al., 2009).

The majority of past and current hyperspectral sensors are designed to be used airborne. In the latest decades advances in hyperspectral sensor technology have been remarkable. In the early 80s the first airborne sensor AIS (Airborne Imaging Spec-

trometer) was introduced. The key technology of the hyperspectral sensors is the detector technology. Although the first detectors of AIS contained only 32x32 elements, they enabled the construction of an imaging spectrometer that covered the spectral range of 1200-2400 nm (Vane et al., 1984). In the late 1980's several commercial hyperspectral imagers were introduced like CASI (Compact Airborne Spectrographic Imager) and DAIS (Digital Airborne Imaging Spectrometer), for example (Nakashima et al., 1989; Richter, 1996). The introduction of these sensors started the spread of hyperspectral imaging towards commercial applications. The development of AVIRIS (Airborne Visible/infrared Imaging Spectrometer) by the NASA Jet Propulsion Laboratory is probably the most comprehensive research and development project related to hyperspectral imaging. AVIRIS development was started in 1984 and the imager first flew aboard a NASA ER-2 aircraft in 1987. Since then it has gone through major upgrades as technology has advanced in detectors, electronics and computing (Goetz, 2009). In addition to sensors referred above, two instruments, AISA and HyMap, have been deployed for commercial and scientific operations around the world. Both sensors provide excellent signal-to-noise ratio (<500:1) and image quality. The total setup needed for airborne hyperspectral acquisition can be quite complex. It typically consists of a sensor (optoelectronic unit), power supply, data accumulation and control unit, vibration damping platform, operator display, GPS receiver, inertial measurement unit, and data processing device (Ortenberg, 2011). Hyperspectral acquisition systems are traditionally expensive, space consuming and heavy. One of the biggest trends in remote sensing is the use of unmanned aerial vehicles (UAV). The use of UAVs can provide low cost and flexible approaches to hyperspectral imaging.

2.2   Atmospheric Correction of Hyperspectral Data

In order to use hyperspectral imaging data for quantitative remote sensing of environment, the atmospheric effects must be removed. Over the years, atmospheric correction algorithms have evolved from the simple empirical methods to more recent methods based on rigorous radiative transfer modeling approaches. The objective of atmospheric correction is to retrieve the surface reflectance (that characterizes the

surface properties) from remotely sensed imagery by removing the atmospheric effects. The data after radiometric correction is given as radiance, i.e., the energy reflected from a unit surface area (W/m^2). In atmospheric correction, the radiance values are converted into reflectance data, expressing the fraction of radiation reflected from the surface. Atmospheric correction is a difficult procedure due to the complex nature of atmosphere; the correction procedure must be done individually for each flight line. Atmospheric correction should be done with utmost care because it largely determines the usability of the final data. The use of most algorithms and indices requires well calibrated reflectance data. Accurate change detection cannot be accomplished without atmospheric correction because otherwise it is impossible to determine whether the change occurred in the continuously varying atmosphere conditions or in the target under study. Several methods for the atmospheric correction have been proposed in the literature. Methods can be divided into three categories: 1) empirical-based, 2) model-based methods and 3) combined methods. The empirical-based methods rely on the scene information and do not use physical information as the model-based methods do. The scene information means the information that is embedded in the image, i.e., the radiance at certain location. Model-based correction approaches use methods in which the radiance at the sensor is modeled using radiative transfer models and data from detailed atmospheric and sun information archives. In the following, a short overview of combined methods is given as these are most relevant from this thesis' point of view.

2.2.1 Combined methods

Combined methods, also referred as hybrid methods use both radiative modeling and empirical approaches for the derivation of surface reflectances from hyperspectral imaging data. The surface reflectance spectra retrieved using radiative transfer models often contain residual atmospheric absorption and scattering effects (Gao et al., 2009). The reflectance spectra may also contain artifacts due to errors in radiometric and spectral calibrations. These errors can sometimes be corrected using combined atmospheric correction methods. A combined Empirical Line (EL) and model-based

method was first suggested by Clark et al. (1993). The combined method produced better results than empirical- or model-based methods alone. The EL correction complemented model-based method by correcting for fine details such as errors in solar flux or radiance calibration, and could better correct for unusual path radiance due to aerosols.

Uniform calibration ground targets needed in the EL method can be hard to find. Goetz et al. (1998) proposed a technique that combines ground measurements of spectral irradiance with existing radiative transfer model to derive the model equivalent of an empirical line method correction without the need for uniform ground targets of different reflectance. The method is based on determining atmospheric parameters from the spectral irradiance measurements made at the earth's surface which are fed into the MODTRAN model to provide an at-sensor modeled radiance (Berk et al., 1989).

Another combined correction method is EFFORT (the Empirical Flat Field Optimal Reflectance Transformation) that makes a linear adjustment to the data in order to increase the accuracy of model-based atmospheric correction (Broadman, 1998). EFFORT has its roots in the EL method often used to correct data from uncalibrated sensors using field measured spectra. The empirical gains and offsets are applied to the data after a model-based atmospheric correction has been done using the ATEREM radiative transfer code. However, in this method gains and offsets are not derived from field measurements. By using the data themselves EFFORT generates "pseudo field" spectra by fitting each observed spectrum with a parametric model of Legendre polynomials optionally augmented with real spectra. Gains and offsets for every band are calculated by comparing the modelled spectra to the data spectra.

Ben-Dor et al. (2004) presented a comprehensive study where atmospheric correction techniques were evaluated using model-based HATCH, EL and their combined methods. The study utilized a synthetic data set that represented at-sensor radiance data of the AVIRIS sensor in order to have well defined controlled conditions. It was found that application of the EL to model-based corrected data was much more effective than applying it to the original radiance data. The thematic analysis using

a SAM classifier showed that the combination of EL and HATCH methods produces best classification accuracy. The atmospheric features are stronger when spaceborne data is used as the travel in the atmosphere is longer. Matsunaga et al. (2013) proposed the use of combined Dark Pixel method and MODTRAN 5 code for correcting hyperspectral spaceborne HISUI data.

2.2.2 Atmospheric correction of sea areas

The atmospheric correction methods presented in remote sensing literature are primarily designed for remote sensing of land surfaces. However, these methods in most cases are not directly applicable for hyperspectral remote sensing of sea areas. The main reason is that sea surfaces are much darker than land surfaces. Due to the high absorption and transmission of water bodies the reflected radiation level is much lower compared to land areas (Gao et al., 2009). Another reason is that the reflection from air/water interface is not Lambertian. Accurate modeling of atmospheric absorption and scattering effects and the specular sea surface reflection effects is required in order to derive the so called "water leaving reflectance" from hyperspectral imaging data. Water leaving reflectance is the reflectance resulting from scattering by water bodies excluding contributions from specular reflection at the air-water interface.

Severe problems related to atmospheric correction of sea areas have been published in several research papers. Reinart and Kutser (2006) concluded that model-based algorithms cannot model some marine climates such as that prevailing at the Baltic Sea area, for example. Kutser et al. (2011) concluded that spectral library approaches of benthic mapping failed because of the problems related to atmospheric correction of hyperspectral data. The sun glint effect is yet another contributing factor disturbing atmospheric correction of sea areas. When water surface is not flat, the direct radiance originating from the sun can be reflected from the crests or slopes of the waves (Kutser et al., 2009). The reflected radiance does not contain any information about the water constituents and benthic features. Sun glint effect is often a factor in wide field-of-view acquisition of airborne or satellite data.

In the late 1990s Naval Research Laboratory presented a TAFKAA algorithm

for atmospheric correction of hyperspectral remote sensing data of sea areas (Gao et al., 2000). The algorithm uses lookup tables generated using a vector radiative transfer code and a spectral matching technique. In this algorithm channels located at wavelengths longer than 0.86 μm, where the water leaving reflectances are close to zero, are used for the derivation of information on atmospheric aerosols. The aerosol information is then extrapolated back to the visible range based on aerosol models in order to retrieve the water leaving radiances. The proposed algorithm has produced excellent results when tested using both satellite and airborne hyperspectral data.

After the presentation of TAFKAA, more model-based algorithms have been developed for hyperspectral remote sensing of sea areas. Adler-Golden and Acharya (2005) developed a special version of the FLAASH code, which is applicable to hyperspectral and multispectral data, for retrieving coastal water properties and for estimating bathymetry of shallow waters. Sterckx and Debruyn (2004) described a code nicknamed WATCOR for remote sensing of coastal and lake waters. Both the special version of FLAASH and WATCOR codes used MODTRAN-4 for radiative transfer modeling.

2.3   Remote sensing of water quality

Even when some basic life forms can manage in polluted water, most organisms require water that is relatively clean. The shortage of clean water is one of the major threats to human life and health globally. The quality of surface waters is determined by the type and the quantity of various suspended and dissolved substances (Koponen, 2006). The large amount of these substances correlates with poor water quality. Some of the substances are of natural origin while others originate from human activities.

In traditional water quality monitoring, water samples are regularly collected from the same sampling sites and analyzed for various water quality parameters such as biological parameters (e.g. phytoplankton biomass) as well as physical and chemical parameters (e.g. nutrients). Standardized sampling and measurement methods are used so that the results are comparable.

Remote sensing is a suitable technique for large scale monitoring of inland and

coastal water quality and its advantages have long been recognized. Remote sensing provides a synoptic view of the spatial distribution of different biological, chemical and physical variables of both the water column and, if visible, the substrate (Dekker et al., 2011). Currently the following water quality parameters can be estimated using optical remote sensing methods (Koponen, 2006):

- phytoplankton (chlorophyll *a*)
- suspended inorganic material (e.g. clay, sand and dust)
- colored dissolved organic matter (CDOM)
- turbidity
- secchi depth
- temperature
- occurrence and extent of algal blooms.

Natural water bodies differ from each other substantially. The terminology and rationale for Case 1 and Case 2 water classifications were established by Morel and Prieur (1977) in their work on the bio-optical basis for ocean color variations. The reflectance spectra of Case 1 waters are largely dominated by: 1) living phytoplankton cells; 2) organic tripton (detritus) particles from death and decay of phytoplankton and the grazing products of zooplankton; and 3) the dissolved organic matter produced by phytoplankton metabolism as well as the decay of organic tripton (Schalles, 2006). Case 1 waters can range from very clear (oligotrophic) to very productive (eutrophic) waters, depending on the phytoplankton concentration. Case 2 waters are 'everything else', i.e., waters where inorganic particles or dissolved organic matter from land drainage contribute significantly to the reflectance spectra so that absorption by pigments is relatively less important in determining the total absorption (Mobley, 1994). Roughly 98 % of the world's oceans and coastal waters fall into the Case 1 category, and almost all bio-optical research has been directed towards these phytoplankton dominated waters. However, near shore and estuarine, Case 2 waters are disproportionately important to human interests such as recreation, fisheries, and military operations (Mobley, 1994).

Finland has a long coast line with the Baltic Sea. It can be difficult to define where

the coastal area ends and where open sea starts. Outer islands of the Archipelago can be used as limit, but, in some approaches, it is assumed that the whole Baltic Sea belongs to Case 2 waters. In addition to sea areas, Finland has thousands of lakes covering approximately 10 % of the total area. The water quality varies widely according to the lake type (trophic state, humus content).

2.3.1   Hyperspectral remote sensing of turbidity, TSM, TSS and CDOM

While chlorophyll content remains the most important water quality parameter in coastal waters, there are other parameters such as: turbidity, total suspended matter (TSM), total suspended solids (TSS) and colored dissolved organic matter (CDOM) which can be estimated using hyperspectral data.

Bhatti et al. (2010) demonstrated that simple band ratio algorithms can successfully be used to estimate turbidity, TSS and CDOM. The wavelengths to be used were selected using regression analysis. Turbidity is an optical characteristic or property of a liquid, which in general terms describes the clarity, or haziness of the liquid. The first-derivative spectrum has been successfully used to estimate turbidity (Fraser, 1998). The derivatives of reflectance spectra at 429, 628 and 695 nm are significantly correlated with turbidity over a wide range of water quality conditions. TSM is essentially related to the total scattering of particles in the water column. The method of partial least squares (PLS) regression was successfully applied to retrieving the TSM (Xu et al., 2009). The results showed that the proposed method can outperform traditional linear regression as well as the first-derivative and logarithmic models.

CDOM is an important component in coastal waters. CDOM can have significant effects on biological activity in aquatic ecosystems by diminishing light penetration and, consequently, influencing bacterial respiration. Yu et al. (2010) analyzed hyperspectral data using a functional linear model (FLM) in order to establish a relationship between the measured reflectance spectrum and CDOM concentration. One advantage of using hyperspectral data in water quality monitoring, is that several parameters can be retrieved simultaneously. For example, Pan et al. (2015) used

hyperspectral CASI-1500 data and support vector regression to successfully retrieve both turbidity and water depth from a shallow river.

2.3.2   Hyperspectral remote sensing of clay content

Suspended marine clay can have a significant effect on primary production in several ways: (1) it increases the attenuation of light, hence reducing the light available for photosynthesis in plants and (2) it may absorb certain nutrients (e.g. phosphate) in the water column, making them less available for algal uptake. Gin et al. (2003) studied the spectral profiles of suspended marine clay for the estimation of suspended sediment concentration in tropical waters. The amount of inorganic suspended sediment was controlled by diluting marine clay in the measured water samples. It was found that the dominant reflectance peak lays between 595 and 690 nm when inorganic marine sediments (clay) are suspended in water. Another reflectance peak was found in the infra red region at 814 nm. The regression analysis showed that the best estimate of clay concentration can be obtained using the band ratio of 595/754 nm.

Remote sensing of water quality parameters in coastal waters is challenging. This is mainly due to the complex interactions of the several optically active substances. Gin et al. (2002) studied the effects of suspended marine clay on the reflectance spectra of phytoplankton. The results showed clear correlation between clay concentration and measured spectra, but the shape of the spectra was largely defined by the fresh water phytoplankton. Based on the research referred above, it can be concluded that the development of a clay retrieval algorithm, robust against the variation of chlorophyll, can be very challenging.

2.4   Hyperspectral Benthic mapping

Europe's marine environment is deteriorating rapidly and existing measures to reverse the situation are clearly insufficient. The amounts of nutrients in the Baltic Sea increased several times during the last century with severe ecological effect on the biota. During the last few decades the perennial seaweed *Fucus vesiculosus L.*

has rapidly declined in large parts of the Baltic Sea. Indirect effects of eutrophication such as increased turbidity and sedimentation have generally been suggested as major factors causing the decline. (Berger et al., 2004)

Benthic vegetation is an important part of the coastal zone ecosystem. It contributes to the primary production in coastal areas in a fundamental way. Submerged aquatic vegetation provides important habitats feeding, spawning and serving as nursery grounds for many fish and invertebrate species (Vahtmäe, 2009). Species composition of the benthic vegetation cover is a powerful indicator of environmental conditions in both marine and fresh water ecosystems (Wolter et al., 2005). Macroalgae species differ in their tolerance to environmental factors. Their presence or absence and diversity have been used to assess the status of coastal systems. Health and survival of these submerged plant communities in coastal waters depend on suitable environmental conditions. The growth, survival and depth penetration of submerged vegetation is directly related to light availability (Dennison, 1987).

On the other hand, knowing of bottom type (sand, clay, etc.) and/or water depth in shallow coastal waters is important for several reasons (e.g. safe navigation, recreation areas). Mapping shallow water bottom types by diving is time consuming and expensive. Some coastal regions may be too dangerous for diving (due to swell) or not accessible to hydrographical ships due to shallow water and/or dangerous bottom topography (Vahtmäe and Kutser, 2007).

There is an increasing need for reliable information on benthic cover types. Knowledge on the distribution and quantity of benthic habitats is sparse if not absent. Mapping benthic algal cover using conventional methods can yield to very good accuracy and high resolution (Werdell and Roesler, 2003). However, traditional *in situ* measurements like diving, submerged video and grab sampling cannot cover large areas without excessive costs. Even if the issue of the cost is ignored, insufficiency of manpower and logistical problems would be unbearable. Mapping of benthic cover types and their biophysical properties based on their optical properties has been carried out successfully in optically clear waters (Phinn et al., 2005). Majority of the remote sensing studies of submerged mapping have been carried out in clear ocean waters, so the limits of the technique are still somewhat vague. Vahtmäe et al. (2006) have pub-

lished promising results where the feasibility of submerged remote sensing is tested in challenging turbid waters of the Baltic Sea. The study is based on model-based simulations, so some empirical validation would be needed. Mumby et al. (1999) studied the cost-effectiveness of different remote sensing techniques and the conventional methods. The overall conclusion was that remote sensing is the most cost-effective method available.

2.4.1 The effects of water column in benthic mapping

When light penetrates water, its intensity decreases exponentially as a function of increasing depth. This phenomenon is known as attenuation and it exerts a profound effect on remotely sensed data of aquatic environments (Green et al., 2000). The magnitude of attenuation differs with the wavelength of electromagnetic radiation. In benthic mapping the visible part of the spectrum is most commonly considered, because the attenuation in the NIR region is so high. In the region of visible light, the red part of the spectrum attenuates more rapidly than the shorter wavelength blue part. As depth increases, the separability of benthic cover types by theirs wavelength spectra declines. The spectral radiances recorded by a sensor are therefore dependent both on the reflectance of the substrate and on depth. These two factors on the signal create considerable confusion when attempting to use visual inspection or image classification to map benthic cover types.

The exponential decay of light intensity with increasing depth results from two phenomena: absorption and scattering. Absorption involves the conversion of electromagnetic energy into other forms such as heat or chemical energy (e.g. photosynthesis in phytoplankton). Absorption itself is a fundamental process that determines the shape and magnitude of the reflectance spectrum in the water, while absorption coefficient accounts for the proportion of light lost due to absorption (Pegau et al., 1995). The main absorbers in natural waters are (Holden and LeDrew, 2001):

– Water itself; water has weak absorption in the blue and green portions of electromagnetic spectrum but the absorption increases significantly for wavelengths greater than 550 nm.

  – Yellow substance, or dissolved organic matter (DOM) resulting from decomposition; yellow substance presents significant consequences for light absorption in the blue end of the spectrum.

  – Phytoplankton, absorbing strongly in the red region of the spectrum depending on the total amount of photosynthetic pigments.

While light is mostly absorbed immediately in the water column, a significant part of the photons is are still scattered before being absorbed. Since scatter does not remove light but simply diverges light from its original path, it effectively impedes the vertical penetration of light. This process of scattering is largely caused by inorganic and organic particulate matter and increases with the suspended sediment load (turbidity) of the water.

The most important characteristic of water column in benthic mapping is the diffuse attenuation coefficient. The diffuse attenuation coefficient in water indicates how strongly light intensity at a specified wavelength is attenuated within the water column. A large attenuation coefficient means that the light is quickly attenuated (weakened) as it passes through the water column. Attenuation coefficient is measured using units of reciprocal length. This parameter, is directly related to the presence of scattering particles in the water column, either organic or inorganic, is an indicator of water clarity. Any increase in the concentration of optically active substances increases the diffuse attenuation coefficient and may change its spectral composition.

2.4.2   Water column correction techniques

The most common difficulty related to remote sensing of submerged environment is the confounding influence of variable depth on bottom reflectance (Green et al., 2000). Removal of the influence of depth on bottom reflectance would require (1) a measurement of depth for every pixel on the image, and (2) knowledge of the attenuation characteristics of the water column. The attenuation characteristics are mainly determined by the concentration of dissolved organic matter (Mumby et al., 1998). Good digital depth maps are rarely available. Depth maps are mostly acquired for marine safety purposes, which often restricts their use for benthic mapping purposes.

There are new techniques such as LiDAR based bathymetry that can produce accurate and high resolution depth maps (Tulldahl et al., 2011). Unfortunately, the use of such techniques can be quite expensive. Mumby et al. (1998) reported only four studies out of forty five (9 %) that attempted water column correction and concluded that authors were generally unaware of such methods.

In order to avoid the need for accurate depth map, Lyzenga (1978) put forward a simple image based approach to compensate for the effect of variable depth when mapping bottom features (hereafter referred to as water column correction). Rather than predicting the reflectance of the seabed, the method produces a depth invariant bottom index from each pair of spectral bands.

The attractive aspect of this approach is that *in situ* or auxiliary data are not required. Yet, it is only applicable where water properties are moderately constant across an image. Lyzenga's pioneering work has inspired many researchers to test and develop the original method. Spitzer and Dirks (1987) used a two flow radiative transfer model to predict the sensitivity of the Lyzenga's model and concluded that increased turbidity was a major limiting factor when using Lyzenga's method. Tassan (1996) proposed a modified Lyzenga's method which is mathematically quite complex. Lyzenga's original method is not applicable if the suspended sediment content is higher in shallow waters compared to deep waters. Tassan's study was based on numerical simulations and requires field validation. Mumby et al. (1998) tested Lyzenga's method in coral reef mapping using CASI hyperspectral data. When combined, depth compensation and contextual editing made a significant improvement upon simple classification using original bands.

Some new methods, not directly based on Lyzenga's original work have been proposed as well. Armstrong et al. (2007) presented an approach where at-sensor radiances are transformed into underwater reflectance factors. The transformation was derived by using submerged black and white tarpaulins as underwater calibration targets. Unlike Lyzenga's approach to water column correction, the presented field calibration methodology preserves the full dimensionality of the remote sensing data in its original spectral space. In addition, no field data of image based estimates of the spectral attenuation coefficients are required. The main limitation of this approach

is the logistics of placing calibration targets of adequate size underwater and the measurement of their reflectance properties during the overflight. Karpouzli et al. (2003) proposed a method based on the variables of water depth, distance to and size of mangrove beds, and distance to and size to towns. The method was developed by using an extensive number of optical *in situ* water measurements and laboratory analysis of water samples. Karpouzli et al. concluded that the results of studies where single measurements of 'average' attenuation have been used to depth correct remotely sensed imagery should be interpreted with a high degree of caution. Both methods referred above require a considerable amount of fieldwork.

In addition to rather simple methods described above, some more complex approaches have been presented. Cho et al. (2010) proposed an experimentally derived algorithm for water column correction. The energy absorbed by water and scattered from the water column was separated using reflectance measurements in an indoor water tank with hypothetical surfaces that either reflect or absorb all the incoming light. Using these experimental measurements, a hyperbolic tangent function was developed to correct reflectance measured from a shallow water body for the water effects. This experimentally derived algorithm can improve the quality of mapping seagrass beds and invasive aquatics in shallow water bodies. Mishra et al. (2007) proposed a sophisticated algorithm that accounts for variable depth and optical properties of water. The hyperspectral data were used in band ratio algorithms to derive water depth and water column optical properties (e.g., absorption and backscattering coefficients). Mobley et al. (2005) proposed an approach based on spectrum-matching and look-up-table methodology: first, a database of remote sensing reflectance spectra corresponding to various water depths, bottom reflectance spectra and water-column IOPs is constructed using a special version of the HydroLight radiative transfer numerical model. Second, the measured spectrum for a particular image pixel is compared with each spectrum in the database, and the closest match to the image spectrum is found using a least-squares minimization. Zoffoli et al. (2014) evaluated a comprehensive set of water column correction methods proposed in the literature using simulated data. They concluded that the best method depends on the marine environment, available input data and desired outcome or scientific application. There are a few

software products for water column correction, although not commercially available. Kobryn et al. (2013) used a WATCOR softwave module to water column correction and successfully retrieved bathymetric data and sea floor reflectance over a large reef site in north-western Australia.

2.5   Hyperspectral Mapping of Wetlands

The coastal wetlands are important as natural ecosystems offering wildlife habitat and recreational areas, as well as functioning as important nutrient cycling environment for maintaining water quality (Schmidt and Skidmore, 2003). Wetlands are also an excellent indicator for early signs of any physical or chemical degradation in wetland environments (Dennison et al., 1993). The management of these environments, especially in response to human activities, requires information on the quality and quantity of vegetation. Wetland plants and their properties are not as easily detectable as terrestrial plants due to several reasons. First, the reflectance spectra of wetland vegetation are often very similar and are combined with reflectance spectra of the underlying soil, understory vegetation and atmospheric vapor (Adam et al., 2010). Second, wetland vegetation exhibits high spectral and spatial variability because of the steep environmental gradients and sharp demarcation between the vegetation unit (Zomer et al., 2009). Hence, it is often difficult to identify the boundaries between vegetation community types, even in the field. Last, tidal changes cause rapid variation in environmental factors such as salinity and water intake.

Several research publications have demonstrated the feasibility of hyperspectral remote sensing in wetland vegetation mapping. Artigas and Yang (2005) discriminated vegetation species in north-eastern New Jersey, USA, using field-collected hyperspectral seasonal reflectance spectra of marsh species in coastal wetland. The results indicated that NIR range and wavelengths 670-690 nm in the visible region can be used to discriminate between the most marsh species. Wang et al. (2007) attempted to map highly mixed vegetation in salt marshes in Venice, Italy. The use of CASI hyperspectral data and Vegetation Community based Neural Network Classifier (VC-NNC) produced classification accuracy higher than (91 %). Kamal and Phinn (2011)

used CASI-2 hyperspectral data for Mangrove species mapping. The results demonstrated that the object-based approach, combining a rule-based and nearest-neighbor classification methods, produced best results (76 %) when compared to Spectral Angle Mapper (SAM). Hunter et al. (2010) studied the mapping of macrophytic vegetation in shallow lakes using the Compact Airborne Spectrographic Imager (CASI) data and Maximum Likelihood Classifier (MLC) and Support Vector Machine (SVM) methods. The classification accuracy rose near 80% for both methods. Several seasonal time-series spectral of common reed have been published as well (Gilmore et al., 2008; Ouyang et al., 2013; Artigas and Yang, 2005).

Chapter 3

Remote Sensing of Coastal Environment: Data and Methods

In this chapter the study sites and data acquisition methodology are described. Finally, the methods used to process these data are presented.

3.1   Data

The data used in this study was collected using a variety of sensors. All the employed data are hyperspectral, i.e., the spectra are continuous and the spectral resolution is high. Both airborne and field measurements were used. All study sites shown in Figure 3.1 are located in Satakunta region at the West Coast of Finland. The data used in this doctoral study were obtained from the following measurements.

1. The spectral laboratory measurements of water samples were carried out in Reposaari Environmental Research Centre in Pori. The reflected light from a water surface at the wavelength range of 350-2500 nm was measured with a portable field spectroradiometer FieldSpec Pro from Analytical Spectral Devises Inc. ASD; Boulder, Colorado, USA. The spectral resolution of the device is 3 nm between 350-1000 nm and 10 nm between 1000-2500 nm. At pre-processing, the spectrum is interpolated to have a value at every nanometer. The total number of six water samples with added clay were measured. The clay concentration in the prepared water sam-

ples varied between 10.6 and 142 mg/l. A particular challenge for the measurement was the illumination of the water sample in glass container. The container was illuminated with an Oriel research arc lamp source having a power consumption of 1000 W. The Oriel lamp is a laboratory equipment designed for spectral measurements providing constant spectral characteristics. The oriel lamp is a heavy equipment and it was not possible to mount it above the container to provide nadir angle of light. The water sample had to be illuminated through glass, which caused the need to develop a method that corrects the effect of glass. The arrangement of reflectance measurements is shown in Figure 3.4. Measurements were carried out by the author and Senior Researcher Viljo Kuosmanen from Geological Survey of Finland. These data were used in [P1].

2. The HYPE08 flight campaign was carried out in July 2008. The main goal of the hyperspectral data acquisition was to capture the hyperspectral baseline of the environment around Olkiluoto repository site before the permission of the construction license. Baseline data is the reference used in change detection when the data of future campaigns will be analyzed. The planning phase preceding the actual flight campaign included calculation of flight lines, search and verification of sites used for field measurements and co-timing of operations. The size of the imaged area is over 600 km^2. Half of the imagery covers coastal water areas. The rest of the data covers rural forest and agricultural areas as well as urban area around the city of Rauma. The start of the flight campaign and the selection of flights days were planned based on the information provided by the commercial weather forecast service Foreca Ltd. Despite of careful planning, the campaign suffered from severe cloud cover in many days. The total number of recorded flight lines was 27, of which 23 flight lines were recorded on 4th of July and 4 flight lines on 13th of July. The cloud cover on both days was absent providing homogenous solar irradiation from ground surface. The acquisition of 4 pre-planned flight lines was cancelled due to excessive cloud cover. The flight altitude during the acquisition was 1.9 km leading to ground resolution of 2.5*2.5 m per pixel. The acquisition was done using Piper Pa23-250 aircraft carrying an AISA dual imaging spectrometer. The AISA dual spectrometer collects reflected solar radiation in 481 bands from 399 to 2452 nm wavelength. This includes the
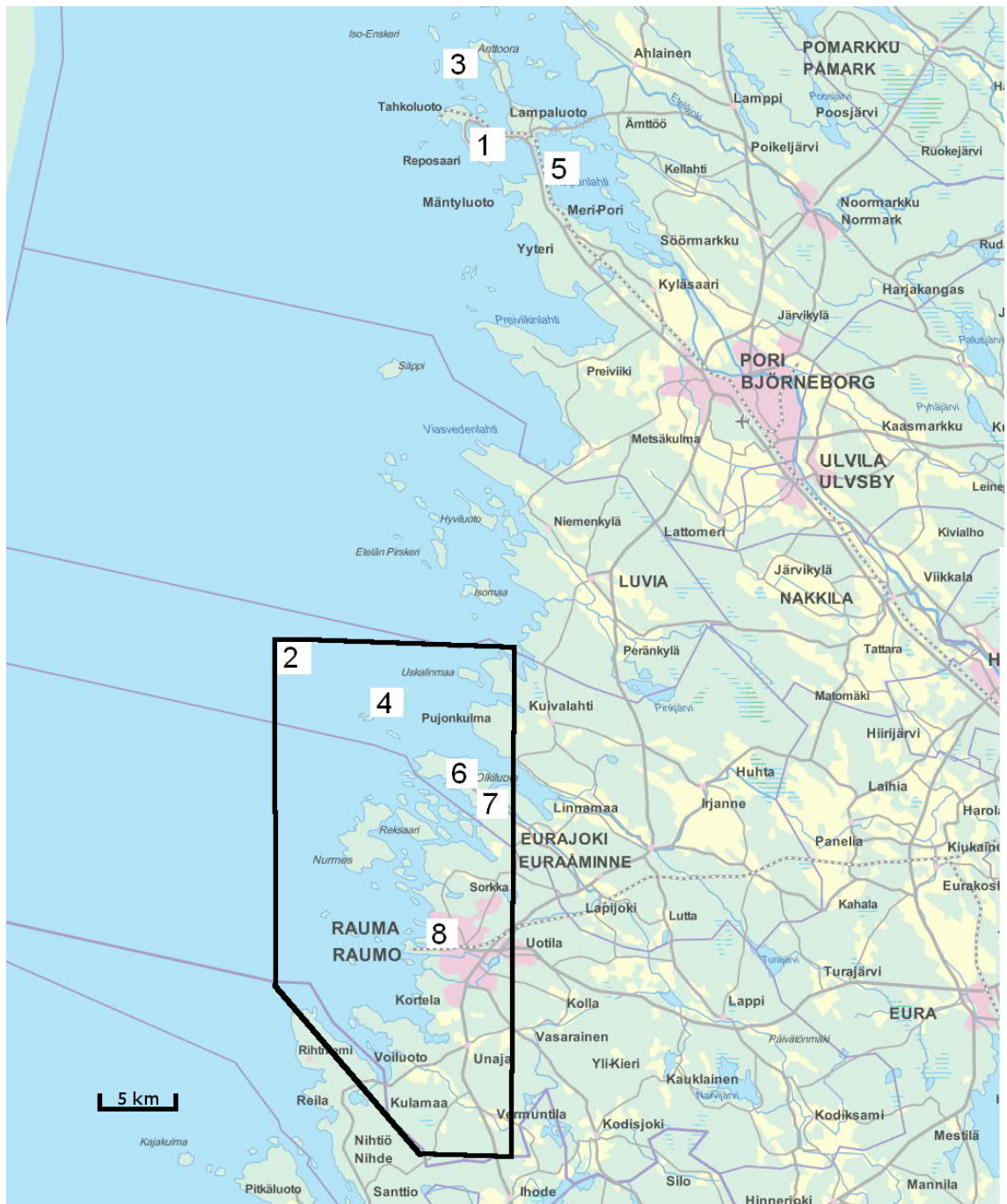
Figure 3.1: Geographic location of data aquisition sites: 1) laboratory measurements of water samples 2) area of HYPE08 flight campaign 3) spectral field measurements of water quality parameters 4) spectral field measurements of benthic cover type samples 5) spectral time-series measurements of reed beds, Pori 6) spectral field measurements of reed beds in Olkiluoto 7) spectral field measurements during HYPE08 8) spectral field measurements of Satakunta spectral library

visible, near infrared and shortwave infrared regions of the electromagnetic spectrum. The spectral resolution is 3.3 nm at Visible Near Infrared (VNIR) range and 12 nm at Short Wave Infrared (SWIR) range. The HYPE08 campaign was a joint effort of Aero Media Ltd., University of Debrecen, Hungary, Pöyry Environment Ltd., Geological Survey of Finland, Luode Consulting Ltd., Tampere University of Technology, Pori, and Posiva Ltd. These data were used in [P1] and [P5].

3. Spectral water-quality parameters were measured at the four sites in Reposaari archipelago on 26th of May 2011. Spectral measurements on board a small boat are challenging. Interfering factors like sun glint and reflections from the boat hull can easily ruin acquired data. Two spectral parameters were measured at each site: the optically deep water reflectance R and the water attenuation coefficient K. Optically deep water reflectance was measured using a GER 1500 spectroradiometer (Spectra Vista Corporation, Poughkeepsie, New York, U.S.A.) equipped with the optical fiber extension. Reflectance was calculated as the ratio of radiance from the measured object to the radiance from the reflectance standard, i.e., 99% Spectralon panel (Labsphere, North Sutton, New Hampshire, U.S.A.). The spectral range of the instrument is 300-1100 nm. Spectra were sampled with 1.5 nm intervals, and spectral resolution of the GER 1500 instrument is 3 nm. The water attenuation coefficient K was measured using a white reference plate. The plate was set at a depth of 30 cm, and the reflectance was measured. Then the reflectance of the wet reference plate was measured again on board without the water column. Measurements were carried out by the author and boatman Jukka Jussila from Reposaari Environmental Research Centre. These data were used in [P2] and [P4].

4. The samples of benthic cover types were collected near Island Kalla, Eurajoki on 6th of July 2010. Benthic cover types for this study were selected based on an initial submerged survey in the study site. Research divers explored the area using side-scan sonar and underwater video. Specimens of typical green (*Cladophora glomerata*), brown (*Fucus vesiculosus*), and red (*Ceramium tenuicorne*) benthic macroalgae were selected. In addition to benthic vegetation, three typical bottom covers, i.e., sand, clay, and reddish pebble, were selected. Divers collected samples and transported them in water filled containers to mainland. Reflectance spectra of samples were

measured using a GER 1500 spectroradiometer immediately after the transportation. Measurements were carried out by the author and research divers Ari Ruuskanen and Niko Nappu from Monivesi Ltd. These data were used in [P2] and [P4].

5. The spectral time-series measurements of three observed reed beds were carried out at Hilskansaari Island, Pori between 12th of June and 3rd of October 2012. Reflectance spectra of reed beds were measured using a portable GER 1500 spectroradiometer. The fiber optic light guide connected to the instrument was raised above the reed bed by using a 6 meters long fiberglass pole. The end of the optical fiber was placed above plant canopies at approximately 4 meters' height from the canopy. This arrangement provided a nadir view of the reed bed. The field-of-view of the optical fiber is 25 degrees resulting in circular measurement area of 1.7 meters in diameter. Three repeated measurements at each measurement point were taken and the results were averaged. Each individual measurement was calibrated using a reflectance standard. Measurements were carried out by the author and research assistant Juha Ståhlnacke. These data were used in [P3].

6. Spectral field measurements of reed beds in Olkiluoto were carried out in summer 2012. Reflectance spectra of reed beds were measured using a GER 1500 spectroradiometer in the same manner as in Hilskansaari. These data were used in [P3].

7. A field campaign was conducted during the airborne data acquisition of HYPE08. The purpose of the field campaign was to collect data for the validation and calibration process of the hyperspectral data. Selected Reference (REF) and Pseudo Invariant Feature (PIF) targets were measured using a ASD FieldSpec Pro portable spectrometer. REF targets are spectrally homogenous tarpaulins laid to the ground during the overflight. PIF targets are natural homogenous areas on the ground surface. The distance of optical fiber from the target was approximately 1.5 meters resulting in circular measurement area of 0.7 meters in diameter. Measurements were carried out by senior researcher Viljo Kuosmanen and geophysicist Jukka Laitinen from Geological Survey of Finland. These data were used in [P5].

8. In summer 2009 a field campaign was arranged in order to collect a spectral library from Satakunta Region. On 23rd of July measurements were carried out in

Otanlahti area, Rauma using a ASD FieldSpec Pro spectrometer. Measurements were made in the same manner as during the HYPE08 campaign. Measurements were carried out by the author and senior researcher Viljo Kuosmanen from Geological Survey of Finland. These data were used in [P5].

3.2 Methods

The methods applied in this doctoral thesis can be divided into the following categories:

- methods for estimating the difference between two spectra and/or to classify targets according to their spectral signature in [P2] and [P4]
- methods for generating simulated hyperspectral data in [P2] and [P4]
- methods for various corrections in [P1] and [P2] (such as the effect of glass container, for example).

Below the most important algorithms and methods are briefly presented while more detailed description of the methods are given in the respective papers.

3.2.1 Methods for estimating the difference between two spectra

Spectral Angle Mapper (SAM)

SAM measure is defined by Kruse et al. (1993) as:

$$\alpha = cos^{-1} \frac{\sum_{l=1}^{N} \mathbf{X}_l \mathbf{Y}_l}{\sqrt{\sum_{l=1}^{N} (\mathbf{X}_l)^2 \sum_{l=1}^{N} (\mathbf{Y}_l)^2}} \tag{3.1}$$

where α is the angle formed between the reference spectrum $\mathbf{Y}$ and the image spectrum $\mathbf{X}$ and N is the number of bands used.

Euclidean Distance (ED)

Euclidean distance measure is defined by

$$ED(\mathbf{X}, \mathbf{Y}) = \|\mathbf{X} - \mathbf{Y}\| \equiv [\sum_{l=1}^{N}(\mathbf{X}_l - \mathbf{Y}_l)^2]^{0.5} \tag{3.2}$$

where $\mathbf{X}$ is the reference spectrum and $\mathbf{Y}$ is the image spectrum and N is the number of bands used.

Spectral Correlation Mapper (SCM)

The SCM measure is defined by Carvalho and Meneses (2000) as:

$$R = \frac{\sum_{l=1}^{N}(\mathbf{X}_l - \overline{\mathbf{X}_l})(\mathbf{Y}_l - \overline{\mathbf{Y}_l})}{\sqrt{\sum_{l=1}^{N}(\mathbf{X}_l - \overline{\mathbf{X}_l})^2 \sum_{l=1}^{N}(\mathbf{Y}_l - \overline{\mathbf{Y}_l})^2}} \tag{3.3}$$

where $\overline{\mathbf{X}}$ and $\overline{\mathbf{Y}}$ are the means of corresponding spectra.

Spectral Information Divergence (SID)

The SID measure is defined by Chang (2000) as:

$$SID(\mathbf{X}, \mathbf{Y}) = D(\mathbf{X}\|\mathbf{Y}) + D(\mathbf{Y}\|\mathbf{X}) \tag{3.4}$$

where $D(\mathbf{X}\|\mathbf{Y})$ can be considered as directed divergence or cross-entropy from pixel $\mathbf{Y}$ to pixel $\mathbf{X}$ [**P4**]. Thus $D(\mathbf{X}\|\mathbf{Y})$ quantifies the information in $\mathbf{Y}$ about $\mathbf{X}$ and, $D(\mathbf{Y}\|\mathbf{X})$ quantifies the information in $\mathbf{X}$ about $\mathbf{Y}$. The algorithm was implemented using an ENVI (Exelis Inc., Boulder, Colorado) software package.

Jeffries-Matusita Distance (JM)

The Jeffries-Matusita distance (JM) is defined by Richards (2013) as:

$$\boldsymbol{JM}_{ij} = 2(1 - e^{-B_{ij}}) \tag{3.5}$$

in which

$$B_{ij} = \frac{1}{8}(\boldsymbol{m}_i - \boldsymbol{m}_j)^T(\frac{\boldsymbol{C}_i + \boldsymbol{C}_j}{2})^{-1}(\boldsymbol{m}_i - \boldsymbol{m}_j) + \frac{1}{2}\ln\left(\frac{|(\boldsymbol{C}_i + \boldsymbol{C}_j)/2|}{\sqrt{|\boldsymbol{C}_i| \times |\boldsymbol{C}_j|}}\right) \tag{3.6}$$

which is referred to as the *Bhattacharyya distance*. i and j are the two classes being compared. $\boldsymbol{C}_i$ is the covariance matrix of class i. $\boldsymbol{m}_i$ is the mean vector of class i.

3.2.2   Methods for generating synthetic hyperspectral data

When the sea bottom is measured through the water column, the resulting reflectance R can be considered to two partial reflectances R_b and R_∞. R_∞ is the reflectance of optically deep water, i.e., the depth is so large that bottom is no longer visible and R_b is bottom reflectance without water column. In extreme cases, $R = R_b$ when the depth is zero and $R = R_\infty$ when the depth reaches certain level. That level is dependent on the attenuation of light in water. It has been shown by Maritorena et al. (1994) that diffuse reflectance of shallow waters just below the water surface can be calculated using the equation

$$R(o-, z) = R_\infty + (R_b - R_\infty)exp(-2Kz) \tag{3.7}$$

where z is the water depth and K is the diffuse attenuation coefficient of the water. In order to simulate the bottom reflectance through the water column all variables are known, except the attenuation coefficient K. The coefficient K was obtained by measuring a white reference plate (Figure 3.2). The plate was set at a depth of 30 cm, and the reflectance was measured. Then the reflectance of the wet reference plate was measured again on board without the water column.
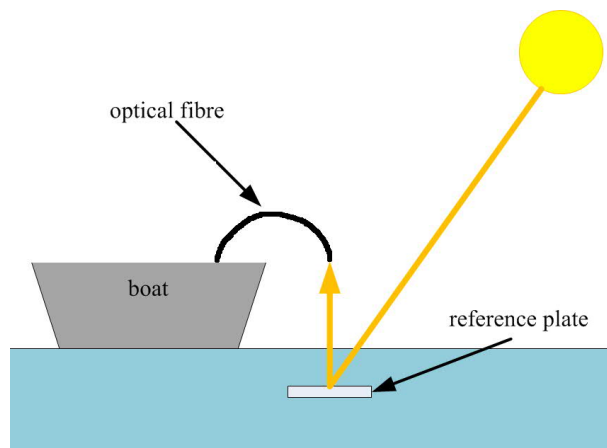

Figure 3.2: The arrangement of diffuse attenuation measurement

The coefficient K was solved using the equation

$$K = \frac{ln\frac{R-R_\infty}{R_b-R_\infty}}{-2z} \tag{3.8}$$

The simulation of benthic reflectance through water column using *in situ* field measurements is illustrated in Figure 3.3. The simulated water depth varies between 0.01 m and 3.0 m at 0.01 m intervals. Four different water type classes were used: Q1, Q2, Q3, and Q4, where Q1 represents the least turbid and Q4 the most turbid water. Classes are based on empirical spectral water quality measurements. The simulated data are calculated using Equation 3.9. The simulated spectrum R is calculated using deep water reflectance R and attenuation coefficient K corresponding to the simulated water type.

$$R(0-,z) = R_\infty + (R_b - R_\infty)\exp(-2Kz)$$
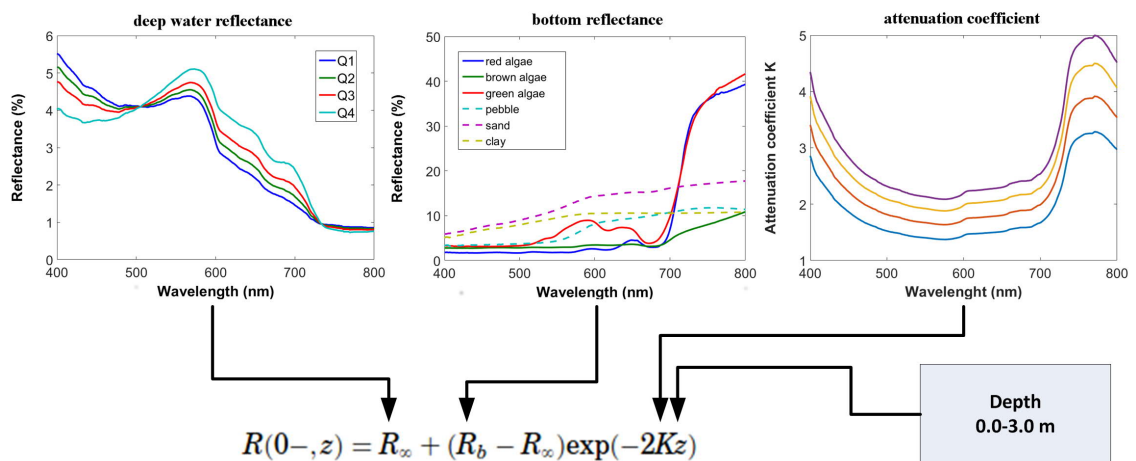
Figure 3.3: Simulation of bottom reflectance through water column

3.2.3 Methods for correction of unwanted effects

Correction for the optical effect of glass container

Reflectance measurements of water samples in glass container need a specific correction for the removal of the optical effect of the container (Figure 3.4). The radiance at water surface is dependent on the transmittance of glass. The correction coefficients were calculated using an empirical method where a white reference target was measured inside and outside the empty container. The number of wavelength channels is 2151 being constant throughout the work. Therefore, indexing of the channels has been omitted in the notation.
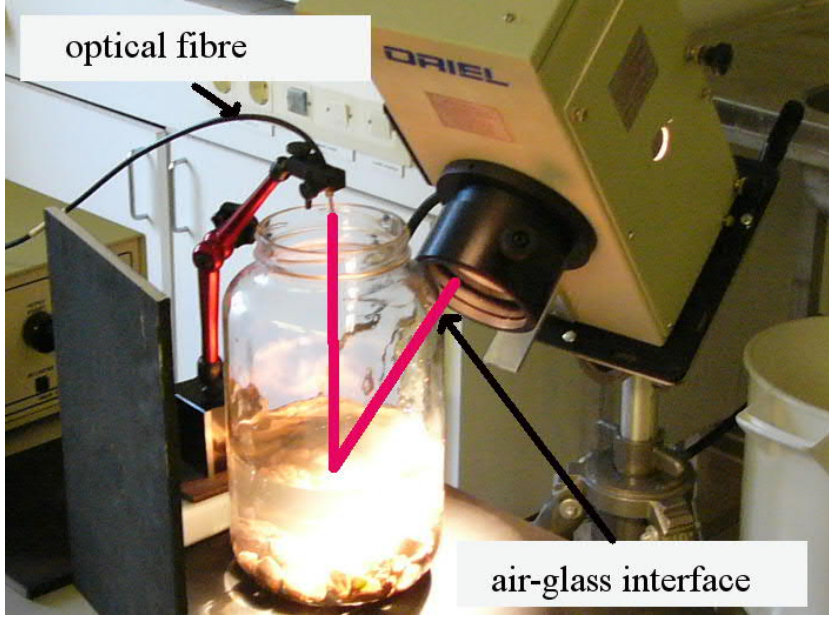
Figure 3.4: The arrangement of reflectance measurements of water samples

The measured reflectances are as follows:

T_p = Reflectance of the empty container

P_p = Reflectance of homogenous reference target in the same container

P_i = Reflectance of homogenous reference target outside the container

Denoting the apparent reflectance as A_{Tp} and the corrected reflectance as A_{Pi}, it follows:

$$A_{Tp} = c_1 \frac{P_p}{P_i} - c_2 \tag{3.9}$$

$$A_{Pi} = \frac{c_1 P_p}{T_p + c_2} \tag{3.10}$$

where $c_1 \approx 4.233$ and $c_2 \approx 3.994$. The constants c_1 and c_2 were estimated by minimizing the total sum of the absolute difference $A_{Tp} - T_p$. The optical effect of the glass container can be removed from the reflectance R_w of a water sample measured in that container using the following relation:

$$A_{Rw} = \frac{c_1 R_w}{T_p + c_2} \tag{3.11}$$

where A_{Rw} denotes the corrected reflectance.

Water column correction

Water column correction techniques are used for compensating the effects of variable water depths. In this thesis a simple water column correction method was tested in publications [P2] and [P4]. The advantage of the method is that it only requires one water quality measurement. The method does not assume any knowledge about the characteristics of the water column covering the underwater target. The correction is based on Equation 3.9, with water depth z taken to be half of the considered depth range (e.g., assuming water depth in the range of 0.0 m to 3.0 m, $z = 1.5$ was chosen) and water quality assumed to be water type $Q1$. This means that the optically deep water reflectance and the diffuse attenuation coefficient measured at site $Q1$ are used when a new reference spectrum is calculated. The use of water type $Q1$ helps to preserve more features of the reference spectra compared to more turbid waters. A new water column corrected reference spectrum for each benthic cover type was calculated using Equation 3.9 and used in the classification instead of the original measured spectra.

Sun glint correction

Sun glint, the specular reflection of light from water surfaces, is a serious confounding factor in remote sensing of water quality and benthos. Sun glint correction was used in publication [P2]. Kutser et al. (2009) proposed a method that utilizes the presence and depth of the oxygen absorption feature near 760 nm as an indicator of glint contamination. The method is based on two assumptions. First, it is assumed that there is no spectral absorption feature in the reflectance spectrum of natural waters at 760 nm if reflected light does not contain glint. Second, the depth of the oxygen absorption feature D at 760 nm is proportional to the amount of glint in the spectrum. In this thesis a modified version of the proposed method was used. In the original method it was assumed that pixels with D values close to zero do not contain glint and the pixels with the highest D value contain mainly glint. Remote sensing images can contain hundreds of thousands of pixels, and it is safe to assume that in this large set there exist pixels with no glint as well as pixels resulting mainly

from glint. However, in this study there are only 12 measured spectra that contain significant amounts of glint, and none of them contains mainly glint or is totally glint free. In sun glint correction it is assumed that the measured reflectance originates from both the reflectance of water and the reflectance due to sun glint. Therefore, if the depth D is proportional to the amount of glint, it is also proportional to the reflectance of water. It is not well established whether this proportion is linear or non-linear; however, linear correction seems to produce reasonable results.

Figure 3.5: Graphical representation of the sun glint correction method. The correction is illustrated at the wavelength of 440 nm. M1 through M3 represent the three measured spectra. For each spectrum the absorption depth D is calculated according to Equation 3.14. Then the regression Equation 3.15 is solved for each wavelength band, and the deglinted reflectance value at the corresponding wavelength is determined by the point where the regression line crosses the Y-axis ($D = 0$).

In our modified approach, the depth of the absorption feature was calculated to be

$$D = \frac{R_{750} + R_{780}}{2} - R_{764} \tag{3.12}$$

where D is the depth of the oxygen absorption feature and R_{750}, R_{764} and R_{780} are reflectances at these particular wavelengths. Three measurements of deep water reflectance were used to scale the relationship between the reflectance R and absorption depth D. For each band a linear regression was applied between R and D (Figure 3.5), using the equation

$$R = a \times D + b \tag{3.13}$$

The corrected value of R can be calculated by setting $D=0$

Chapter 4

Results and discussion

In this chapter the main results concerning assessment of water quality (more specifically, clay concentration), mapping of benthic cover and assessment of temporal and spatial variability of reed bed spectra are presented. All the mentioned applications deal with the analysis of hyperspectral field measurements in coastal areas. The results form the basis for successful interpretation of air- and spaceborne hyperspectral remote sensing data.

4.1 Hyperspectral assessment of clay concentration in water

The aim of this study was to compare the performance of widely used band-ratio measures with that of the Spectral Angle Mapper in water quality assessment applications. The question concerning the influence of the number of wavelength bands on the accuracy and robustness of the assessment results was also addressed. The difference of accuracy between SAM and band-ratio algorithms was insignificant, although in favor of proposed SAM. The initial question was: how many bands should be used in order to obtain best accuracy for retrieval algorithm. The result of the correlation test indicated that no more than five bands should be used. The basic problem in water quality retrieval applications is that when the measured property,

in this case clay concentration, stays the same, the quantity of other optically active substances can change, resulting in altered spectrum. The robustness of the algorithm to the presence of organic suspension was evaluated using simulated reflectance spectra representing water samples containing both clay and organic suspension.

The SAM algorithm outperforms band-ratio algorithms, but the differences are quite moderate. The RMS error of the SAM algorithm increases from 14.1 to 32.2 when the concentration of organic suspension increases (Table 4.1). Schalles et al. (2001) studied the influence of suspended clays on waters containing chlorophyll. The published spectra were quite similar in shape than measured in this study. The accuracy of the proposed SAM algorithm was better than that published by Gin et al. (2003), however, the number of samples was only 6 in our study. It can be expected that the accuracy decreases when the number of samples increases.

Table 4.1: RMSE values for the band-ratio and spectral angle algorithms calculated using varying percentage of organic suspension.

Organic suspension	0	10	20	30	40	50	%
RMSE Band-ratio	14.5	17.1	20.4	24.6	30.1	38.7	%
RMSE Spectral angle	14.1	14.8	17.4	20.8	25.3	32.2	%

Noise is a major problem in water quality applications, mainly because the the reflectance of water is low. Atmospheric and sun glint correction can also increase the noise present in spectrum. The robustness of the algorithms against noise was tested by adding random noise to the spectrum. The average RMSE for the spectral angle algorithm was about 10% smaller compared to the band-ratio algorithm (Table 4.2). This indicates the robustness of the spectral angle algorithm although the difference between the algorithms was quite small.

The proposed algorithm was tested using real hyperspectral data recorded during the HYPE08 campaign (Figure 4.1). The test site is located at Eurajoki strait in SouthWest Finland. Two rivers, Eurajoki and Lapinjoki, transport clay particles to the test area. The produced clay concentration map could not be validated due to lack of ground truth measurements, but the results are rational. In site A high clay

concentration is due to river Eurajoki whereas in site B it's due to river Lapinjoki.

Table 4.2: The relationship between the RMSE of the tested algorithms and signal to noise ratio (SNR) of hyperspectral data.

SNR	100	30	10	
RMSE Band-ratio	$1,61$	4.89	16.25	%
RMSE Spectral angle	1.45	4.41	14.6	%
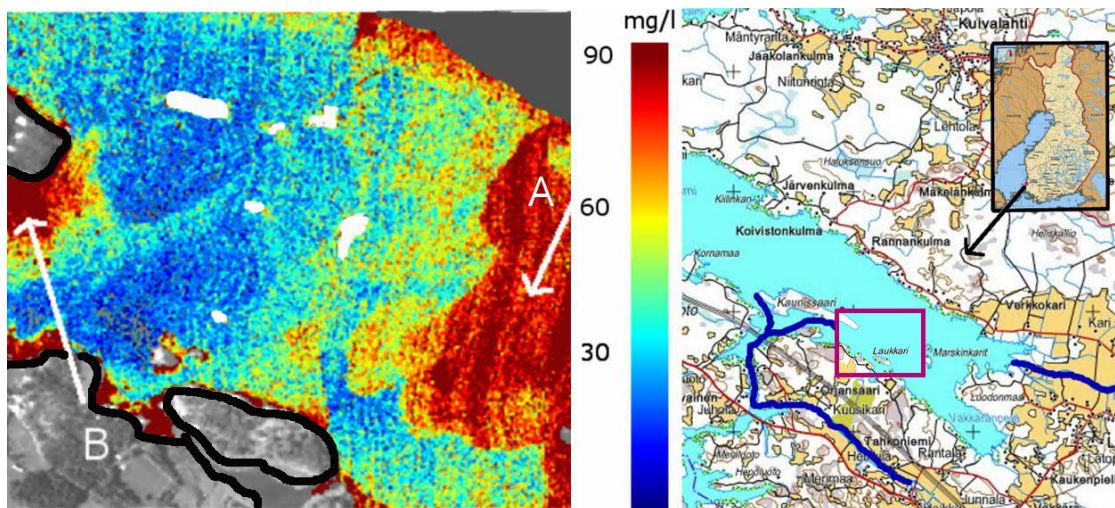
Figure 4.1: Clay concentration map of Eurajoki strait and the geographic location of the test site.

4.2 Hyperspectral classification of benthic cover type in turbid waters

Though several research papers exploring the possibilities of benthic cover type classification have been published, little emphasis has been given to comparison of the performance of the various spectral classification methods. In many cases the classification method is chosen without testing. In paper [P4] four different classification methods were tested with and without water column correction. The results showed

significant differences in mapping accuracy among the tested classification methods. The Spectral Correlation Mapper (SCM) clearly outperformed the others when water column correction was not in use. The mapping accuracy of 75% obtained by SCM is quite remarkable when compared to 41.4% of widely used Spectral Angle Mapper (SAM) method. One possible explanation is that SAM can not distinguish between positive and negative correlation and considers only the absolute value, whereas SCM eliminates negative correlation (Kumar et al., 2011). Best accuracy was obtained using the ED classification when water column correction is used. All classification methods except SCM seem to benefit from water column correction. When water column correction was applied the Euclidean Distance (ED) method produced best accuracy 84.5%. The differences between methods were lower than without water column correction. In the literature the best method varies depending on the application. Mapping methods like Spectral Angle Mapper, analysing the shape of the spectra, work better in the case of the forward modeled spectral library (Kutser et al., 2006). On the other hand, in some other benthic mapping applications Maximum Likelihood Classification (MLC) has produced best results (Casal et al., 2011).

In paper [P2] the feasibility of benthic cover type mapping in turbid waters near estuaries using hyperspectral remote sensing is studied. The major problem involved in remote sensing of submerged cover types is that the water column affects the signal received at the sensor depending on water depth and water quality. The influence of the water column is demonstrated in Figure 4.2. The measured spectra of red, green and brown algae are drawn using solid line and simulated spectra corresponding to 40 cm deep column of least turbid water (Q1) are drawn using dashed line. Features like local maxima are diminished and reflectance level is decreased especially in the Near Infra-Red (NIR) region. When the depth increases to certain level, the spectral features of the bottom substrate are no longer visible.

Results showed that water quality varies significantly within the studied area. The impact of this variation is clearly shown in the classification results. If the water quality is Q4 (most turbid) meaningful results can not be expected in benthic mapping applications. The classification accuracy is very much dependent on the cover type in question. Classification of sand gave poor results whereas algae species were detected
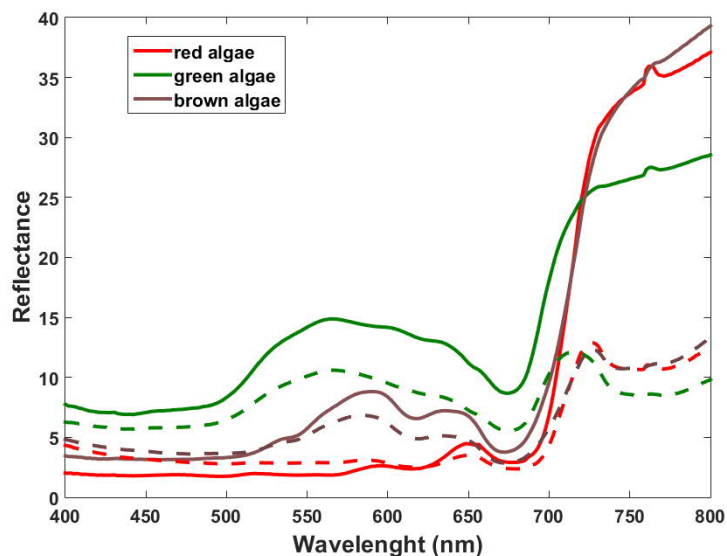
Figure 4.2: The spectra of red, green and brown algae. The simulated spectra of these three algae corresponding to 40 cm deep column of least turbid water (Q1) are drawn using dashed line

with greater certainty. This can be considered as a good thing, hence there are usually much more interest in submerged vegetation than sand bottoms. Some macroalgae species are used as an indicator of the ecological status of sea areas. The poor results of sand are most likely due to flat spectrum, there are no spectral features that could discriminate it from other substrates. The benthic mapping method can be considered operational when the discrimination accuracy of cover types exceeds 80%. The ED classifier together with simple water-column correction can almost fulfill this criterion up to depths of 2 m when water quality is Q1.

4.3 Assessment of temporal and spatial variability of reed bed spectra

The spatial and temporal variability of reed bed spectra was studied in paper [P3]. Seasonal time-series studies can provide important information on spectral variability. Given the dynamic character of vegetation cover, a snapshot in time is

not nearly as revealing as a time sequence (Goetz, 2009). Seasonal variability of the reflectance spectra of type 'old reed bed', i.e., reed bed where dead stems are present, is remarkable, when it is significantly smaller for type 'new reed bed', i.e., reed bed where only live stems are present. When the measured seasonal spectra were compared to those published in the literature, it was found that the shape of the spectra is quite similar at same phenological stages as published by Ouyang et al. (2013) and Artigas and Yang (2005). This applies for targets 1 and 2 representing old reed beds. On the other hand, it was found that the shape and reflectance level of target 3, representing 'new reed bed', spectra is surprisingly similar to that published by Gilmore et al. (2008) shown in Figure 4.3.
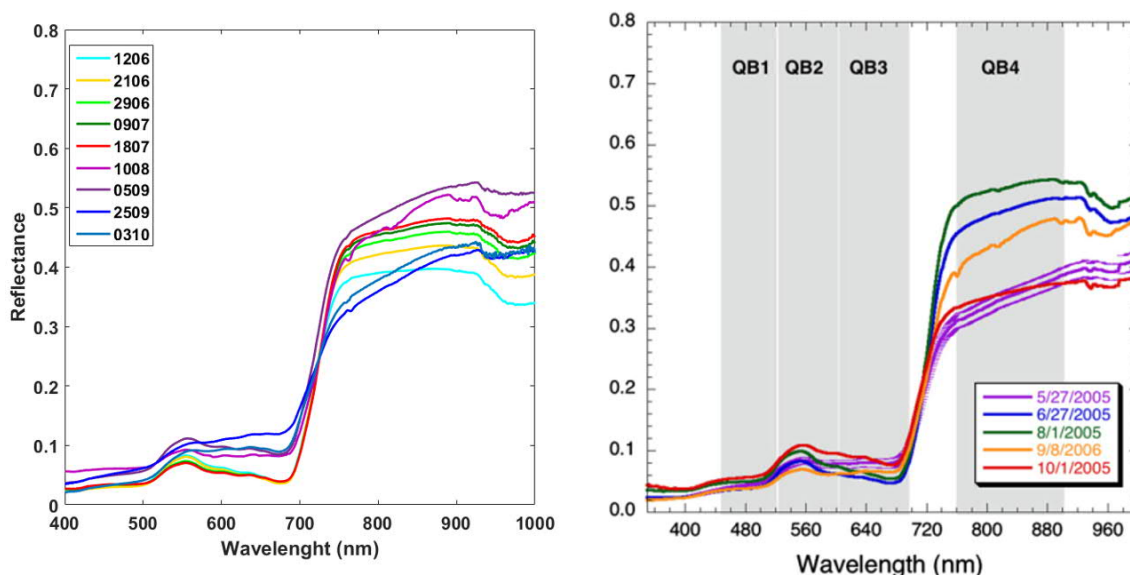
Figure 4.3: Seasonal reed bed spectra measured at target 3 at Hilskansaari and at Ragged Rock Creek, Connecticut River, U.S.A. by Gilmore et al. (2008)

In order to measure the separability of target and reference spectra, Euclidean Distance (ED), JeffriesMatusita distance (JM) and Spectral Angle Mapper (SAM) values were calculated between all targets and the moss spectra. When the seasonal separability values for targets 1, 2 and 3 were studied, it was found that optimal time window can be determined to discriminate the reed bed from surrounding vegetation, but the time is dependent on reed bed type and separability measure.

The vegetation type that most likely causes confusion in reed bed discrimination is meadows. The determination of the boundary between reed bed and meadow is difficult even in the field yet to mention remote sensing approaches. Meadows tends to have large spectral within-class variability, hence meadow class contains several species, i.e., grasses, weeds and flowers. Local variability of the vegetation and spectra were studied in a small neighborhood for assessing the feasibility of discriminating between the reed bed and the meadow. The mean reed bed and meadow spectra are rather similar both in shape and reflectance level. The best separability is achieved in the blue region of the visible part of spectrum. Separability values were calculated between the mean spectra of the classes and the spectra of each target (both reed bed and meadow) separately. 10 out of 11 targets had lower SAM value to the mean spectrum of the corresponding class than that of the other class. The results deteriorated when ED and JM-distance measures were used.
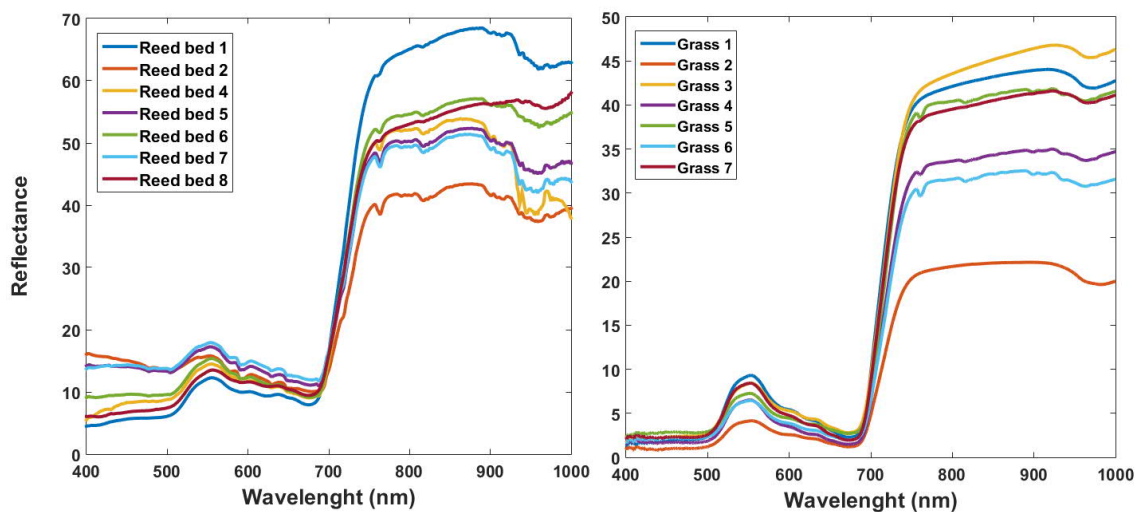
Figure 4.4: Within-class variability of Reed and Grass classes

The within-class variability of both classes was calculated and compared to a few references. The variability of reed (15.95) and meadow (24.62) was high compared to that of grass (8.86) and savannah trees (5.57). The within-class variability of reed and grass classes is demonstrated in Figure 4.4 by showing the spectra of both classes. For both classes one particular measurement is contributing to the within-class variability

more than others. Purely by chance it is measurement 2 in both cases. The within-class variability of grass is lower mainly because the variability is significantly lower in the blue region under 500 nm.

The spatial variability of reed bed spectra in Olkiluoto was studied using four reed bed sites. The results on within-class spectral variability of reed bed at four test sites within the Olkiluoto Island showed that while the reed spectra from the sites of Kornamaa and Munakari were close to each other, the spectra measured in Satama and Flutanperä differed significantly. This is at least partly due to the variation in the density and height of live and dead reed stems among the four sites. Field studies made in August 2012 showed that there is considerable variability in the ratio of live and dead stems. The fraction of dead stems varied from 0 to 83 in percentage.

Chapter 5

Conclusions

The thesis contributes to its scientific field by testing and developing methods for i) water quality monitoring ii) benthic mapping iii) wetlands mapping, and iv) atmospheric correction. As such, the thesis contributes to research related to airborne hyperspectral remote sensing and its applications to environmental monitoring and mapping in Finland or elsewhere where the conditions are similar.

The vast majority of the methods used in water quality retrieval are based on simple band ratio algorithms. Often only two bands are used. The results of P[1] show that the use of more bands can lead to better results. The accuracy of the proposed spectral angle algorithm was just slightly better compared to the band-ratio algorithm, but it is more robust against the effects of other optically detectable substances and noise. It can be concluded that there is a certain optimal number of bands to be used, in this case it was five. Results also emphasized the importance of local calibration of semi-empirical algorithms. The results obtained using locally calibrated algorithms were quite different from those obtained by algorithms calibrated elsewhere.

The results of [P4] showed that the selection of the classification method in benthic mapping has clear influence on classification accuracy reached. Results indicate that depending on the selected water column correction and modeling methods, benthic cover types can be discriminated either using a classifier based on spectral shape or distance measures. The SCM classifier is rarely, if ever, used in benthic mapping

applications. It might not outperform other classifiers in every case, but it is certainly worth trying. The benthic mapping method can be considered operational when the discrimination accuracy of cover types exceeds 80 %. The ED classifier together with simple water column correction can almost fulfill this criterion up to depths of 2 m when water quality is least turbid in the test area. When turbidity increases, depths slightly less than 1 m could be mapped with reasonable accuracy. It can be concluded that the hyperspectral remote sensing of benthic cover types is limited to rather shallow areas. The used test method has some limitations; it does not account for correction errors related to real images or within-species variability of benthic cover types. Even though the results showed quite limited operability of the hyperspectral benthic mapping, it should not be rejected without further research. The tested methods were quite simple. The use of the state of the art methodology such as simultaneous water quality and depth retrieval, spectrum matching and look-up-tables could increase the feasible depth range considerably.

The temporal variability of reed bed spectra was found to be significant. The main challenge related to temporal variability is that there are two different types of reed beds having different seasonal spectra. The optimal time of data acquisition depends on the reed bed type. Careful timing of the data acquisition is needed. The spectral within-class variability of both reed bed and meadow in local neighborhood was found to be large when compared to references. Both classes have similar mean spectra, however, 10 out of 11 targets had lower Spectral Angle Value to the mean spectrum of the corresponding class than that of the other class.This gives a positive indication for successful reed bed mapping. The results on within-class spectral variability of reed bed at four test sites within the Olkiluoto Island showed that while the reed spectra from the sites of Kornamaa and Munakari were close to each other, the spectra measured in Satama and Flutanperä differed significantly. This is at least partly due to the variation in the density and height of live and dead reed stems among the four sites. It can be concluded that if features such as reed characteristics, temporal variation and surrounding habitats are known and can be controlled, mapping of reed beds is feasible based on their spectral properties; otherwise LiDAR data or textural features would be needed.

Hybrid atmospheric correction methods are rarely seen in scientific literature. The overall conclusion of [P5] is that the accuracy of atmospheric correction can be increased by using combined methods rather than a model based method alone. Even in situations where the number of spectral ground truth measurements is limited, the proposed method can improve atmospheric correction accuracy over the whole acquisition area. The improvement is shown especially in certain wavelength regions which are $(950\ldots1100$ nm) and $(2300\ldots2500$ nm).

Chapter 6

Overview of Publications

In this chapter a brief overview of the publications is given, emphasizing the new contribution of each publication.

6.1 Water quality monitoring [P1]

Clay induced turbidity is the major cause of complex changes in the ecosystem of coastal water areas. The motivation of publication [P1] was to develop an accurate and robust algorithm for the clay concentration retrieval using high spectral resolution hyperspectral data. The study was based on controlled experiment and spectral laboratory measurements. The accuracy of the proposed spectral angle algorithm was just slightly better compared to the band ratio algorithm, but it is more robust against the effects of other optically active substances and noise. Spectral angle mapper (SAM) method is widely used in remote sensing applications, yet it is not proposed for water quality retrieval in literature before this publication.

6.2 Benthic mapping [P2] [P4]

The information on the underwater marine environment is needed both for the planning of nature conservation and for the exploitation of natural resources. The motivation of publications [P2] and [P4] was to estimate the feasibility of hyperspec-

tral remote sensing in benthic mapping at the coastal areas of Finland. In publication [P4] four different classification methods were tested using simulated data and spectral *in situ* measurements. The influence of water column correction was evaluated as well. The results showed significant differences in mapping accuracy among the tested classification methods. The motivation of [P2] was to study the effects of water depth and water quality on benthic cover type classification. The overall mapping accuracy of SCM classification without water column correction reached 47.8 % when the depth range 0.0-3.0 m was studied. The mapping accuracy increased to 66.0 % using the ED classifier with water column correction. The majority of research papers addressing remote sensing of benthic cover types concentrate on optically clear, shallow coastal and reef waters. A few comprehensive research papers exploring the feasibility of benthic mapping in the Baltic Sea using remote sensing have been published. In these two papers the hyperspectral benthic mapping in coastal Finland is addressed first time in literature.

6.3   Wetlands mapping [P3]

Common reed (*Phragmites Australis*) has significantly spread on the Finnish coast during the last decades. Reed beds are the second largest producer of biomass in Olkiluoto Island. Quantitative information on the extent and amount of reed stands is an integral part of the biosphere assessment related to long-term safety analysis of nuclear fuel repository site currently under construction. Spectral field measurements were used to study the temporal and spatial variability of spectral characteristics of reed beds. It can be concluded that if features such as reed characteristics, temporal variation and surrounding habitats are known and can be controlled, mapping of reed beds is feasible based on their spectral properties; otherwise LiDAR data or textural features would be needed. Time-series analysis of reed bed spectra in North America and China have been publish, yet this is the first publication presenting results measured in Europe, specifically in Finland. The analysis of local spatial variability is a new contribution to the field as well.

6.4 Atmospheric Correction [P5]

One of the major drawbacks of hyperspectral imaging is the need for complicated correction procedures. Atmospheric correction can be very challenging, especially in marine environment. The proposed method has two phases. In the first phase the hyperspectral radiance data is corrected using the model-based ATCOR 4 software followed by the second phase where the modeled reflectance data is corrected using the Empirical-Line (EL) method. The average RMSE error of the PIF targets was 6.8 % when the reflectance was derived using the ATCOR 4 software. The average RMSE error decreased to 1.8 % when the reflectance was derived using the proposed combined method. Combined methods in atmospheric correction are rarely proposed in the literature, yet the proposed method is not exactly a new one. The new contribution of this paper is the use of Empirical-Line method on large geographic area using only a two measurements of reference targets. The relationship between on-board radiance and reflectance changes as a function of time. The acquisition of the study are took several hours, yet only two measurements was enough to increase the accuracy of model based method.

Bibliography

Adam, E., Mutanga, O., and Rugege, D. (2010). Multispectral and hyperspectral remote sensing for identification and mapping of wetland vegetation: a review. *Wetlands Ecology and Management*, 18(3):281–296.

Adler-Golden, S. M. and Acharya, P. K. (2005). Remote bathymetry of the littoral zone from AVIRIS, LASH, and QuickBird imagery. *IEEE Transactions on Geoscience and Remote Sensing*, 43(2):337–347.

Armstrong, R., Guild, L., Gilbes, F., Lobitz, B., and Detres, Y. (2007). Water column corrections of AVIRIS data for hyperspectral characterization of benthic marine communities in Puerto Rico. In *In proceedings of 5th EARSeL workshop on imaging spectroscopy*, Bruges, Belgium.

Artigas, F. and Yang, J. (2005). Hyperspectral remote sensing of marsh species and plant vigour gradient in the New Jersey Meadowlands. *International Journal of Remote Sensing*, 26(23):5209–5220.

Ben-Dor, E., Kindel, B., and Goetz, A. F. H. (2004). Quality assessment of several methods to recover surface reflectance using synthetic imaging spectroscopy data. *Remote Sensing of Environment*, 90(3):389–404.

Berger, R., Bergström, L., Graneli, E., and Kautsky, L. (2004). How does eutrophication affect different life stages of Fucus vesiculosus in the Baltic Sea? – a conceptual model. *Hydrobiologia*, 514:243–248.

Berk, A., Bernstein, L., and Robertson, D. (1989). MODTRAN: A Moderate Resolution Model for LOWTRAN7," Rpt. No. GL-TR-89-0122. Technical report, Air Force Geophysical Laboratory, Bedford, MA.

Bhatti, A., Schalles, J., Rundquist, D., and Ramirez, L. (2010). Application of hyperspectral remotely sensed data for water quality monitoring: accuracy and limitation. In *Accuracy 2010 Symposium*, pages 349–352, Leicester, UK.

Broadman, J. (1998). Post-ATREM polishing of AVIRIS apparent reflec- tance data using EFFORT: A lesson in accuracy versus precision. In *Summaries of the seventh JPL airborne earth science workshop*, page 53, Pasadena, California.

Brook, A. and Ben-Dor, E. (2011). Supervised vicarious calibration (SVC) of hyperspectral remote-sensing data. *Remote Sensing of Environment*, 115(6):1543–1555.

Carvalho, O. and Meneses, P. (2000). Spectral Correlation Mapper (SCM): An improvement on the Spectral Angle Mapper (SAM). In *Summaries of the 9th Airborne Earth Science Workshop*, Pasadena, California. Jet Propulsion laboratory.

Casal, G., Kutser, T., Domínguez-Gómez, J., Sánchez-Carnero, N., and Freire, J. (2011). Mapping benthic macroalgal communities in the coastal zone using CHRIS-PROBA mode 2 images. *Estuarine, Coastal and Shelf Science*, 94(3):281–290.

Chang, C.-i. (2000). An Information-Theoretic Approach to Spectral Variability, Similarity, and Discrimination for Hyperspectral Image Analysis. *IEEE Transactions on Geoscience and Remote Sensing*, 46(5):1927–1932.

Cho, M. A., Debba, P., Mathieu, R., Naidoo, L., Aardt, J. V., and Asner, G. P. (2010). Improving Discrimination of Savanna Tree Species Through a Multiple-Endmember Spectral Angle Mapper Approach : Canopy-Level Analysis. *IEEE Transactions on Geoscience and Remote Sensing*, 48(11):4133–4142.

Clark, R. (1999). Spectroscopy of Rocks and Minerals, and Principles of Spectroscopy. In Rencz, A., editor, *Manual of Remote Sensing*, pages 3–58. John Wiley and Sons, New York.

Clark, R., Swayze, G., Heidebrecht, K., Goetz, A., and Green, R. (1993). Comparison of methods for calibrating AVIRIS data to ground reflectance. In *Proceedings of the fourth annual JPL airborne geoscience workshop*, pages 35–36, Pasadena, California.

de Leeuw, J., Georgiadou, Y., Kerle, N., de Gier, A., Inoue, Y., Ferwerda, J., Smies, M., and Narantuya, D. (2010). The Function of Remote Sensing in Support of Environmental Policy. *Remote Sensing*, 2(7):1731–1750.

Dekker, A., Brando, E., Anstee, J., Pinnel, N., Kutset, T., Hoogenboom, H., Pasterkamp, R., Peters, S., Vos, J., Olbert, C., and Malthus, T. (2011). Imaging spectrometry of water. In *Imaging Spectrometry: Basic Principles and Prospective Applications*, pages 307–359. Kluwer, Dordrecht.

Dennison, W. (1987). Effects of light on seagrass photosynthesis, growth and depth distribution. *Remote Sensing of Environment*, 27(1):15–26.

Dennison, W. C., Orth, R. J., Moore, K. A., Stevenson, J. C., Carter, V., Kollar, S., Bergstrom, P. W., Batiuk, R. A., Dennison, W. C., Orth, R. J., Moore, K. A., Stevenson, J. C., Carter, V., Kollar, S., Bergstrom, P. W., and Batiuk, R. A. (1993). Assessing Water Quality with Submersed Aquatic Vegetation Habitat requirements as barometers of Chesapeake Bay health. *BioScience*, 43(2):86–94.

Fraser, R. (1998). Hyperspectral remote sensing of turbidity and chlorophyll a among Nebraska Sand Hills lakes. *International Journal of Remote Sensing*, 19(8):1579–1589.

Gao, B. C., Montes, M. J., Ahmad, Z., and Davis, C. O. (2000). Atmospheric correction algorithm for hyperspectral remote sensing of ocean color from space. *Applied optics*, 39(6):887–896.

Gao, B.-C., Montes, M. J., Davis, C. O., and Goetz, A. F. H. (2009). Atmospheric correction algorithms for hyperspectral remote sensing data of land and ocean. *Remote Sensing of Environment*, 113(S1):S17—-S24.

Gilmore, M. S., Wilson, E. H., Barrett, N., Civco, D. L., Prisloe, S., Hurd, J. D., and Chadwick, C. (2008). Integrating multi-temporal spectral and structural information to map wetland vegetation in a lower Connecticut River tidal marsh. *Remote Sensing of Environment*, 112(11):4048–4060.

Gin, K., Koh, S., and Lin, I. (2002). Study of the effects of suspended marine clay on the reflectance spectra of phytoplakton. *International Journal of Remote Sensing*, 23(11):2163–2178.

Gin, K., Koh, S., and Lin, I. (2003). Spectral irradiance profiles of suspended marine clay for the estimation of suspended sediment concentration in tropical waters. *International Journal of Remote Sensing*, 24(16):3235–3245.

Goetz, A., Heidebrecht, K., Kindel, B., and Broadman, J. (1998). Using ground spectral irradiance for model correction of AVIRIS data. In *Summaries of the Seventh JPL Airborne Earth Science WorkshopJPL Publication*, pages 159–168, Pasadena, California.

Goetz, A., Vane, G., Solomon, J., and Rock, B. (1985). Imaging spectrometry for Earth remote sensing. *Science*, 228:1147–1153.

Goetz, A. F. H. (2009). Three decades of hyperspectral remote sensing of the Earth: A personal view. *Remote Sensing of Environment*, 113(S1):S5—-S16.

Green, E., Mumby, P., Clark, C., and Edwards, T. (2000). *Remote sensing handbook for tropical coastal management*. UNESCO Publishing, Paris.

Holden, H. and LeDrew, E. (2001). Effects of the water column on hyperspectral reflectance of submerged coral reef features. *Bulletin of Marine Science*, 69(2):685–699.

Hunter, P. D., Gilvear, D. J., Tyler, a. N., Willby, N. J., and Kelly, A. (2010). Mapping macrophytic vegetation in shallow lakes using the Compact Airborne Spectrographic Imager (CASI). *Aquatic Conservation: Marine and Freshwater Ecosystems*, 20:717–727.

Kallasvuo, M. (2010). *Coastal environmental gradients – Key to reproduction habitat mapping of freshwater fish in the Baltic Sea*. University of Helsinki, Helsinki.

Kamal, M. and Phinn, S. (2011). Hyperspectral Data for Mangrove Species Mapping : A Comparison of Pixel-Based and Object-Based Approach. *Remote Sensing*, 3(10):2222–2242.

Karpouzli, E., Malthus, T., Place, C., Chui, A. M., Garcia, M. I., and Mair, J. (2003). Underwater light characterisation for correction of remotely sensed images. *International Journal of Remote Sensing*, 24(13):2683–2702.

Kerr, J. T. and Ostrovsky, M. (2003). From space to species: ecological applications for remote sensing. *Trends in Ecology & Evolution*, 18(6):299–305.

Kobryn, H. T., Wouters, K., Beckley, L. E., and Heege, T. (2013). Ningaloo Reef: Shallow Marine Habitats Mapped Using a Hyperspectral Sensor. *PLoS ONE*, 8(7):1–22.

Koponen, S. (2006). *Remote sensing of water quality for Finnish lakes and coastal areas* . Helsinki University of Technology, Espoo.

Kruse, F., Lefkoff, A., Boardman, J., Heidebrecht, K., Shapiro, A., Barloon, P., and Goetz, A. (1993). The spectral image processing system (SIPS)—interactive visualization and analysis of imaging spectrometer data. *Remote Sensing of Environment*, 44(2-3):145–163.

Kumar, M., Seshasai, M. V. R., Vara Prasad, K. S., Kamala, V., Ramana, K. V., Dwivedi, R. S., and Roy, P. S. (2011). A new hybrid spectral similarity measure for discrimination among Vigna species. *International Journal of Remote Sensing*, 32(14):4041–4053.

Kutser, T., Kotta, J., Vahtmäe, E., Pärnoja, M., Möller, T., and Lennuk, L. (2011). Using high spatial resolution remote sensing, spatial modelling and web map services for spatial planning is shallow coastal water environments. In *In proceedings of 34th International Symposium on Remote Sensing of Environment*, Sydney, Australia.

Kutser, T., Miller, I., and Jupp, D. L. B. (2006). Mapping coral reef benthic substrates using hyperspectral space-borne images and spectral libraries. *Estuarine, Coastal and Shelf Science*, 70(3):449–460.

Kutser, T., Vahtmäe, E., and Praks, J. (2009). A sun glint correction method for hyperspectral imagery containing areas with non-negligible water leaving NIR signal. *Remote Sensing of Environment*, 113(10):2267–2274.

Lyzenga, D. (1978). Passive remote sensing techniques for mapping water depth and bottom features. *Applied Optics*, 17(3):379–383.

MacDonald, J. S., Ustin, S. L., and Schaepman, M. E. (2009). The contributions of Dr. Alexander F.H. Goetz to imaging spectrometry. *Remote Sensing of Environment*, 113(s1):S2—-S4.

Mäkisara, K., Meinander, M., Rantasuo, M., Okkonen, J., Aikio, M., and Sipola, K. (1993). Airborne Imaging Spectrometer for Applications (AISA). In *Geoscience and Remote Sensing Symposium (IGARSS)*, pages 479–481, Tokyo.

Maritorena, S., Morel, A., and Gentili, B. (1994). Diffuse reflectance of oceanic shallow waters: influence of water depth and bottom albedo. *Limnology and Oceanography*, 39(7):1689–1703.

Matsunaga, T., Iwasaki, A., Tsuchida, S., Tanii, J., Kashimura, O., Yamamoto, H., and Rokugawa, S. (2013). Current Status of Hyperspectral Imager Suite (HISUI). In *IGARSS 2013 IEEE International Geoscience and Remote Sensing Symposium*, pages 3510–3513, Melbourne.

Milton, E. (1987). Principles of field spectroscopy. *International Journal of Remote Sensing*, 8(12):1807–1827.

Milton, E. J., Schaepman, M. E., Anderson, K., Kneubühler, M., and Fox, N. (2009). Progress in field spectroscopy. *Remote Sensing of Environment*, 113(s1):S92—-S109.

Mishra, D. R., Narumalani, S., Rundquist, D., Lawson, M., and Perk, R. (2007). Enhancing the detection and classification of coral reef and associated benthic habitats: A hyperspectral remote sensing approach. *Journal of Geophysical Research*, 112(C8):C08014.

Mobley, C. (1994). *Light and Water: Radiative Tranfer in Natural Waters* . Academic Press, San Diego.

Mobley, C. D., Sundman, L. K., Davis, C. O., Bowles, J. H., Downes, T. V., Leathers, R. a., Montes, M. J., Bissett, W. P., Kohler, D. D. R., Reid, R. P., Louchard, E. M., and Gleason, A. (2005). Interpretation of hyperspectral remote-sensing imagery by spectrum matching and look-up tables. *Applied optics*, 44(17):3576–3592.

Morel, A. and Prieur, L. (1977). Analysis of variations in ocean color. *Limnology and Oceanography*, 22:709–722.

Mumby, P., Green, E., Edwards, A., and Clark, C. (1999). The cost effectiveness of remote sensing for tropical coastal resources assessment and management. *Journal of Environmental Management*, 55(3):157–166.

Mumby, P. J., Clark, C. D., Green, E. P., and Edwards, a. J. (1998). Benefits of water column correction and contextual editing for mapping coral reefs. *International Journal of Remote Sensing*, 19(1):203–210.

Nakashima, B., Borstad, G., Hill, D., and Kerr, R. (1989). Remote Sensing of Fish Schools: Early Results from a Digital Imaging Spectrometer. In *12th Canadian Symposium on Remote Sensing*, pages 2044–2047.

Ortenberg, F. (2011). Hyperspectral Sensor Characteristics. In Thenkabail, Prasad S.; Lyon, John G.; Huete, A., editor, *Hyperspectral Remote Sensing of Vegetation*, pages 39–69. CRC Press, New York.

Ouyang, Z. T., Gao, Y., Xie, X., Guo, H. Q., Zhang, T. T., and Zhao, B. (2013). Spectral Discrimination of the Invasive Plant Spartina alterniflora at Multiple Phenological Stages in a Saltmarsh Wetland. *PLoS ONE*, 8(6):1–12.

Pabich, P. (2002). *Hyperspectral imagery: warfighting through a different set of eyes.* Air University USAF, Maxwell Alabama.

Pan, Z., Glennie, C. L., Legleiter, C. J., and Overstreet, B. T. (2015). Estimation of Water Depths and Turbidity from Hyperspectral Imagery Using Support Vector Regression. *Submitted to IEEE Geoscience and Remote Sensing Letters*, 12(10):2165–2169.

Pegau, W. S., Cleveland, J. S., Doss, W., Kennedy, C. D., Maffione, R. A., Mueller, J. L., Stone, R., Trees, C. C., Weidemann, A. D., Wells, W. H., and Zaneveld, J. R. V. (1995). A comparison of methods for the measurement of the absorption coefficient in natural waters attenuation coefficient and chlorophyll a fluorescence profiles) were. *Journal of Geophysical Research*, 100(C7):13201–13220.

Pere, T., Aro, L., and Tuohimaa, M. (2015). Results of Monitoring at Olkiluoto in 2013 Environment. Technical report, Posiva Ltd, Eurajoki.

Phinn, S. R., Dekker, a. G., Brando, V. E., and Roelfsema, C. M. (2005). Mapping water quality and substrate cover in optically complex coastal and reef waters: an integrated approach. *Marine pollution bulletin*, 51(1-4):459–469.

Rees, W. (2001). *Physical Principles of Remote Sensing.* Cambridge University Press, Cambridge, 2 nd edition.

Reinart, A. and Kutser, T. (2006). Comparison of different satellite sensors in detecting cyanobacterial bloom events in the Baltic Sea. *Remote Sensing of Environment*, 102(1-2):74–85.

Richards, J. (2013). *Remote Sensing Digital Image Analysis.* Springer, Heidelberg.

Richter, R. (1996). Atmospheric correction of DAIS hyperspectral image data. *Computers and Geosciences*, 22:785–793.

Schaepman, M. (2007). Spectrodirectional remote sensing: From pixels to processes. *International Journal of Applied Earth Observation and Geoinformation*, 9:204–223.

Schalles, J. (2006). Optical remote sensing techniques to estimate phytoplakton chlorophyll a concentrations in coastal waters with varying suspended matter and cdom concentrations. In Richardson, L. and LeDrew, E., editors, *Remote Sensing of Aquatic Coastal Ecosystem Processes*, pages 27–79. Springer-Verlag, Dordrecht.

Schalles, J., Rundquist, D., and Schiebe, F. (2001). The influence of suspended clays on phytoplankton reflectance signatures and the remote sensing of chlorophyll. *Vehr. Intern. Verein. Limnol.*, 27:3619–3625.

Schmidt, K. and Skidmore, A. (2003). Spectral discrimination of vegetation types in a coastal wetland. *Remote Sensing of Environment*, 85(1):92–108.

Shippert, M. (2004). Why use hyperspectral imagery. *Photogrammetric Engineering and Remote Sensing*, (April):377–379.

Spitzer, D. and Dirks, R. (1987). Bottom influence on the reflectance of the sea. *International Journal of Remote Sensing*, 8(3):279–290.

Sterckx, S. and Debruyn, W. (2004). A hyperspectral view of the North Sea. In *Proceedings of the Airborne Imaging Spectroscopy Workshop*, Bruges, Belgium.

Tassan, S. (1996). Modified Lyzenga's method for macroalgae detection in water with non-uniform composition. *International Journal of Remote Sensing*, 17(8):1601–1607.

Tulldahl, M., Philipson, P., and Tolt, G. (2011). Sea Floor Classification with WorldView-2 and Bathymetry Data. In *Proceedings of the 34th International Symposium on Remote Sensing of Environment*, Sydney, Australia.

Tuominen, J. and Lipping, T. (2011). Detection of Environmental Change Using Hyperspectral Remote Sensing at Olkiluoto Repository Site. Technical report, Posiva Oy.

Vahtmäe, E. (2009). *Mapping benthic habitat with remote sensing in optically complex coastal environments.* Tartu University Press, Tartu.

Vahtmäe, E. and Kutser, T. (2007). Mapping of bottom type and water depth in shallow coastal waters with satellite remote sensing. *Journal of Coastal Research*, SI50:185–189.

Vahtmäe, E., Kutser, T., Martin, G., and Kotta, J. (2006). Feasibility of hyperspectral remote sensing for mapping benthic macroalgal cover in turbid coastal waters—a Baltic Sea case study. *Remote Sensing of Environment*, 101(3):342–351.

Vane, G., Goetz, A., and Wellman, J. (1984). Airborne Imaging Spectrometer: A New Tool for Remote Sensing. *IEEE Transactions on Geoscience and Remote SensingIEEE*, GE-22(6):546–549.

Wang, C., Menenti, M., Stoll, M.-p., Belluco, E., and Marani, M. (2007). Mapping mixed vegetation communities in salt marshes using airborne spectral data. *Remote Sensing of Environment*, 107(4):559–570.

Werdell, J. and Roesler, C. (2003). Remote assessment of benthic substrate composition in shallow waters using multispectral reflectance. *Limnology and Oceanography*, 48(1):557–567.

Wolter, P., Johnston, C., and Niemi, G. (2005). Mapping submerged aquatic vegetation in the US Great Lakes using Quickbird satellite data. *International Journal of Remote Sensing*, 26(23):5255–5274.

Xu, J., Zhang, B., Li, F., Song, K., Wang, Z., Liu, D., and Zhang, G. (2009). Retrieval of total suspended matters using field spectral data in Shitoukoumen Reservoir, Jilin Province, Northeast China. *Chinese Geographical Science*, 19(1):77–82.

Yu, Q., Tian, Y. Q., Chen, R. F., Liu, A., Gardner, G. B., and Zhu, W. (2010). Functional Linear Analysis of in situ Hyperspectral Data for Assessing CDOM in Rivers. *Photogrammetric Engineering and Remote Sensing*, 76(10):1147–1158.

Zoffoli, M., Frouin, R., and Kampel, M. (2014). Water Column Correction for Coral Reef Studies by Remote Sensing. *Sensors*, 14(9):16881–16931.

Zomer, R. J., Trabucco, A., and Ustin, S. L. (2009). Building spectral libraries for wetlands land cover classification and hyperspectral remote sensing. *Journal of Environmental Management*, 90(7):2170–2177.

Chapter 7

Publication P1

HYPERSPECTRAL DETECTION OF MARINE CLAY IN COASTAL WATERS USING THE SPECTRAL ANGLE METHOD

Jyrki Tuominen[1], Tarmo Lipping[1], Viljo Kuosmanen[2], and Sari Repka[3]

1. Tampere University of Technology, Signal Processing, Pori, Finland;
   {jyrki.tuominen / tarmo.lipping}(at)tut.fi
2. Geological Survey of Finland, Remote Sensing, Espoo, Finland;
   viljo.kuosmanen(at)gtk.fi
3. University of Turku, Marine Biology, Pori, Finland; sari.repka(at)utu.fi

ABSTRACT

Clay induced turbidity is the major cause of complex changes in the ecosystem of coastal water areas. The accuracy of the algorithms for the assessment of the clay concentration may suffer significantly from the presence of other substances like Algal chlorophyll or dissolved organic matter, highly influencing the optical properties of the water. The objective of this study was to develop an accurate and robust algorithm for the clay concentration retrieval using high spectral resolution hyperspectral data. In order to provide necessary information for the spectral analysis of the water samples, a controlled experiment was arranged. Carefully weighted clay portions were diluted in water and reflectance spectra were recorded using a field spectrometer. Traditionally simple algorithms are used to estimate the remotely sensed water quality variables. In this paper a novel algorithm based on the principle of spectral angle measure is presented. The accuracy of the proposed algorithm was just slightly better compared to the band-ratio algorithm, but it is more robust against the effects of other optically detectable substances and noise.

INTRODUCTION

Increasing water turbidity is one of the human-induced environmental changes in coastal areas. Human activity causes both organic (algal) and non-organic (clay) turbidity to rise in aquatic environments. Rivers and brooks transport clay particles to coastal waters from agricultural land; and other human activities such as landfill activities, dredging, gravel take, ships turbines, building etc. may cause non-organic turbidity to rise (1). The effects of increasing organic turbidity on the ecosystem and biochemical cycles are complex. Especially the underwater biological diversity may be harmed by increasing turbidity, e.g., *Fucus vesiculosus* is sensitive to the turbidity (2). It may also be possible that clay turbidity influences the phytoplankton community structure. The planktonic food web may change due to the increasing turbidity (3). Organic particles (alive or dead) enter the food web either by grazing or via decomposition by micro-organisms. Clay particles cannot provide energy to the grazers or bacteria. They may, however, contain nutrients and trace-elements that can be utilised by phytoplankton or bacteria (4). In lakes, the clay-turbidity has been shown to have serious effects on the food web and to prevent the improvement of the lake condition due to the restoration methods (5). These effects can be assumed to take place in coastal marine environments as well.

Information revealing the environmental effects of the non-organic turbidity in coastal areas is badly needed by the environmental administration for the Environmental Impact Analysis of projects that will increase the clay induced turbidity. Remote sensing has already demonstrated its ability to provide water quality relevant data. Excellent work has been performed to extract the essential water quality parameters such as chlorophyll content, turbidity and the total amount of suspended matter (6,7,8). Yet, it appears that there is no standard algorithm for the estimation of suspended sediments in coastal waters (9). From the remote sensing perspective, the water environment can be divided into two categories: Case 1 and Case 2. Case 1 refers to phytoplankton dominated waters (e.g. open oceans) whereas case 2 refers to coastal waters which contain re-suspended sediments, terrigenous particles and dissolved organic matter (yellow substances) (10). Remote sensing in the coastal zone has generally been far less successful than in other areas, such as open oceans or

terrestrial environment (11). This is mainly due to complex interactions of the three optically detectable substances: algal chlorophyll, suspended sediments and dissolved organic substances. These substances have significant impact on the water quality. Each substance has its own reflectance and absorption trends complicating the derivation of the clay concentration estimation algorithms based on the remotely sensed data.

Several studies have been conducted to address the impact of the suspended sediments on the spectral signature of the surface waters (12,13,14,15). Researchers have usually addressed the general trends in the spectral responses of water samples with varying concentrations of organic and inorganic suspension. Quibell (1992) showed that the addition of the particulates generally increases the reflectance at the wavelengths longer than 550nm (16). Gin et al. (2003) proposed a band ratio algorithm R_{595}/R_{754} for the estimation of the marine clay concentration. The algorithm produced rather good results with the coefficient of determination r^2 varying from 0.53 to 0.86 according to the particle size of the marine clay.

Case 2 water quality retrieval algorithms traditionally use simple band-ratio or band- difference techniques. However, promising techniques utilising more information have been introduced in recent years. Gitelson et al. (2008) presented a three-band NIR-Red algorithm producing excellent results in chlorophyll-a concentration retrieval in turbid case 2 waters (17). Cococcioni et al. (2004) presented an approach to case 2 water quality retrieval based on the use of fuzzy logic (18). The proposed method produced promising results for the estimation of concentrations of optically active constituents of case 2 seawater. Doerffer & Schiller (2007) proposed the use of neural network in order to overcome the problems related to the complex nature of case 2 waters in water quality retrieval (19).

It is quite likely that the derivation of a general algorithm for the clay concentration estimation to be used globally is not feasible. This is mainly due to the different clay types and different particle sizes. In addition, the concentrations of the other optically detectable substances than clay vary too much in the coastal water areas around the world. Yet, an algorithm developed for a smaller geographic region such as the Baltic Sea can be used as a valuable tool in the studies of the clay's re-suspension and biological effects. In this study, a controlled experiment was conducted to measure the reflectance spectra of seawater samples with varying clay concentration. The purpose of the spectral analysis was to develop a robust and accurate algorithm for the clay concentration estimation for the coastal water areas of the Baltic Sea using high resolution hyperspectral data.

METHODS

Test data

Reflectance spectra of seawater samples of varying clay concentrations were measured in a laboratory environment. The seawater was collected from board of a boat at an offshore location where both the organic and the non-organic suspension is very low. Total Suspended Matter (TSM) of the collected water was 5 mg/l and it can be assumed that the matter was mainly organic.

Marine clay was collected from the seaside of the town Pori in South-West Finland (61°36.842'N 21°26.765'E). The small portions of clay were carefully weighted using a precision laboratory scale. The spectral measurements were carried out in a glass container filled with 24 centimetres of seawater. The small portions of clay were ground into powder and diluted in the seawater in the container. The reflectance spectrum of each water sample was recorded using an ASD FS-2500 portable spectrometer. A total number of six water samples with added clay were measured. The clay concentration in the prepared water samples varied between 10.6 and 142 mg/l. The clay concentration values are typically in that range at the coast of the Baltic Sea. A black sheet painted with black Synthal paint was positioned under the container in order to ensure that the bottom reflectance does not influence the measured reflectance of the water sample. The Synthal paint has a very low reflectance throughout the measured wavelength range. The measured reflectance of the paint is under 0.03 in the range 350 to 2500 nm.

The container was illuminated with an Oriel research arc lamp source having a power consumption of 1000 W. The Oriel lamp is a laboratory equipment designed for spectral measurements providing

constant spectral characteristics. The Oriel lighting source was operated with a voltage stabiliser unit which ensured a constant illumination of the measured water sample. Black sheets were installed around the container in order to block out all stray light from other sources. It was necessary to illuminate the measured water sample through the glass because the straight mirror reflection from the water sample had to be avoided. In order to verify the absence of bottom effects the reflectance spectrum of the empty container bottom was measured. The measured reflectance was very low throughout the measured wavelength range. Reflectance peaks and absorption points of the bottom spectrum could not be observed in the water sample spectra. Hence it is safe to assume that there were no reflections from the bottom involved in water sample measurements. The arrangement of reflectance measurements is shown in Figure 1.
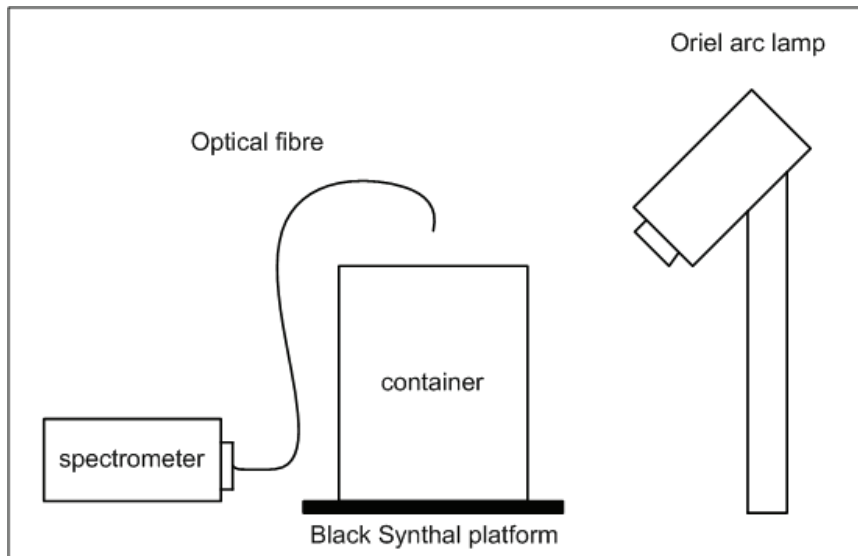

Figure 1: The arrangement of reflectance measurements.

Reflectance measurements of water samples in glass containers need a specific correction for the removal of the optical effect of the container. The correction coefficients were calculated using an empirical method where a white reference target was measured inside and outside the empty container. The number of wavelength channels is 2151 and is constant throughout the work. Therefore, indexing of the channels has been omitted in the notation.

The measured reflectances are as follows:

T_p = Reflectance of the empty container
P_p = Homogenous reference target in the same container
P_i = Homogenous reference target outside the container

Denoting the apparent reflectance T_p as A_{Tp} and the corrected reflectance P_i as A_{Pi}, it follows:

$$A_{Tp} = c_1 \frac{P_p}{P_i} - c_2 \tag{1}$$

$$A_{Pi} = \frac{c_1 P_p}{T_p + c_2} \tag{2}$$

where $c_1 \approx 4.233$ and $c_2 \approx 3.994$.

The constants c_1 and c_2 were estimated by minimising the total sum of the absolute difference A_{Tp} - T_p. The optical effect of the glass container can be removed from the reflectance R_w of a water sample measured in that container using the following relation:

$$A_{Rw} \approx \frac{c_1 R_w}{T_p + c_2} \tag{3}$$

where A_{Rw} denotes the corrected reflectance.

Algorithms

A linear regression is perhaps the most often used empirical method in the remote sensing of water quality. The use of channel ratios in the regression algorithm has been found to be suitable for the retrieval of many water quality parameters (20). Quite often the wavelength channels are called ocean colour bands in the literature addressing the remote sensing of water quality, so the ocean colour band ratio algorithms are as essential as the band ratio algorithms. The use of band-ratio algorithms for the estimation of the clay concentration has been proposed in the literature and therefore, they are used for a comparison in the evaluation of the spectral angle method proposed in this paper(8). The general form of a band ratio algorithm used in the assessment of clay concentration C is:

$$C = a\frac{R_1}{R_2} + b \tag{4}$$

where R_1 and R_2 are the remotely sensed reflectances at predefined wavelengths and a and b are empirically determined regression parameters. High spectral resolution imaging spectrometers such as AISA dual can provide information on as many as 481 wavelength channels. When the simple band-ratio algorithms are calculated based on such data the majority of the information is not utilised. The use of more than two wavelength channels can lead to more robust and accurate algorithms.

Spectral Angle Mapper (SAM) is a spectral classification method that uses an n-dimensional angle to match remotely sensed pixels to a reference spectrum. The algorithm determines the similarity between two spectra by calculating the angle between the spectra, treating them as vectors in a space with a dimensionality equal to the number of bands (21). A small angle means close match to the reference spectrum. The spectral angle α can be expressed as:

$$\alpha = \cos^{-1}\left(\frac{\sum\limits_{i=1}^{nb} t_i r_i}{\left(\sum\limits_{i=1}^{nb} t_i^2\right)^{1/2}\left(\sum\limits_{i=1}^{nb} r_i^2\right)^{1/2}}\right) \tag{5}$$

where nb is the number of bands, t is the target spectrum and r is the reference spectrum. The spectral angle between the target and the reference spectra in the case of a two-band image is shown in Figure 2.

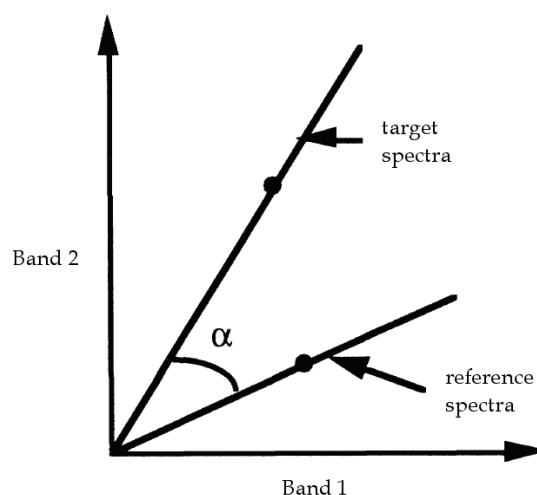*Figure 2: The spectral angle between target and reference spectra shown in the case of a two-band image.*

The feasibility of the SAM method in clay concentration retrieval is not self-evident, the method has some shortcomings. When using the spectral angle method, a normalisation of spectra is carried out. Only the shape of these spectra, and not their brightness, is taken into account. Furthermore, SAM

does not distinguish between negative correlation and positive correlation as it uses absolute values. In order to overcome the limitations of the SAM method, improved spectral methods such as Spectral Correlation Mapper (SCM) and Spectral Multiple Correlation Mapper (SMCM) have been proposed (22,23,24). The main difference between these methods concerns the criteria of similarity used for comparing the spectra. SCM and SMCM offer some benefits in certain situations but in this kind of application where the whole spectrum is not employed there is no clear advantage when compared to SAM. The only essential requirement for a spectrum-dependent variable in this application is a strong correlation between the variable and clay concentration.

In the proposed algorithm the spectrum of the water sample without added clay suspension was used as the reference. The spectral angle between the measured water sample spectrum and the reference spectrum representing water with a very low organic and non-organic suspension was calculated. The clay concentration C was calculated using the following equation:

$$C = a'\alpha + b'$$ (6)

where α is the spectral angle between the reference and the measured spectra and a' and b' are empirically determined regression parameters. In this paper this equation is referred to as the spectral angle algorithm. It is quite usual that all the available wavelength bands are not used in the spectral angle based classification. It is very likely that some of the wavelength bands do not contain information relevant to the clay concentration of the water. There are several methods for dimensionality reduction of hyperspectral data presented in the literature such as feature selection, Principal Component Analysis (PCA) and Minimum Noise Fraction (MNF) (25). The PCA and MNF components are always image dependent and therefore cannot be used in general algorithms. The wavelength bands used in the algorithm proposed in this paper were chosen depending on the correlation analysis. The band combination that produces the strongest correlation between the spectral angle α and the clay concentration C leads to the highest retrieval accuracy when using Eq. (6).

A very desirable property of a clay concentration estimation algorithm would be its robustness, i.e., insensitiveness to the presence of other substances than clay. An organic suspension is often present in case 2 waters. Therefore, the robustness of algorithms to withstand organic suspensions was tested. In our study the spectra of the combined clay and organic suspension were obtained by simulation. The simulated reflectance spectra of the combined suspension were calculated as a linear combination of the measured spectrum of a water sample with added clay and the spectrum of a water sample with strong organic suspension. Water samples with a strong organic suspension were manufactured by diluting green algae in water with very low suspension.

The simulated reflectance spectrum R_s was calculated using the following equation:

$$R_s = R_c \frac{100 - P}{100} + R_o \frac{P}{100}$$ (7)

where R_c is the spectrum of the water sample with added clay, R_o is the spectrum of the water sample with the organic suspension and P is the percentage of the water with organic suspension in the mix. R_s is the simulated spectrum of the water sample containing both suspensions, i.e, clay and organic. An example of R_s is shown in Figure 3. R_c is the measured spectrum of the water sample with a clay concentration of 67.4 mg/l and R_o the measured spectrum of the water sample with organic suspension. The percentage of the water with organic suspension in the simulated spectrum is 20%. Hence, 20% of the simulated reflectance spectrum R_s is determined by R_o and 80 % is determined by R_c. The reflectance peak around 715 nm and absorption around 680 nm due to chlorophyll can clearly be seen in the reflectance spectrum of the water sample with organic suspension. This indicates a significant chlorophyll concentration although the exact value could not be measured. The Total Suspended Matter (TSM) of seawater used as a reference (with very low suspension) was 5 mg/l before the addition of clay, so there is a small amount of organic suspension; however, this amount is very small compared to the amount of added clay or the amount of organic suspension in the water sample represented by the green line.
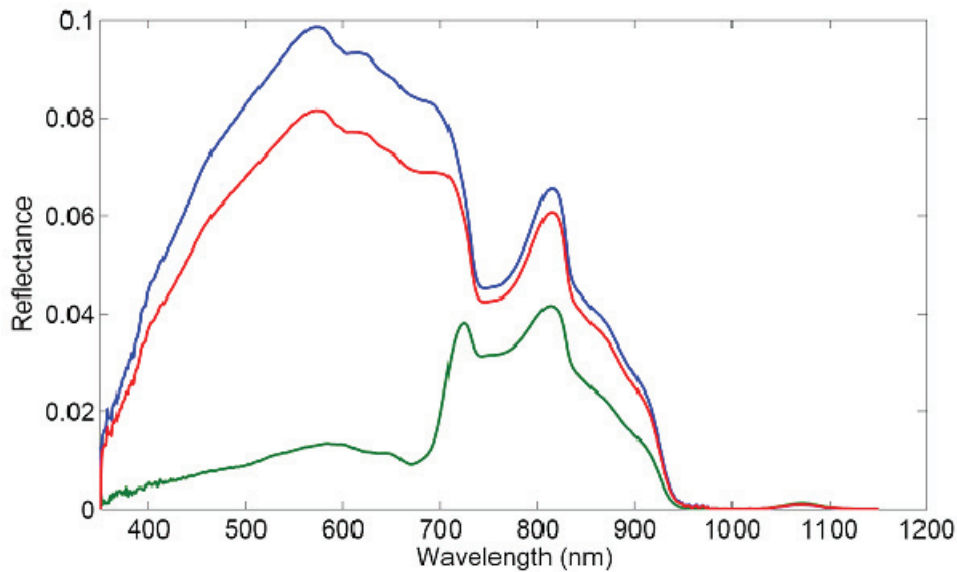
Figure 3: The reflectance spectrum of water sample with added clay R_c (blue), the spectrum of water sample with organic suspension R_o (green) and simulated water sample with combined clay and organic suspension R_s (red).

In many cases hyperspectral data have noisy channels due to the poor alignment of the hyperspectral sensor or other factors related to signal quality (26). In the worst cases channels containing excessive noise have to be excluded from the dataset before processing the hyperspectral data. Generally, the signal-to-noise ratio of satellite-borne hyperspectral sensors is rather poor (27). It is important that an algorithm used to retrieve clay concentration is not sensitive to noise. The sensitivity of algorithms to noise was evaluated by generating simulated reflectance spectra where random noise was added to the measured reflectance of water samples with the known clay concentration. The simulated reflectance spectra were calculated using the following equation:

$$R_s = R_c + \frac{N}{SNR} \tag{8}$$

where R_c denotes the spectrum of a water sample with added clay, N is a random noise signal which has the same mean value as R_c and SNR is the signal-to-noise ratio of R_s.

RESULTS

The measured reflectance spectra of the water samples containing varying amounts of the added clay are shown in Figure 3. Ten repeated measurements were used to calculate the spectra for each water sample. Original measurements covered the wavelength range from 350 to 2500 nm, but the range above 1150 nm was excluded in this study because the reflectance of the water at that range is close to zero. All the measured reflectance spectra have two local maxima and one local minimum. The reflectance maxima are centred at the wavelengths 590 and 815 nm. The local reflectance minimum is centred at the wavelength 760 nm. The increase of the reflectance around 815 nm seems to have a quite linear relationship with the clay concentration of the water, but the increase of reflectance around 590 nm saturates when the clay concentration becomes higher. The decrease of the reflectance at 760 nm also saturates at higher clay concentrations.

In order to determine the best wavelength channels to be used in a band-ratio based algorithm, the correlation between clay concentration and hyperspectral band ratio was calculated for all possible wavelength combinations. The band ratio R_{709}/R_{585} produced the best result with the coefficient of determination $r^2 = 0.941$. The band ratio R_{595}/R_{754} proposed in the literature had a weaker correlation giving the coefficient of determination $r^2 = 0.519$. The correlation between R_{754} and the clay concentration is not strong. This is most likely because the type or particle size of the added clay was differ-

ent in the measurements described in this paper compared to the referenced paper. The regression parameters *a* and *b* in Eq. (4) were determined and the clay concentration *C* in milligram per litre was calculated with the following equation:

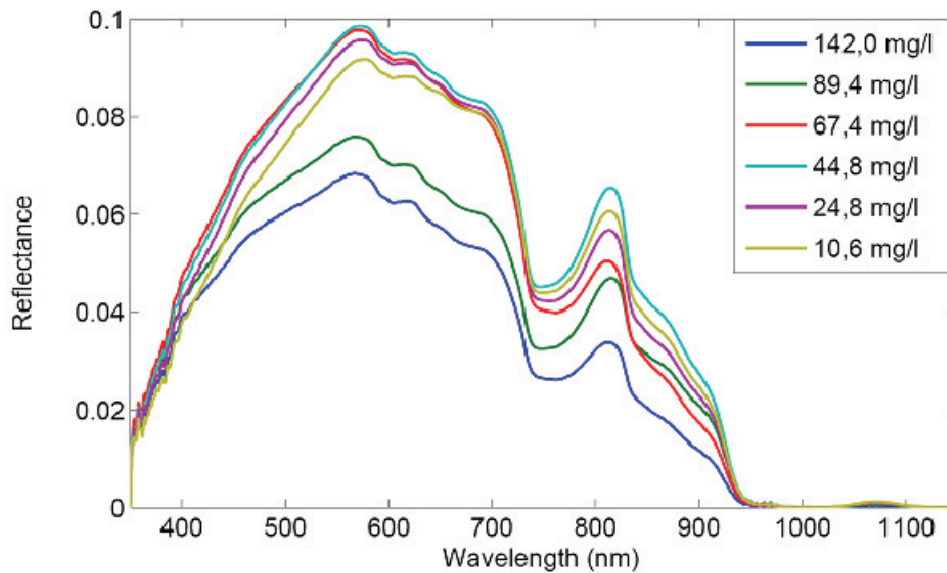$$C = 8702 \frac{R_{709}}{R_{585}} + (-6498) \tag{9}$$

Figure 4: Reflectance spectra of water samples containing varying amounts of added clay.

Not all wavelength bands contain information relevant for clay concentration. Therefore, only a small number of bands was selected to be used in the spectral angle calculation. Band selection was done using a correlation analysis. The correlation between the spectral angle and the clay concentration was calculated for all possible band combinations. The correlation was calculated using different numbers of wavelength bands in order to determine how many bands should be used in the spectral angle calculation. The correlation between the spectral angle and the clay concentration is not an adequate criterion for the band selection without restrictions. There are band combinations that provide a good correlation between the spectral angle and the clay concentration, but the change in the spectral angle is very small with respect to the change in the clay concentration. This makes the algorithms based on such band combinations very sensitive to noise and other possible interferences. Therefore, additional restrictions were imposed on a band selection: the spectral angle corresponding to the lowest clay concentration 10.6 mg/l cannot be higher than 10% of the spectral angle corresponding to the highest clay concentration 142 mg/l. The best obtained coefficients of determination r^2 using a different number of wavelength bands are shown in Table 1.

Table 1: Results of correlation analysis using different number of wavelength bands.

Number of bands	4	5	6	7	8	9	10
r^2	0.932	0.967	0.962	0.954	0.944	0.933	0.922

The strongest correlation was obtained using five wavelength bands. Only a certain number of bands correlate strongly with the clay concentration. When more bands are used, bands with a weaker correlation decrease the correlation between spectral angle and the clay concentration. The correlation weakens gradually when more than 5 bands are employed, but the weakening is not dramatic. The wavelengths that produced the strongest correlation were: 437, 637, 685, 749 and 952 nm. The regression parameters a' and b' in Eq. (6) were determined and the clay concentration *C* in mg/l was calculated using the following equation:

$$C = 643.7 \cdot \cos^{-1}\left(\frac{\sum\limits_i t_i r_i}{\left(\sum\limits_i t_i^2\right)^{1/2}\left(\sum\limits_i r_i^2\right)^{1/2}} \right) + 73.9 \tag{10}$$

where t denotes the remotely sensed target spectrum, r denotes the reference spectrum of the water sample without clay suspension, and $i = \{437,637,685,749,952\}$. The root mean square error (*RMSE*) of the clay concentration estimate was calculated according to:

$$RMSE = \sqrt{\frac{1}{N-2}\sum_{i=1}^{N}\left(C_{IV,i} - C_{RS,i}\right)^2} \tag{11}$$

where N is the number of measurements at different clay concentrations, $C_{IV,i}$ is the measured *in vivo* clay concentration and $C_{RS,i}$ is the estimated clay concentration. RMSE values calculated for the band-ratio and spectral angle algorithms measurements at different concentrations are shown in Table 2.

Table 2: The percentage of RMSE error of the mean clay concentration for band-ratio and spectral angle algorithm.

Algorithm	Band-ratio	Spectral angle
RMSE	14.5%	14.1%

The RMSE was slightly lower for the spectral angle algorithm as was expected on the basis of the correlation analysis.

The sensitivity of the algorithm to the presence of organic suspension was evaluated using simulated reflectance spectra representing water samples containing both the clay and the organic suspension. RMSE values for both presented algorithms corresponding to the varying percentage of organic suspension are shown in Table 3.

Table 3: RMSE values for the band ratio and spectral angle algorithms calculated using varying percentage of organic suspension.

Organic suspension	0%	10%	20%	30%	40%	50%
RMSE (Band-ratio)	14.5%	17.1%	20.4%	24.6%	30.1%	38.7%
RMSE(Spectral angle)	14.1%	14.8%	17.4%	20.8%	25.3%	32.2%

As can be seen from Table 3, RMSE values are significantly lower (about 15%) for the spectral angle algorithm. When the simulated water sample contained equal volumes of water with different suspension, i.e., clay and organic, the *RMSE* for the spectral angle algorithm was 32.2%. The result indicates that the spectral angle algorithm can provide reasonable results even when other optically detectable substances than clay are present in the water area under study.

In order to evaluate the sensitivity of the algorithms to noise, random noise was added to the reflectance spectra and the RMSE caused purely by the noise was measured. In order to get statistically representative RMSE values this process was repeated 10,000 times and the average *RMSE* for all measurements was calculated. The relationship between the *RMSE* of the algorithms and the *SNR* of the hyperspectral data is shown in Table 4.

The average *RMSE* for the spectral angle algorithm was about 10% smaller compared to the band-ratio algorithm. This indicates the robustness of the spectral angle algorithm although the difference between the algorithms was quite small.

Table 4: The relationship between the RMSE of algorithms and SNR of hyperspectral data.

SNR	100	30	10
RMSE(Band-Ratio)	1.61%	4.89%	16.25%
RMSE(Spectral angle)	1.45%	4.41%	14.6%

CONCLUSIONS

In this paper a spectral angle based algorithm for clay concentration retrieval is presented. The proposed algorithm was tested using reflectance spectra of water samples with added clay suspension. A controlled experiment was arranged in the laboratory environment in order to record the necessary reflectance spectra. The band-ratio algorithm proposed earlier in the literature was compared against the band-ratio algorithm using optimal wavelength bands. The algorithm using optimal wavelength bands produced significantly better results, which demonstrates the need for a local calibration when developing an algorithm. The optimal number of wavelength bands used in the SAM algorithm was quite small, indicating that only a few bands have a very strong correlation to the clay concentration. The correlation decreases quite slowly when the number of bands increases from the optimal value.

The difference in the retrieval accuracy between the SAM and band-ratio algorithms was small, although in favour of the SAM algorithm. The results clearly demonstrate the robustness of the proposed SAM algorithm. The retrieval error caused by the presence of organic suspension in the water sample is smaller using the SAM algorithm when compared to the band-ratio algorithm. The retrieval error caused by the presence of noise in the measured spectrum was also smaller.

The results of this study clearly show the potential of the spectral angle algorithm, but more research should be done in order to understand the optical properties of optically detectable substances in case 2 seawater areas. Future work will contain controlled experiments where water samples with combined suspension are prepared and the reflectance spectra are recorded. A comprehensive spectral library would provide necessary information on the mixed suspension water spectra, which would make it possible to derive more accurate algorithms for the estimation of clay concentration.

ACKNOWLEDGEMENTS

REFERENCES

1   Lindholm T, M Svanström, L Spoof & J Meriluoto, 2001. Effects of ship traffic on archipelago waters off the Langnas harbor in Åland, SW Finland. Hydrobiologia, 444: 217-225

2   Korpinen S & V Jormalainen, 2008. Grazing and nutrients reduce recruitment success of *Fucus vesiculosus L.* (Fucales: Phaeophyceae). Estuarine, Coastal and Shelf Science, 78: 437-444

3   Engström-Öst J & M Salonen, 2007. Can zooplankton escape predation in turbid water? Human and Climate Forcing of Zooplankton Populations 2007, p. 102
    http://www.pices.int/publications/book_of_abstracts/2007_4th_Zooplankton_Symposium.pdf
    (last access: 06.12.2010)

4   Niemistö J, H Holmroos, Z Pekcan-Hekim. & J Horppila, 2008. Interactions between sediment resuspension and sediment quality decrease the TN:TP ratio in a shallow lake. Limnology and Oceanography, 53: 2407-2415

5   Horppila J & A Liljendahl-Nurminen, 2005. Clay-turbid interactions may not cascade – a reminder for lake managers. Restoration Ecology, 13: 242-246

6   Dekker A G, 1993. Detection of Optical Water Quality Parameters for Eutrophic Waters by High Resolution Remote Sensing. PhD Thesis, Vrije University, The Netherlands

7   Koponen S, J Pulliainen, K Kallio, M Hallikainen, & J Vepsäläinen, 2001. Use of MODIS data for monitoring turbidity in Finnish Lakes. International Geoscience and Remote Sensing Symposium (IGARSS'01), pp. 3, Sydney, Australia, 9-13 July, 2001

8   Miller R L & B A McKee. 2004. Using MODIS Terra 250 m imagery to map concentrations of total suspended matter in coastal waters. Remote Sensing of Environment, 93: 259-266

9   Gin K Y H, S T Koh & I I Lin, 2003.Spectral irradiance profiles of suspended marine clay for the estimation of suspended sediment concentration in tropical waters. International Journal of Remote Sensing, 24: 3235-3245

10   Nichol J E, 1993. Remote sensing of water quality in the Singapore Johor-Riau growth triangle. Remote Sensing of Environment, 43: 139-148

11   Cracknell A P, 1999. Remote sensing techniques in estuaries an coastal zones – an update. International Journal of Remote Sensing, 19: 485-496

12   Gin K Y H, S T Koh & I I Lin, 2003.Study of the effects of suspended marine clay on the reflectance spectra of phytoplankton. International Journal of Remote Sensing, 23: 2163-2178

13   Han L, D C Rundquist, L L Liu, R N Fraser & J F Schalles, 1994. The spectral responses of algal chlophyll in water with varying levels of suspended sediments. International Journal of Remote Sensing, 18: 3707-3718

14   Ritchie J C, C M Cooper & F R Schiebe, 1994. The relationship of MSS and TM digital data with suspended sediments, chlorophyll and temperature in Moon Lake, Missisippi. Remote Sensing of Environment, 33: 137-148

15   Han L, D C Rundquist, L L Liu, R N Fraser & J F Schalles, 1994. Analysis of suspended solids in water using remotely sensed high resolution derivative spectra. Photogrammetric Engineering and Remote Sensing, 59: 505-510

16   Quibell G, 1994. Estimating chlorophyll concentrations using upwelling radiance from different fresh water genera. International Journal of Remote Sensing, 13: 2611-2621

17   Gitelson A A, D Dall'Olmo, W Moses , D C Rundquist, T Barrow, T R Fisher, D Gurlin & J Holtz, 2008. A simple semi-analytical model for remote estimation of chlorophyll-a in turbid waters. Remote Sensing of Environment, 112: 3582-3593

18   Cococcioni M, G Corsini, B Lazzerini & F Marcelloni, 2004. Approaching the ocean color problem using fuzzy rules. IEEE Transactions on Systems, Man and Cybernetics, 34: 1360-1373

19   Doerffer R & H Schiller, 2007.The MERIS Case 2 water algorithm. International Journal of Remote Sensing, 28: 517-535

20   Koponen S, 2006. Remote Sensing of Water Quality for Finish Lakes and Coastal Areas (Helsinki University of Technology, Doctoral Thesis) 35pp.

21   Kruse F A, A B Lefkoff, J B Broadman, K B Heidebrecht, A T Shapiro, P J Barloon & F H Goetz, 1993.Spectral Image Processing System (SIPS) – interactive visualization and analysis of imaging spectrometer data. Remote Sensing of Environment, 44: 145-163

22   Carvalho A C & P R Meneses, 2000. Spectral Correlation Mapper (SCM): an improvement on the Spectral Angle Mapper (SAM). In: Proceedings of the 10th AVIRIS Airborne Geoscience Workshop, JPL Publication 00-18

23 O de Carvalho Jr, R Guimaraes, R Gomes, A Carvalho, N da Silva & E Martins, 2006. Spectral multipole correlation mapper. In: <u>IEEE International Conference on Geoscience and Remote Sensing</u>, IGARSS 2006 (Denver, USA) 31 July - 4 August 2006

24 Green A A, M Berman, B Switzer & M D Graig, 1988. A transformation for ordering multispectral data in terms of image quality with implications for noise removal. <u>IEEE Transactions on Geoscience and Remote Sensing</u>, 26: 65-74

25 Keshava N, 2001. Best bands selection for detection in hyperspectral processing. Proceedings of IEEE international conference on Acoustics, Speech and Signal Processing, 26: 65-74

26 Stephan K, C A Hibbits, H Hoffman & R Jaumann, 2003. Reduction of instrument-dependent noise in hyperspectral image data using the principal component analysis: Applications to Galileo NIMS data. <u>Planetary and Space Science</u>, 56: 406-419

27 Pearlman J S, P S Barry, C C Segal, J Shepanski, D Beiso & S L Carman, 1993. Hyperion, a space-based imaging spectrometer. <u>IEEE Transactions on Geoscience and Remote Sensing</u>, 41: 1160-1173

Chapter 8

Publication P2

Tuominen, J. and Lipping, T. (2014). Feasibility of Benthic Cover-Type Mapping in Turbid Waters near Estuaries Using Hyperspectral Remote Sensing. *Journal of Coastal Research*, 30(6): 1131-1139

Feasibility of Benthic Cover-Type Mapping in Turbid Waters near Estuaries Using Hyperspectral Remote Sensing

Jyrki Tuominen and Tarmo Lipping

Tampere University of Technology
Pohjoisranta 11 A
28100 Pori, Finland
jyrki.tuominen@tut.fi

www.cerf-jcr.org

www.JCRonline.org

ABSTRACT

Tuominen, J. and Lipping, T., 0000. Feasibility of benthic cover-type mapping in turbid waters near estuaries using hyperspectral remote sensing. *Journal of Coastal Research,* 00(0), 000–000. Coconut Creek (Florida), ISSN 0749-0208.

In this study the feasibility of benthic cover-type mapping in turbid waters near estuaries using hyperspectral remote sensing is explored. The majority of research papers addressing remote sensing of benthic cover types concentrate on optically clear, shallow coastal and reef waters. In order to study the effects of water depth and water quality on benthic cover-type classification, a synthetic data set was generated. Synthetic spectra were calculated using *in situ* optical measurements of water quality and spectra of different bottom types. The data set was classified using the spectral correlation mapper (SCM) and the Euclidean distance (ED) classifier. A simple water-column correction method was also tested. The overall mapping accuracy of SCM classification without water-column correction reached 47.8% when the depth range 0.0–3.0 m was studied. The mapping accuracy increased to 66.0% using the ED classifier with water-column correction. When water quality was changed from least turbid to most turbid, the overall accuracy decreased to 50.4%.

ADDITIONAL INDEX WORDS: *Baltic Sea, water-column correction.*

INTRODUCTION

Increasing water turbidity is one of the human-induced environmental changes in coastal areas. Maritime spatial planning is a key instrument for implementing the European Union's Integrated Maritime Policy (Meiner, 2010). At present authorities are often forced to carry out spatial planning of marine areas based on insufficient or incomplete data. Reliable information on benthic habitats is urgently needed in many marine areas. The Finnish Inventory Programme for the Underwater Marine Environment (VELMU), designed to provide information for the protection of the Baltic Sea, collects data on the diversity of underwater marine biotopes and species (Kohonen, 2003). One of the main goals of the research programme is to maintain and increase diversity in the marine environment. The protection programme is difficult to implement, as knowledge of the underwater marine environment and its state in general is insufficient.

Benthic algal cover and trends in changes of algal cover could be used as indicators of biological state in coastal areas (Juanes *et al.*, 2008; Kutser, Miller, and Jupp, 2006). Such indicators are valuable tools when the protection and preservation of marine environments is planned. Maritime spatial planning requires data covering large areas; traditional *in situ* measurements taken by diving, submerged video, and grab sampling cannot cover such large areas without excessive costs. Remote sensing based submerged mapping has been shown to be more cost-effective than *in situ* measurements (Mumby *et al.*, 1999). Classification of benthic cover types has been suggested in several research papers, as it is a spatially comprehensive method (Dekker *et al.*, 2001).

Mapping of benthic cover types based on remote-sensing data has been carried out successfully in optically clear, shallow coastal and reef waters (Dekker *et al.*, 2001; Kutser and Jupp, 2002). Louchard *et al.* (2003) showed that hyperspectral classification of benthic cover types can produce satisfactory results in the clear coastal waters of the Bahamas. Bertels *et al.* (2008) used airborne hyperspectral data in coral reef mapping, yielding desirable classification accuracy even in depths above 10 m. Turbid waters, however, are far more challenging for remote-sensing techniques (Phinn *et al.*, 2005). The limited exchange of marine waters of the North Sea through narrow channels and large discharge from rivers significantly influence the optical properties of the Baltic Sea (Darecki and Stramski, 2004). Colored dissolved organic matter (CDOM) is the major light absorber in these waters (Kowalczuk *et al.*, 2005). CDOM in coastal environments generally has a terrestrial origin and is transported to the ocean *via* rivers. The highest concentrations of CDOM are found in coastal margins of oceans and in semienclosed seas, where direct sources of terrestrial organic matter are found.

A few comprehensive research papers exploring the feasibility of benthic mapping in the Baltic Sea using remote sensing have been published. The feasibility of multi- and hyperspectral remote sensing was studied using model-based simulations. The modelling results indicate that to some extent it is possible to map the macroalgal species in turbid waters of the Baltic Sea using multispectral satellite sensors. However, the depths at which the macroalgae can be detected are often shallower than the maximum depths to which the studied species grow (Kutser, Vahtmäe, and Martin, 2006). The modelling results of the hyperspectral method indicate that the feasibility of mapping benthic macroalgal cover in CDOM-dominated environments such as the Baltic Sea is not much lower than in clear waters (Vahtmäe *et al.*, 2006). In addition to studies based on model-based simulations, some empirical studies on benthic mapping in the Baltic Sea have been published. Kutser *et al.* (2011) used airborne hyperspectral data to classify benthic cover types on the coast of Estonia. The results were promising; however, the need for more satisfactory atmospheric correction of the data was pointed out. Vahtmäe and Kutser (2007) published a study assessing the suitability of high-spatial-resolution multispectral and medium-spatial-resolution hyperspectral data for mapping benthic macroalgal cover in shallow coastal waters of the Baltic Sea. Results of the study indicate that the use of multispectral satellite data with high spatial resolution is preferable to hyperspectral medium-resolution data in mapping benthic macroalgal cover in areas where the spatial heterogeneity is very high.

The water near the coastline of Finland is largely influenced by discharge from numerous rivers. In the case of large rivers, this influence can cover wide areas near the coastline. In summer 2008 an airborne hyperspectral campaign was carried out in SW Finland. The data acquisition covered the SW coastline using an AISA dual sensor. Unfortunately benthic field survey data was not collected during the flight campaign, so the usability of the data in benthic mapping could not be evaluated. Such missions are planned in the future. The objective of our study was to determine whether such hyperspectral flights could be used for benthic mapping in these challenging conditions. The maximum depth at which reasonably accurate classification can be performed was estimated, as well as the influence of water type on the accuracy of classification. Studies using hyperspectral flight campaigns with simultaneous *in situ* submerged measurements are often hard to carry out, both in terms of excessive cost and the considerable amount of work related to field measurements. In this study simulated data were used instead of remote-sensing imagery. Synthetic data generated using empirical spectral and water-quality measurements were used to determine classification accuracy of benthic mapping. The reflectance spectra of typical benthic cover types in the study site were measured using a handheld spectroradiometer. In order to calculate the effect of the water column on bottom reflectance, several spectral water-quality measurements were performed. The optically deep water reflectance was measured and the water attenuation coefficient assessed at four locations of different turbidity. A simulated data set was generated using these spectral *in situ* measurements.

MATERIALS AND METHODS

Study Area

The study area is located on the coast of the city of Pori in SW Finland (Figure 1). The river Kokemäenjoki flows from inland into the large estuary of Kolpanlahti. The average flow in the river Kokemäenjoki is 260 m^3/s, and flow rates exceeding 500 m^3/s are not exceptional. The discharge from a smaller river, Kristiskerinjoki, also contributes to increased turbidity in the study area, but not at the same scale as the Kokemäenjoki. From the estuary, water flows towards the open sea *via* three narrow outlets. A Landsat ETM+ image covering the study area was acquired on 6 June 2011, ten days after spectral water-quality measurements were taken (Figure 2). Increased turbidity due to discharge from rivers can be seen as brownish colour. Clearer-water bodies appear as dark blue areas. According to remotely sensed estimates provided by the Finnish Environment Institute, turbidity near *in situ* measurement sites typically varies from 3 to 5 Formazin Turbidity Unit (FNU). The Landsat image is shown in order to illustrate the variation of turbidity in the study area; it was not used in the classification process.

In Situ Measurements of Benthic Reflectance Data

Benthic cover types for this study were selected based on an initial submerged survey in the study site. Research divers explored the area using side-scan sonar and underwater video. Specimens of typical green (*Cladophora glomerata*), brown (*Fucus vesiculosus*), and red (*Ceramium tenuicorne*) benthic macroalgae were selected. In addition to benthic vegetation, three typical bottom covers, *i.e.* sand, clay, and reddish pebble, were selected. Reflectance spectra of benthic cover types were measured using a handheld GER 1500 spectroradiometer (Spectra Vista Corporation, Poughkeepsie, New York, U.S.A.). The spectral range of the instrument is 300-1100 nm. Spectra were sampled with 1.5 nm intervals, and spectral
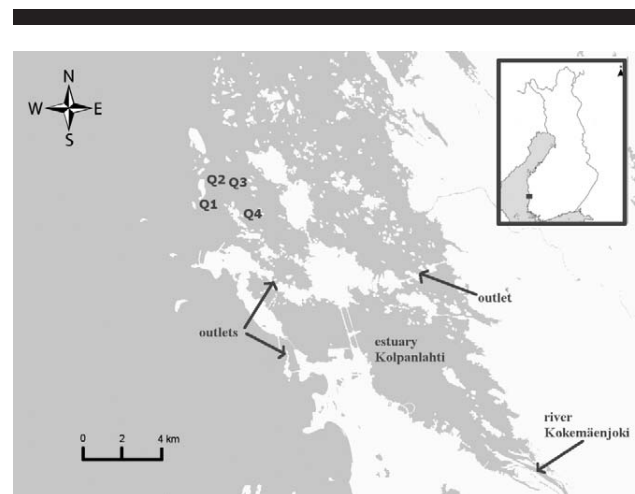

Figure 1. The geographic location of the study area. The sites of *in situ* spectral water-quality measurements are labelled according to water type (Q1 through Q4). Water type Q1 represents the least turbid and Q4 the most turbid water.
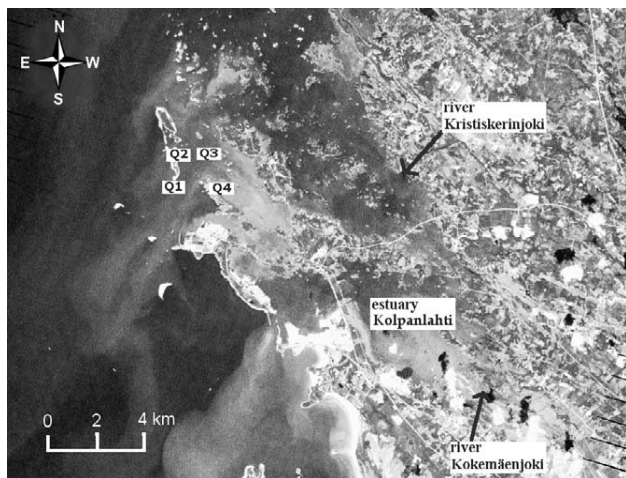
Figure 2. Enhanced Landsat satellite image (channels 3, 2, and 1) of the study area. (Color for this figure is available in the online version of this paper.)

resolution of the GER1500 instrument was 3 nm. Reflectance was calculated as the ratio of radiance from the measured object to the radiance from the reflectance standard, *i.e.* 99% Spectralon panel (Labsphere, North Sutton, New Hampshire, U.S.A.). Samples of each studied cover type were collected into water-filled plastic containers. Reflectance measurements of wet samples were carried out on the shore immediately after landing of the boat. Three reflectance spectra of each sample were measured, and the average spectrum of each cover type was used in the following data-generation and classification procedures.

In Situ Measurements of Spectral Water-Quality Parameters

Spectral water-quality parameters were measured at the four sites indicated in Figure 1 on 26 May 2011. Two spectral parameters were measured at each site—the optically deep water reflectance R_∞ and the water attenuation coefficient K. The sites were selected by the following criteria:

(1) Depth must be at least 6 m in order to ensure the measurement of deep water reflectance. Deep water reflectance R_∞ means that the bottom albedo has no influence on the reflectance value.
(2) Increased turbidity caused by the river must be present.
(3) The location of the site must provide some shelter from the waves to allow spectral measurements aboard a small boat.

Optically deep water reflectance was measured using a GER 1500 spectroradiometer equipped with the optical fibre extension. The side of the boat was covered with a black low-reflectance sheet in order to prevent interfering reflections from the boat. The water attenuation coefficient K was measured using a white reference plate. The plate was set at a depth of 30 cm, and the reflectance was measured. Then the

reflectance of the wet reference plate was measured again on board without the water column.

It has been shown by Maritorena, Morel, and Gentili (1994) that the diffuse reflectance of shallow waters just below the water surface can be calculated using the equation

$$R(0-,z) = R_\infty + (R_b - R_\infty)\exp(-2Kz), \qquad (1)$$

where z is the water depth, R_b is bottom reflectance, R_∞ is reflectance of optically deep water, and K is the diffuse attenuation coefficient of the water. In this case R is the reflectance of the reference plate at the depth of 30 cm and R_b is the reflectance of the reference plate measured without the water column; the depth z and deepwater reflectance R_∞ are known. Hence the only unknown variable in Equation (1) is the water attenuation coefficient K, which can be solved using the equation

$$K = \frac{\ln\left(\frac{R-R_\infty}{R_b-R_\infty}\right)}{-2z}. \qquad (2)$$

Three reflectance spectra of each water type were measured and average spectra were calculated for the assessment of both R_∞ (without the reference plate) and K (obtained from the measurement with the reference plate at 30 cm using Equation [2]). In this study the diffuse attenuation coefficient was measured at a depth range of 0.0–0.3 m, and it is assumed that the obtained value is valid for the depth range of 0.0–3.0 m. This assumption might not be completely correct, but the approach provides a reasonable estimate of the attenuation coefficient. Although vertical attenuation coefficients are bound to change with depth, in many cases the exponential decrease of downwelling irradiance in the euphotic zone appears to be satisfactorily given by a single value of K (Gons, Ebert, and Kromkamp, 1998). The water at the measurement sites is quite well mixed. Thus the vertical structure of inherent optical properties (IOPs) is quite homogenous. The underwater radiance distribution is altered not only by the absorbing and scattering properties of the water column (IOPs), but also by angular distribution of light incident on the sea surface (Siegel and Dickey, 1987). This angular distribution of light can slightly alter the vertical structure of the diffuse attenuation coefficient near the surface.

Sun-Glint Correction

The sun-glint correction was accomplished through a modification of the method presented by Kutser, Vahtmäe, and Praks (2009). The method is based on two assumptions: First, it is assumed that there is no spectral absorption feature in the reflectance spectrum of natural waters at 760 nm if reflected light does not contain glint. Second, the depth of the oxygen absorption feature at 760 nm is proportional to the amount of glint in the spectrum. The depth of the absorption feature was calculated to be

$$D = \frac{[R(750) + R(780)]}{2} - R(764), \qquad (3)$$

where D is the depth of the oxygen absorption feature and $R(750)$, $R(760)$, and $R(780)$ are reflectances at these particular wavelengths. Kutser, Vahtmäe, and Praks (2009) used corresponding wavelengths selected from available AISA channels:

739 nm, 760 nm, and 860 nm. In this study optimal channels were chosen from high–spectral-resolution data. In the original method it was assumed that pixels with D values close to zero do not contain glint and the pixels with the highest D value contain mainly glint. Remote-sensing images can contain hundreds of thousands of pixels, and it is safe to assume that in this large set there exist pixels with no glint as well as pixels resulting mainly from glint. However, in this study there are only 12 measured spectra that contain significant amounts of glint, and none of them contains mainly glint or is totally glint free. In sun-glint correction it is assumed that the measured reflectance originates from both the reflectance of water and the reflectance due to sun glint. Therefore, if the depth D is proportional to the amount of glint, it is also proportional to the reflectance of water. It is not well established whether this proportion is linear or nonlinear; however, linear correction seems to produce reasonable results. In our modified approach, three measurements of deep water reflectance were used to scale the relationship between the reflectance R and absorption depth D. For each band a linear regression was applied between R and D (Figure 3), using the equation

$$R = a*D + b \qquad (4)$$

The corrected value of R can be calculated by setting $D = 0$.

Generation of Synthetic Data

In order to study the mapping accuracy of benthic cover-type classification, a synthetic data set was generated. The whole data set contains 7200 simulated spectra, 1200 spectra for each cover type representing the situations of varying water quality and water-column height. The simulated water depth varies
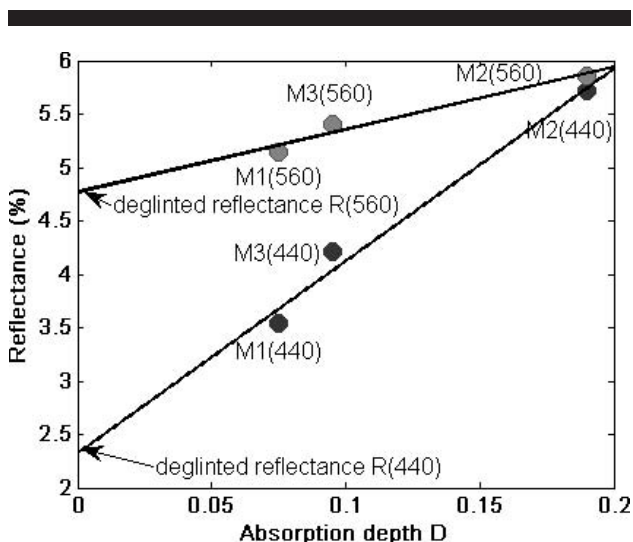

Figure 3. Graphical representation of the glint correction method. The correction is illustrated at two wavelengths, 440 nm and 560 nm. M1 through M3 represent the three measured spectra. For each spectrum the absorption depth D is calculated according to Equation (3). Then the regression equation (Equation [4]) is solved for each wavelength band, and the deglinted reflectance value at the corresponding wavelength is determined by the point where the regression line crosses the axis ($D = 0$).

between 0.01 m and 3.0 m at 0.01 m intervals. Four different water-type classes were studied: Q1, Q2, Q3, and Q4, where Q1 represents the least turbid and Q4 the most turbid water. Classes are based on empirical spectral water-quality measurements. The data set is modelled using Equation (1). The simulated spectrum R is calculated using deep water reflectance R_∞ and attenuation coefficient K corresponding to the simulated water type.

Water-Column Correction

The major problem involved in remote sensing of submerged cover types is that the water column affects the signal received at the sensor depending on the water depth and water quality. In the water-column–correction approach, methods accounting for the effects of water depth and turbidity variation are employed. Mumby *et al*. (1998) reported only 4 studies out of 45 (9%) that attempted water-column correction and concluded that authors are generally unaware of such methods. Several methods for water-column correction have been proposed. Good results have been achieved by a technique that creates a single depth-invariant band from each pair of visible spectral bands (Lyzenga, 1978, 1981). In this method, the exponential attenuation of the water column is first linearized for each band followed by calculation of the ratio of the attenuation coefficients for each pair of bands. However, the method assumes that the water column is uniform over the scene and the signatures of optically deep water pixels are needed to perform the transformations. Several improvements to the Lyzenga method have been since proposed; however, those methods need tuning for particular conditions or make assumptions that are valid only in certain locations.

Recently Armstrong *et al*. (2007) presented an approach in which at-sensor radiances were transformed into underwater reflectance factors. Transformation was derived using submerged black and white tarpaulins as underwater calibration targets. Karpouzli *et al*. (2003) proposed a method based on the variables of water depth, distance to and size of mangrove beds, and distance to and size of towns. The method was developed by using an extensive number of optical *in situ* water measurements and laboratory analysis of water samples. This and the Armstrong *et al*. (2007) method require a considerable amount of fieldwork. Mishra *et al*. (2007) have proposed a method where the depth and water properties are derived from hyperspectral data itself; however, calibration of the method requires extensive *in situ* measurements. There are some methods that allow the retrieval of water depth and bottom type simultaneously. Mobley *et al*. (2005) proposed an approach based on spectrum-matching and look-up-table methodology: First, a database of remote-sensing reflectance spectra corresponding to various water depths, bottom reflectance spectra, and water-column IOPs is constructed using a special version of the HydroLight radiative transfer numerical model. Second, the measured spectrum for a particular image pixel is compared with each spectrum in the database, and the closest match to the image spectrum is found using a least-squares minimization. Kutser, Miller, and Jupp (2006) presented a method that uses spectral libraries created with forward modelling from the sea bottom to the top of the atmosphere. A hyperspectral library of radiance at satellite altitude was

simulated using a spectral library of benthic substrates, a HydroLight radiative transfer model, and an in-house atmospheric model.

In this study a simple water-column–correction method was tested. The advantage of the method is that it only requires one water-quality measurement. The method does not assume any knowledge about the characteristics of the water column covering the underwater target. The correction is based on Equation (1), with water depth z taken to be half of the considered depth range (*e.g.* assuming water depth in the range of 0.0 m to 3.0 m, $z = 1.5$ was chosen) and water quality assumed to be water type Q1. This means that the optically deep water reflectance and the diffuse attenuation coefficient measured at site Q1 are used when a new reference spectrum is calculated. The use of water type Q1 helps to preserve more features of the reference spectra compared to more turbid waters. A new water-column–corrected reference spectrum for each benthic cover type was calculated using Equation (1) and used in the classification instead of the original measured spectra.

Classification of Synthetic Data

The assessment of classification accuracy was performed using simulated data instead of real images. Studies exploring benthic cover-type mapping have usually been done using the maximum likelihood classifier or the spectral angle mapper (SAM). Tuominen and Lipping (2012) tested the accuracy of classification methods in benthic mapping. Four classification methods were tested with and without water-column correction:

(1) Euclidean distance (ED) classifier
(2) SAM classifier
(3) Spectral correlation mapper (SCM) classifier
(4) Spectral information divergence (SID) classifier

SAM is a method for directly comparing image spectra to a known spectrum (usually determined in a laboratory or in the field with a spectrometer). This method treats both spectra (the questioned and known) as vectors and calculates the spectral angle between them (Kruse *et al.* 1993). The SID classifier represents a theoretic approach to hyperspectral classification, comparing the similarity between two pixels by measuring the probabilistic discrepancy between two corresponding spectral signatures (Chang 2000).

The SCM measure is defined by Carvalho and Meneses (2000) as

$$R = \frac{\sum (X - \bar{X})(Y - \bar{Y})}{\sqrt{\sum (X - \bar{X})^2 \sum (Y - \bar{Y})^2}}, \quad (5)$$

where X is the image spectrum, Y is the reference spectrum, and $\bar{X}$ and $\bar{Y}$ are means of the corresponding spectrum vectors.

The Euclidean distance measure is defined as

$$ED(s_r, s_i) = ||s_r, s_i|| \equiv \left[\sum_{l=1}^{L} (s_{rl} - s_{il})^2 \right]^{0.5}, \quad (6)$$

where s_r is the reference spectrum and s_i is the image spectrum.
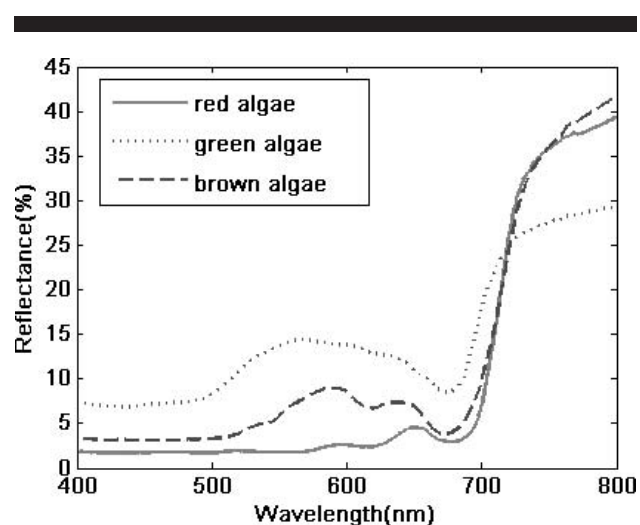
Figure 4. Average reflectance spectra of the studied benthic vegetation types.

Complete details and results of classifier assessment can be found in Tuominen and Lipping (2012). Based on these results, the SCM and ED classifiers were chosen for this study. The whole data set, containing 7200 spectra, was classified using the SCM classification. Water-column correction was not employed, *i.e.* the original spectra of the benthic cover type classes shown in Figures 4 and 5 were used as reference spectra. Each spectrum of the simulated data set was assigned to one of the six classes according to correlation criteria R. The same simulated data set was classified using the ED classifier with water-column correction. Each spectrum of the simulated data set was assigned to one of the six classes according to minimum distance criteria. Classification of synthetic data was

Figure 5. Reflectance spectra of studied nonvegetation benthic cover types.

followed by the assessment of mapping accuracy. The depth ranges under study were 0.0–1.0 m, 0.0–2.0 m, and 0.0–3.0 m.

RESULTS AND DISCUSSION

Three reflectance spectra of each algae sample were measured and the average spectrum of each cover type was used in the following data-generation and classification procedures (Figure 4). All measured vegetation types have high reflectance in the near-i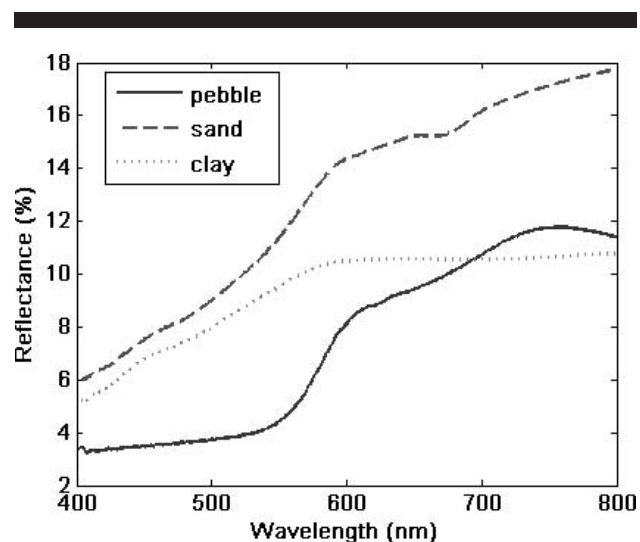nfrared part of the spectrum. The green algae have a more gentle red-edge slope compared to the other algae. The reflectance of green algae is higher than that of the two other algae types in the visible part of the spectrum. Red and green algae have very similar spectra in the near-infrared range. Brown algae have a double peak in reflectance spectra near 590 nm and 640 nm. Red algae have slightly increased reflectance near 590 nm and a stronger peak near 650 nm. Green algae have local reflectance maxima near 580 nm. The most distinctive difference between red and brown algae is the reflectance peak of brown algae near 590 nm. In addition to higher reflectance, the spectrum of the green algae also differs from those of the other two in shape—there are no clear reflectance peaks in the visible part of the spectrum. The measured spectra of green and brown algae are similar to those measured at other parts of the Baltic Sea (Kutser, Vahtmäe, and Metsämaa, 2006). However, the spectra of red algae differ from that measured by Kutser *et al.*, most likely due to the use of different species of red algae: *Furcellaria lumbricalis* seems to have a very similar double-peak spectrum to the brown algae, while *Ceramium tenuicorne* has only one reflectance peak near 650 nm.

In general, the measured nonvegetation spectra resemble each other in shape (Figure 5). Sand and clay have higher reflectance spectra than the algae in the visible range. The reflectances of sand and clay are very similar in shape. Pebble has a steeper slope around 575 nm, and its reflectance decreases above 750 nm compared with sand spectra. The reflectance of clay increases slowly when the wavelength lengthens from 400 nm to around 600 nm and remains almost constant above 600 nm.

When the measurements of optically deep reflectances were compared to published results measured at the Baltic Sea and spectra obtained using bio-optical modelling, it was obvious that the measured spectra contain a significant amount of sun and sky glint (Ficek, Zapadka, and Dera, 2011; Vahtmäe *et al.*, 2006). Three repeated measurements of the same target have considerable variation in the blue green part of the spectrum (Figure 6). The reflectance in the blue part of the spectrum should be considerably lower in CDOM-dominant coastal waters of the Baltic Sea. The oxygen absorption feature near 760 nm is clearly visible in the first measurement. The depth of the absorption feature is lower in the second and third measurements. The sun-glint correction based on the absorption depth removes most of the glint, but reflectance in the blue and near-infrared parts of the spectrum should still be somewhat lower. This indicates that there is probably some sky glint left in the spectra.

In general, sun-glint–corrected optically deep reflectances are quite similar in shape (Figure 7). All measured spectra
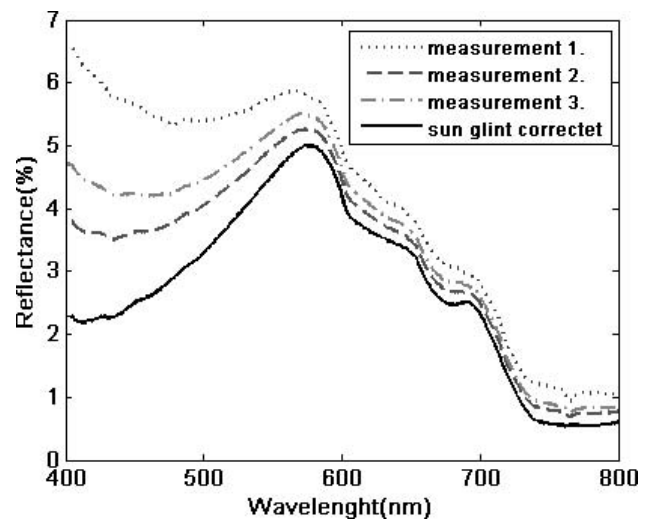
Figure 6. Three measurements of optically deep water reflectance at site Q4 and the sun-glint–corrected spectrum used in the generation of synthetic data.

have a reflectance peak near 570 nm. Water type Q4 has higher reflectance in the blue-red part of the spectrum compared with the other water types, whereas Q1 has higher reflectance in the blue part of the spectrum. Although there seems to be some amount of sun and sky glint left in the spectra, they can be considered useable in this study. Such glint-induced distortion is often present in real remote-sensing images as well.

The diffuse attenuation coefficient was calculated using the spectral measurements of the submerged reference plate (Figure 8). All measured water types have an attenuation
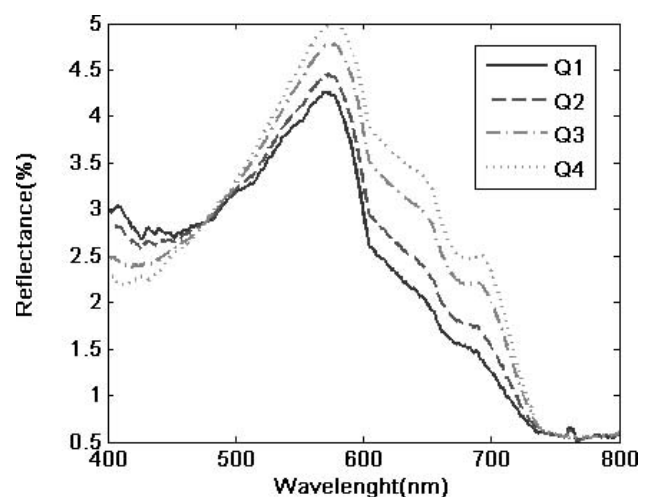
Figure 7. Average reflectance spectra of the sun-glint–corrected optically deep water reflectances.

Figure 8. Attenuation coefficients of the measured water types.

Figure 9. Simulated reflectance spectra representing the spectrum of brown algae through water columns of various heights. The simulated water type is Q1.

minimum near 570 nm. Attenuation increases when the wavelength gets shorter in the blue range of the visible part of the spectrum. All water types have attenuation maxima near 770 nm. The attenuation of water type Q1 is slightly higher when compared with that of clear lakes in South Finland (Reinart *et al.*, 2003). The attenuation of water type Q4 is slightly lower than in moderate lakes. Jerlov (1976) has formally classified oceanic water types according to their optica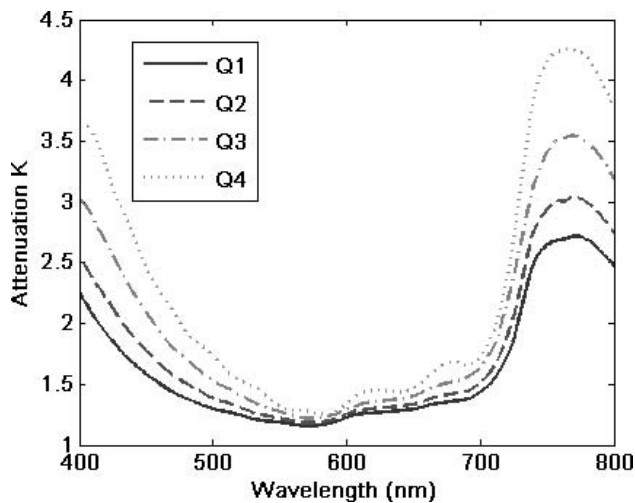l attenuation properties using nine categories. The attenuation of water type Q1 is close to that of Jerlov's category 9, representing the most turbid waters. The attenuations of types Q2, Q3, and Q4 exceed that of Jerlov's category 9.

The water-quality measurements as well as the measured spectra of benthic cover types were used to generate a simulated data set. The confounding effect of the variable water column is clearly visible in the simulated spectra (Figure 9). The spectral features of brown algae are just barely visible when the depth of the water column is 90 cm.

Accuracy for each class together with the overall accuracy of the SCM classifier without water-column correction is presented in Table 1. The overall mapping accuracy varies according to water quality. At a depth range of 0.0–3.0 m, the best overall accuracy, 47.8%, is achieved when the water quality is Q1, and the accuracy deteriorates to 33.7% at water quality Q4. This result can be expected when the attenuation characteristics of the water classes are considered (see Figure 8). The classification of red alga shows better accuracy compared with the other alga types. The mapping accuracy of sand is very modest, varying from 8.9% to 5.3%, according to the water quality (depth range 0.0–3.0 m). The random classification of six classes would produce a mapping accuracy of 9.09% for each class.

Table 2 presents the confusion matrix of the SCM classifier without water-column correction using water type Q1 and depth range 0.0–3.0 m. The most noticeable detail in the confusion matrix is the huge amount of commission errors in
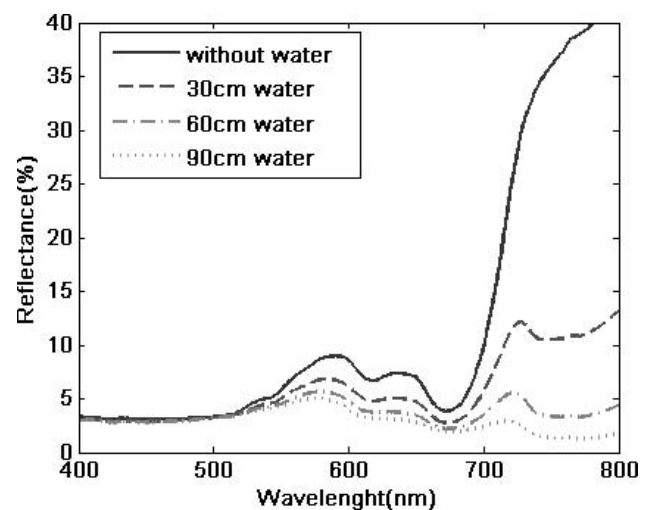
the clay class. The classes of red and green algae were mixed to each other, as were the classes of green and brown algae. Green algae, pebble, and sand were commonly classified as clay.

The mapping accuracy for each class as well as the overall accuracy of the ED classifier with water-column correction is presented in Table 3. As with the SCM classifier, this method was evaluated using three different water depth ranges; the overall mapping accuracy varies according to water quality. At a depth range of 0.0–3.0 m, the best overall accuracy, 66.0%, is achieved when water quality is Q1, and accuracy deteriorates to 50.4% when the water quality is Q4. Two classes, those of red and brown algae, have better classification accuracy compared to other classes. The overall mapping accuracies are better than those obtained without water-column correction. The variation of mapping accuracy between classes is modest when compared to the results obtained without water-column correction.

Table 4 presents the confusion matrix of ED classification with water-column correction using water quality Q1 and depth range 0.0–3.0. Two classes, red and brown algae, are misclassified as pebble whereas green algae are misclassified as clay. The poor classification accuracy of sand is mostly due to the large number of omission errors. The amount of omission errors in the pebble class is quite small, but the amount of commission errors deteriorates the classification accuracy.

Results showed that water quality varies significantly within the studied area. The impact of this variation is clearly shown in the classification results. The benthic mapping method can be considered operational when the discrimination accuracy of cover types exceeds 80%. The ED classifier together with simple water-column correction can almost fulfil this criterion up to depths of 2 m when water quality is Q1. When turbidity increases and water quality is Q4, depths slightly less than 1 m could be mapped with such accuracy. Vahtmäe *et al.* (2006)

Table 1. *Mapping accuracy of the SCM classifier without water-column correction. All data other than depth are presented in percentages.*

Quality	Depth Range (m)	Red Algae	Green Algae	Brown Algae	Pebble	Sand	Clay	Overall
Q1	0.0–1.0	100.0	100.0	100.0	70.0	29.0	58.5	83.2
	0.0–2.0	100.0	47.6	53.0	35.0	14.5	37.4	62.1
	0.0–3.0	72.0	24.2	35.3	23.3	8.9	32.1	47.8
Q2	0.0–1.0	100.0	87.0	85.0	55.0	19.5	50.5	77.3
	0.0–2.0	84.0	32.6	42.5	27.5	10.8	34.2	53.8
	0.0–3.0	59.8	19.3	28.3	18.3	7.4	28.7	41.4
Q3	0.0–1.0	100.0	70.7	70.0	44.0	16.7	44.6	71.0
	0.0–2.0	65.5	23.7	35.0	22.0	9.1	31.6	46.4
	0.0–3.0	43.7	17.5	23.3	14.7	6.3	25.1	36.5
Q4	0.0–1.0	100.0	57.6	61.0	37.0	14.3	40.5	65.8
	0.0–2.0	55.0	20.5	30.5	18.5	7.8	29.2	42.2
	0.0–3.0	37.0	16.2	20.3	12.3	5.3	23.4	33.7

Table 2. *Confusion matrix of the SCM classifier without water-column correction.*

True/Result	Red Algae	Green Algae	Brown Algae	Pebble	Sand	Clay
Red algae	216	84	0	0	0	0
Green algae	0	140	0	0	0	160
Brown algae	0	194	106	0	0	0
Pebble	0	0	0	70	26	204
Sand	0	0	0	0	29	217
Clay	0	0	0	0	0	300

Table 3. *Mapping accuracy of the ED classifier with water-column correction. All data other than depth are presented in percentages.*

Quality	Depth Range (m)	Red Algae	Green Algae	Brown Algae	Pebble	Sand	Clay	Overall
Q1	0.0–1.0	100.0	90.0	100.0	100.0	75.4	84.2	95.3
	0.0–2.0	85.0	61.5	80.0	84.3	37.8	48.5	76.5
	0.0–3.0	76.0	48.0	69.1	53.0	29.1	34.9	66.0
Q2	0.0–1.0	96.0	75.0	90.0	87.7	58.9	74.1	88.5
	0.0–2.0	71.0	52.4	67.0	60.2	39.2	44.8	69.5
	0.0–3.0	63.3	42.6	58.4	44.0	26.0	27.4	58.6
Q3	0.0–1.0	83.0	65.0	78.0	72.0	52.9	64.7	81.3
	0.0–2.0	61.0	46.5	58.0	52.1	30.4	39.4	63.7
	0.0–3.0	54.3	38.1	50.7	38.65	24.0	25.4	53.7
Q4	0.0–1.0	74.0	59.0	71.0	64.5	48.4	59.5	76.7
	0.0–2.0	54.5	42.2	52.5	47.8	28.4	35.5	59.8
	0.0–3.0	48.3	34.7	45.9	34.8	22.8	24.7	50.4

Table 4. *Confusion matrix of ED classification with water-column correction.*

True/Result	Red Algae	Green Algae	Brown Algae	Pebble	Sand	Clay
Red algae	228	0	0	72	0	0
Green algae	0	203	0	0	0	97
Brown algae	0	0	212	88	0	0
Pebble	0	25	7	254	14	
Sand	0	76	0	0	114	110
Clay	0	22	0	23	78	177

indicated that the depth at which sandy bottom can be detected in CDOM-rich estuaries is quite limited (1–3 m). This result is well in coherence with the findings of our study.

Karpouzli *et al.* (2003) concluded that the results of studies in which single measurements of "average" attenuation are used to depth-correct remotely sensed imagery should be interpreted with a high degree of caution. One water-quality measurement is certainly not enough to provide reasonable coverage. Yet the results of this study showed that mapping accuracy can be improved even when a simple correction technique using only one water-quality measurement is employed. In addition to improved accuracy, water-column correction considerably decreased the variation in accuracy between classes.

CONCLUSIONS

In this study the feasibility of benthic cover-type mapping in turbid waters near estuaries using hyperspectral remote sensing was explored. The analysis of measured benthic spectra showed that differences between cover types can be quite subtle; however, they can be discriminated from each

other. The study was based on the analysis of a simulated data set generated using *in situ* measurements of benthic cover types and water-quality parameters. Benthic mapping methods and studies should always be validated using real images. Unfortunately the excessive cost of an airborne hyperspectral flight campaign together with related fieldwork prevented this, and simulations were used instead. Therefore the current study should be regarded as a promising early investigation that must be followed up with validation using real images. Results indicate that hyperspectral remote sensing could provide usable results in areas near outer islands further away from the coastline, as well as in coastal areas which are not in the immediate vicinity of the river mouth. In highly CDOM-rich brown estuarine waters, feasible depths are so modest that the use of remote sensing–based mapping is hardly meaningful. The results also show that water quality can vary significantly within a quite small geographic area near an estuary. A water-column correction method that accounts for variation in water quality would very likely provide better results than the simple method used in this study.

ACKNOWLEDGMENTS

LITERATURE CITED

Armstrong, R.; Guild, L.; Gilbes, F.; Lobitz, B., and Detres, Y., 2007. Water column corrections of AVIRIS data for hyperspectral characterization of benthic marine communities in Puerto Rico. *In: Proceedings of the 5th EARSeL workshop on imaging Spectroscopy* (Bruges, Belgium), pp. 1–6.

Bertels, L.; Vanderstraete, T.; Van Coillie, S.; Knaeps, E.; Sterckx, S.; Goossens, R., and Deronde, B., 2008. Mapping of coral reefs using hyperspectral CASI data; a case study: Fordata, Tanimbar, Indonesia. *International Journal of Remote Sensing*, 29(8), 2359–2391.

Carvalho, O.A. and Meneses, P.R., 2000. Spectral Correlation Mapper (SCM): An improvement on the Spectral Angle Mapper (SAM). *Proceedings of the 9th Airborne Earth Science Workshop*. Pasadena, California: JPL Publication, *00–18*, pp. 65–74.

Chang, C.I., 2000. An information theoretic-based approach to spectral variability, similarity and discriminability for hyperspectral image analysis. *IEEE Transactions on Information Theory*, 46(5), 1927–1932.

Darecki, M. and Stramski, D., 2004. An evaluation of MODIS and SeaWiFS bio-optical algorithms in the Baltic Sea. *Remote Sensing of Environment*, 89(3), 326–350.

Dekker, A.G.; Brando, V.E.; Anstee, J.M.; Pinnel, N.; Kutser, T., and Hoogenboom, E.J., 2001. Imaging spectrometry of water. *In:* Van der Meer, F.D. and De Jong, S.M. (eds.), *Imaging Spectrometry: Basic Principles and Prospective Applications*. Dordrecht, Netherlands: Kluwer Academic Publishers, pp. 307–360.

Ficek, D.; Zapadka, T., and Dera, J., 2011. Remote sensing reflectance of Pomerian lakes and the Baltic. *Oceanologia*, 53(4), 959–970.

Gons, H.J.; Ebert, J., and Kromkamp, J., 1998. Optical teledetection of the vertical attenuation coefficient for downward quantum irradiance of photosynthetically available radiation in turbid inland waters. *Aquatic Ecology*, 31(3), 299–311.

Jerlov, N.G., 1976. *Marine Optics*. Amsterdam: Elsevier, 231p.

Juanes, J.A.; Guinida, X.; Puente, A., and Revilla, J.A., 2008. Macroalgae, a suitable indicator of the ecological status of coastal rocky communities in the NE Atlantic. *Ecological Indicators*, 8(4), 351–359.

Karpouzli, E.; Malthus, T.; Place, C.; Chui, A.M.; Garcia, M.I., and Mair, J., 2003. Underwater light characterization for correction of remotely sensed images. *International Journal of Remote Sensing*, 24(13), 2683–2702.

Kohonen, T., 2003. Finnish strategies for reduction and control of effluents to the marine environment—examples from agriculture, municipalities and industry. *Marine Pollution Bulletin*, 47(1–6), 162–168.

Kowalczuk, P.; Stoń-Egierta, J.; Cooper, W.J.; Whitehead, R.F., and Durako, M.J., 2005. Characterization of chromophoric dissolved organic matter (CDOM) in the Baltic Sea by excitation emission matrix fluorescence spectroscopy. *Marine Chemistry*, 96(3–4), 273–292.

Kruse, F.A.; Lefkoff, A.B; Boardman, J.W.; Heidebrecht, K.B.; Shapiro, A.T.; Barloon, P.J., and Goetz, A.F.H., 1993. The Spectral image processing system (SIPS)—interactive visualization and analysis of imaging spectrometer data. *Remote Sensing of Environment*, 44(2–3), 145–163.

Kutser, T. and Jupp, D.L.B., 2002. Mapping coral reef benthic habitat with a hyperspectral space borne sensor. *In: Proceedings of Ocean Optics XVI* (Santa Fe, New Mexico).

Kutser, T.; Kotta, J.; Vahtmäe, E.; Pärnoja, M.; Möller, T., and Lennuk, L., 2011. Using high spatial resolution remote sensing, spatial modelling and web map services for spatial planning in shallow coastal water environments. *In: Proceedings of the 34th International Symposium on Remote Sensing of Environment* (Sydney, Australia).

Kutser, T.; Miller, I., and Jupp, D.L.B., 2006. Mapping coral reef benthic substrates using hyperspectral space-borne images and spectral libraries. *Estuarine, Coastal and Shelf Science*, 70(3), 449–460.

Kutser, T.; Vahtmäe, E., and Martin, G., 2006. Assessing suitability of multispectral satellites for mapping benthic macroalgal cover in turbid coastal waters by means of model simulations. *Estuarine, Coastal and Shelf Science*, 67(3), 521–529.

Kutser, T.; Vahtmäe, E., and Metsämaa, L., 2006. Spectral library of macroalgae and benthic substrates in Estonian coastal waters. *Proceedings of Estonian Academy of Sciences, Biology-Ecology*, 55(4), 329–340.

Kutser, T.; Vahtmäe, E., and Praks, J., 2009. A sun glint correction method for hyperspectral imagery containing areas with non-negligible water leaving NIR signal. *Remote Sensing of the Environment*, 113(10), 2267–2274.

Louchard, E.M.; Reid, R.P.; Stephens, F.C.; Davis, C.O.; Leathers, R.A., and Downes, T.V., 2003. Optical remote sensing of benthic habitats and bathymetry in coastal environments at Lee Stocking Island, Bahamas: a comparative spectral classification approach. *Limnology and Oceanography*, 48(1), 511–521.

Lynzega, D.R., 1978. Passive remote sensing techniques for mapping water depth and bottom features. *Applied Optics*, 17(3), 379–383.

Lynzega, D.R., 1981. Remote sensing of bottom reflectance and water attenuation parameters in shallow water using aircraft and Landsat data. *International Journal of Remote Sensing*, 2(1), 71–82.

Maritorena, S.; Morel, A., and Gentili, B., 1994. Diffuse reflectance of oceanic shallow waters: influence of water depth and bottom albedo. *Limnology and Oceanography*, 39(7), 1689–1703.

Meiner, A., 2010. Integrated maritime policy for the European Union—consolidating coastal and marine information to support maritime spatial planning. *Journal of Coastal Conservation*, 14(1), 1–11.

Mishra, D.R.; Narumalani, S.; Rundquist, D.; Lawson, M., and Perk, R., 2007. Enhancing the detection and classification of coral reef and associated benthic habitats: a hyperspectral approach. *Journal of Geophysical Research*, 112(C08014), 1–11.

Mobley, C.D.; Sundman, L.K.; Davis, C.O.; Bowles, J.H.; Downes, T.V.; Leathers, R.A.; Montes, M.J.; Bissett, W.P.; Kohler, D.D.R.; Reid, R.P.; Louchard, E.M., and Gleason, A., 2005. Interpretation

of hyperspectral remote-sensing imagery by spectrum matching and look-up tables. *Applied Optics*, 44(17), 3576–3592.

Mumby, P.J.; Clark, C.D.; Green, E.P., and Edwards, A.J., 1998. Benefits of water column correction and contextual editing for mapping coral reefs. *International Journal of Remote Sensing*, 19(1), 202–210.

Mumby, P.J.; Green, E.P.; Edwards, A.J., and Clark, C.D., 1999. The cost effectiveness of remote sensing for tropical coastal resources assessment and management. *Journal of Environmental Management*, 55(3), 157–166.

Phinn, S.R.; Dekker, A.G.; Brando, V.E., and Roelfsema, C.M., 2005. Mapping water quality and substrate cover in optically complex coastal and reef waters: an integrated approach. *Marine Pollution Bulletin*, 51(1–4), 459–469.

Reinart, A.; Herlevi, A.; Arst, H., and Sipelgas, L., 2003. Preliminary optical classification of lakes and coastal waters in Estonia and south Finland. *Journal of Sea Research*, 49(1), 357–366.

Siegel, D.A. and Dickey, T.D., 1987. Observations of the vertical structure of the diffuse attenuation coefficient spectrum. *Deep-Sea Research*, 34(4), 547–563.

Tuominen, J. and Lipping, T., 2012. Assessment of hyperspectral classification methods for benthic cover type mapping. *In: Proceedings of the IEEE International Geoscience and Remote Sensing Symposium* (Munich, Germany), pp. 4837–4840.

Vahtmäe, E. and Kutser, T., 2007. Mapping of bottom type and water depth in shallow coastal waters with satellite remote sensing. *In: Proceedings of the 9th International Coastal Symposium* (Gold Coast, Australia). Journal of Coastal Research, Special Issue No. 50, pp. 185–189.

Vahtmäe, E.; Kutser, T.; Martin, G., and Kotta, J., 2006. Feasibility of hyperspectral remote sensing for mapping macroalgal cover in turbid coastal waters—a Baltic Sea case study. *Remote Sensing of Environment*, 101(3), 342–351.

Chapter 9

Publication P3

Tuominen, J. and Lipping, T. (2016). Spectral Characteristics of Common Reed Beds: Studies on Spatial and Temporal Variability *Remote Sensing*, 8(3): 181

Spectral Characteristics of Common Reed Beds: Studies on Spatial and Temporal Variability

Jyrki Tuominen * and Tarmo Lipping

Information Technology, Tampere University of Technology, Pohjoisranta 11 A, 28100 Pori, Finland; tarmo.lipping@tut.fi
* Correspondence: jyrki.tuominen@student.tut.fi; Tel.: +358-41-75-22-222

Abstract: Reed beds are the second largest producer of biomass in Olkiluoto Island. Quantitative information on the extent and amount of reed stands is an integral part of the biosphere assessment related to long-term safety analysis of nuclear fuel repository site currently under construction. The major challenge in reed bed mapping is discrimination between reed and other green vegetation. Spectral field measurements were used to study the temporal and spatial variability of spectral characteristics of reed beds. Feasibility of discriminating reed beds from other vegetation based on hyperspectral measurements was studied as well. Results indicate that there is large temporal variation of reed bed spectra and the optimal time for data acquisition differs for old and new reed bed types. Comparing spectral characteristics of the reed bed and meadow classes in a local neighborhood indicated that the classes have high within-class spectral variability and similar mean spectra, however, 10 out of 11 targets had lower angle to the mean spectrum of the corresponding class than that of the other class when Spectral Angle Mapper (SAM) was used. Comparing the spectral characteristics of reed beds at four test sites within the Olkiluoto Island indicated that while some of the sites had similar spectra, the difference between others was remarkable. This is partly explained by different density and height of dead and live reed stems at the four sites.

Keywords: reed beds; spectral variability; remote sensing

1. Introduction

Common reed (*Phragmites Australis*), a native helophyte in coastal areas of the Baltic Sea, has significantly spread on the Finnish coast during the last decades raising ecological issues and concerns due to the important role it plays in the ecosystem dynamics of shallow coastal areas [1]. In addition to biodiversity there are other ecological and economic issues such as water protection, bioenergy, construction, farming and landscape. Reed beds have proven to be effective in the treatment of waste waters such as domestic sewage and industrial discharge containing heavy metal wastes [2]. Reed biomass can be used as an energy source in three ways, namely by combustion, biogas production and biofuel production [3]. There are currently studies aiming to develop economical and sustainable methods to harvest reed for bioenergy production in Finland. Reed can be used as a soil conditioner in agriculture thus substituting the use of fertilizers [4].

Recent developments in sensor technology and data processing methods have led to an increase in the use hyperspectral imagery for environmental applications. High spectral and spatial resolution imagery provides researchers the potential to map vegetation at species' level, provided the plant species under study are spectrally distinct [5]. Species discrimination using remote sensing is based

on the assumption that each species is characterized by a set of unique biophysical features and biochemical composition that control the variability in its spectral signature [6].

The fundamental problem in vegetation discrimination using remote sensing is that there is an overall qualitative similarity in the spectral reflectance of green plant species. Furthermore, the assumption that individual plant species have unique spectral signatures may be wrong. Price [7] has argued that several species may actually have quantitatively similar spectra due to the spectral signature variation present within a species.

The capability of discriminating plant species using hyperspectral imagery has been demonstrated in many studies. Clark *et al.* [8] successfully discriminated tropical rain forest tree species. Schmidt and Skidmore [9] studied the discrimination of vegetation types in coastal wetlands. Thenkabail [10] used hyperspectral data to discriminate agricultural crops. Vahtmäe *et al.* [11] demonstrated the feasibility of hyperspectral remote sensing for mapping benthic microalgae cover. The remote sensing of wetlands does, to some extent, differ from remote sensing based mapping of other terrestrial features. Differences exist because wetlands occupy a unique interface between aquatic and terrestrial ecosystems [12]. In addition, the reflectance spectra of wetland vegetation canopies are often very similar and are combined with reflectance spectra of underlying soil [13]. The frequent and rapid changes of water depth and salinity add to the complexity of analyzing wetland environment using remote sensing.

The use of remote sensing in reed bed discrimination has been studied in several publications. Pengra *et al.* [14] evaluated the use of the spaceborne Hyperion sensor. The classification of reed beds showed good overall accuracy of 81.4%. It was found, however, that the small size and spatial arrangement of *Phragmites* stands was less than optimal considering Hyperion's spatial resolution of 30 m. Lopez *et al.* [15] studied the discrimination of *Phragmites* using airborne hyperspectral data collected by the Probe-1 sensor. The study produced *Phragmites* maps showing an estimated accuracy of 80%. Onojeghuo and Blackburn [16] proposed the use of airborne hyperspectral and LiDAR data in reed bed discrimination. A comprehensive set of methods such as Principal Component Analysis (PCA), Spectrally Segmented PCA (SSPCA) and Minimum Noise Fraction (MNF) were applied to the hyperspectral data and combined with LiDAR derived measures including those based on texture analysis. A significant improvement (+11%) in the accuracy of reed bed delineation was achieved when a LiDAR-derived Canopy Height Map (CHM) was used together with the optimal SSPCA data set. Stratoulias *et al.* [17] used airborne AISA Eagle data in order to derive narrow band spectral indices used to characterize reed beds' ecological status. Seasonal time-series studies can provide important information on spectral variability. Given the dynamic character of vegetation cover, a snapshot in time is not nearly as revealing as a time sequence [18]. Ouyang *et al.* [19] studied the spectral characteristics of *Phragmites* and two other wetland species using time-series analysis. The results showed that differences among saltmarsh communities' spectral characteristics were affected by their phenological stages. Artigas and Yang [20] published a field-collected seasonal time-series of *Phragmites* spectra. The measured spectra were used to determine the vigor gradient of plants in marshlands.

Several measures have been proposed to quantify spectral similarity or separability of targets [21], Euclidean Distance (ED) being probably the most well-known measure used. Spectral Angle Mapper (SAM) is another well-established similarity measure in remote sensing applications. SAM is related to Pearson's Correlation Coefficient, sometimes also called Spectral Correlation Mapper (SCM) in remote sensing literature. An advantage of Pearson's Correlation Coefficient over SAM is its ability to distinguish between negative and positive correlation. Spectral Information Divergence (SID) classifier represents an information theoretic approach to hyperspectral classification. SID compares the similarity between two spectra by measuring the probabilistic discrepancy between two corresponding spectral signatures. In principle, the similarity between two spectra has two components: similarity in absolute level of reflectance and similarity in spectral shape. In this study, both of these components of similarity are assessed using the Euclidean Distance and Spectral Angle measures. Jeffries–Matusita distance (JM) was used as a statistical separability measure.

Reed beds cover significant part of the shoreline of the Olkiluoto Island. Reed can be found on gyttja, clay, till or stone bottoms [22]. The extent and vitality of the reed beds varies significantly, depending on the soil type and degree of shelter [22]. A repository site for spent nuclear fuel is currently under construction in Olkiluoto. The disposal is planned to begin in 2022. The results of reed bed studies will be used as input data to the biosphere assessment exercise for the safety analysis of the spent nuclear fuel repository at Olkiluoto [23]. Common reed is a major producer of biomass among wetland species in Olkiluoto and it has significant potential to store and transport radionuclides. Therefore, quantitative information on the extent and biomass of reed stands is an integral part of long-term biosphere assessment. The overall aim of this study is to determine temporal and spatial spectral variability of reed beds in the Olkiluoto Island. More specifically, the objectives of this study are: (1) to characterize the spectral properties of the dominant wetland species *Phragmites Australis* in different phenological stages and to identify the most suitable time to discriminate it from other green vegetation; (2) to study the spatial variability of reed spectra and evaluate the effects of this variability on reed bed mapping; and (3) to suggest promising methods to be used in reed bed mapping.

2. Data and Methods

2.1. Study Area

The main study area is located at the Olkiluoto Island (61°14′23.126′′N, 21° 28′55.58′′E) in southwest Finland (Figure 1). The surface area of Olkiluoto is 12 square kilometers and it is separated from the continent by a narrow strait [22]. Because of long shoreline, coastal ecosystems form a significant part of its nature [22]. The temporal changes in the environment in the coastal zone are rapid because the surrounding sea areas are shallow. The general eutrophication of the Baltic Sea is contributing to these changes by increasing the amount of organic matter in the shallow bays. Another important factor is the post-glacial land uplift [24].
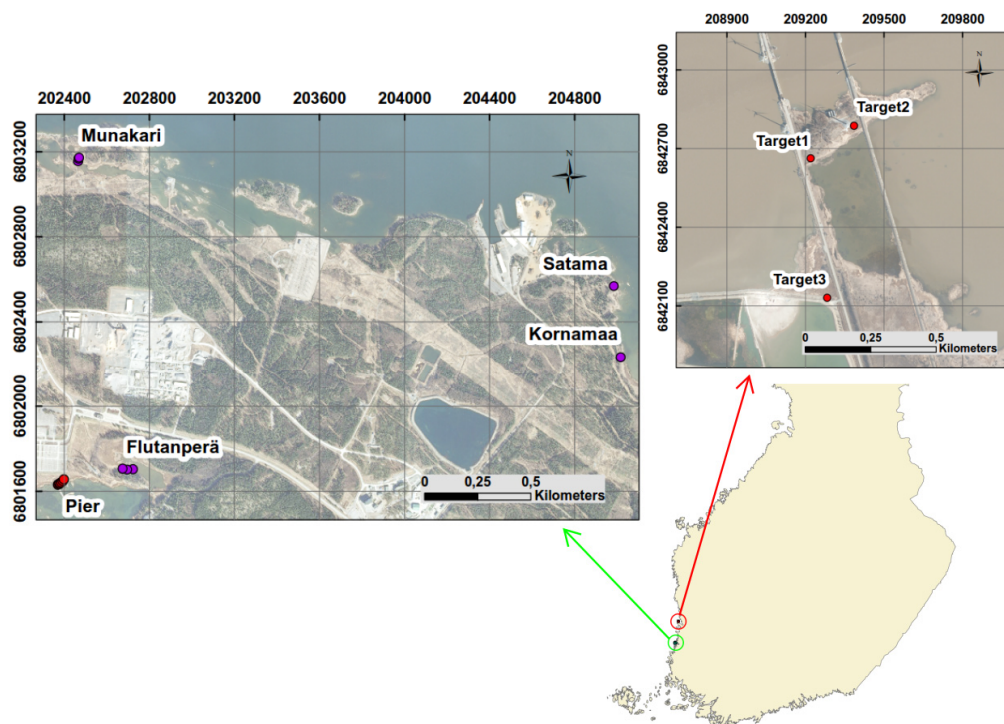
Figure 1. Overview of the study sites Olkiluoto (**left**) and Hilskansaari (**right**).

There are currently two operational nuclear reactors on the island, Olkiluoto 1 and Olkiluoto 2, while a third reactor, Olkiluoto 3, is under construction. In addition, a decision has been made on

the construction of a spent nuclear fuel repository on the island. Another study site, Hilskansaari Island, is located 40 km north of Olkiluoto (Figure 1). The phenological phases of reed beds and the weather conditions at Hilskansaari are similar to those in Olkiluoto. However, due to the effects of the Kokemäenjoki river, the water around Hilskansaari is more turbid and of less salinity. Hilskansaari was chosen as a separate study site in order to broaden the range of underlying environmental conditions and because it was more convenient for multi-temporal measurements as access to Olkiluoto is limited.

2.2. Spectral Field Measurements

All spectral field measurements of reed beds and other vegetation were carried out in the same manner. Reflectance spectra of reed beds were measured using a portable GER 1500 spectroradiometer (Spectra Vista Corporation, Poughkeepsie, NY, USA). The spectral range of the instrument is 300–1100 nm. Spectra were sampled at 1.5 nm intervals, and spectral resolution of the GER 1500 instrument is 3 nm. Reflectance was calculated as the ratio of radiance from the measured object to the radiance from the reflectance standard, *i.e.*, a 99% Spectralon panel. The fiber optic light guide connected to the instrument was raised above the reed bed using a six-meter long fiberglass pole. The end of the optical fiber was placed above plant canopies at a distance of approximately four meters from the canopy. This arrangement provided a nadir view of the reed bed. The field-of-view of the optical fiber is 25 degrees, resulting in circular measurement area of 1.7 meters in diameter. Three repeated measurements at each measurement point were taken and the results were averaged. Each individual measurement was calibrated using a reflectance standard.

The partial spectra of reed beds, described in Section 3.5, were measured using a GER1500 instrument equipped with 2.4-meter-long optical fiber. The material under study was spread on a dark plate on the ground. The end of the fiber was approximately 15 centimeters above the sample. The samples of dead stems, dead inflorescence and live leafs were measured at site Pier, Olkiluoto, on 27 July 2012. The sample of live inflorescence was measured at site Kornamaa, Olkiluoto, on 14 August 2012.

In order to provide reference for the within-class variability studies, spectral field measurements made on 17 August 2010 near Olkiluoto were used. The target was a well-kept grass field in Otanlahti, Rauma. The reflected light from grass canopy at the wavelength range of 350–2500 was measured using a portable field spectroradiometer FieldSpec Pro from Analytical Spectral Devices Inc. ASD (Boulder, CO, USA). The spectral resolution of the device is 3 nm between 350–1000 nm and 10 nm between 1000 and 2500 nm. A total of 7 measurements were made along a straight line using three-meter intervals. The instrument was equipped with a 1.4-meter-long fiber optic light guide. The end of the optical fiber was placed above grass canopy at a distance of approximately 1.2 meters. This arrangement provided a nadir view of the grass field. The field-of-view of the optical fiber is 25 degrees resulting in circular measurement area of 0.5 meters in diameter.

The information related to spectral field measurements used in this study, including date of acquisition, air temperature, relative humidity and water height, is presented in Table 1. The section of the paper describing the respective spectra is also indicated in the table.

Table 1. Spectral field measurements used in this study. The water height is given in centimeters using a Finnish N2000 system. The temperature, humidity and water height data are the courtesy of Finnish Meteorological Institute.

Date	Location	Target	Section	Sensor	T(°c)	Relative Humidity	Water Heigh	Stage
12 June 2012	Hilskansaari	1,2 and 3	3.1, 3.2	GER1500	18	60%	10	Vegetative growth
21 June 2012	Hilskansaari	1,2 and 3	3.1, 3.2	GER1500	14	48%	12	Vegetative growth
29 June2012	Hilskansaari	1,2 and 3	3.1, 3.2	GER1500	19	40%	17	Vegetative growth
9 July 2012	Hilskansaari	1,2 and 3	3.1, 3.2	GER1500	18	94%	8	Vegetative growth
18 July 2012	Hilskansaari	1,2 and 3	3.1, 3.2	GER1500	19	49%	29	Vegetative growth
20 July 2012	Olkiluoto	Haircap Moss	3.2	GER1500	19	56%	31	
20 July 2012	Olkiluoto Pier	4 Meadows	3.3	GER1500	19	56%	31	
27 July 2012	Olkiluoto, Pier	3 partial spectra	3.5	GER1500	18	88%	21	Vegetative growth
27 July 2012	Olkiluoto, Pier	Reed bed ($n = 7$)	3.3	GER1500	18	88%	21	Vegetative growth
10 August 2012	Hilskansaari	1,2 and 3	3.1, 3.2	GER1500	16	48%	20	Flowering
14 August 2012	Kornamaa	partial spectra	3.5	GER1500	21	50%	8	Flowering
14 August 2012	Kornamaa, Munakari	Reed beds ($n = 3$)	3.4	GER1500	21	50%	8	Flowering
15 August 2012	Flutanperä, Satama	Reed beds ($n = 3$)	3.4, 3.5	GER1500	23	53%	6	Flowering
5 September 2012	Hilskansaari	1,2 and 3	3.1, 3.2	GER1500	16	59%	34	Flowering
25 September 2012	Hilskansaari	1,2 and 3	3.1, 3.2	GER1500	9	66%	31	Withering
3 October 2012	Hilskansaari	1,2 and 3	3.1, 3.2	GER1500	13	49%	37	Dormancy
17 August 2010	Rauma, Otanlahti	Grass field ($n = 7$)	3.3	FieldSpec	20	53%		

## 2.3. Description of Study Sites

Common reed begins to grow once the greatest threat of frost has passed in the spring. This happens typically at the beginning of May in southwest Finland. Stems can grow up to 5 centimeters a day if the growing conditions are optimal and the plant will reach its maximum height and density by the end of July. Flowering takes place typically in August. The leaves and stems die along with first frosts in autumn. Although dead, the strong stems will remain erect throughout the winter. In Finland, moving ice often cuts some of the stems. While common reed produces seeds, its primary method of reproduction is vegetative via a vast underground rhizome network [25]. The spectral characteristics of the reed bed are largely influenced by the phenological stage of reeds [26]. Time-series field measurements provided the means to study these changes.

The water at both study sites, Olkiluoto and Hilskansaari, is brackish meaning that it is a mixture of seawater and freshwater from a river. Field survey showed that there are two basic types of reed beds in Olkiluoto and Hilskansaari. In this paper, they are called "old reed bed" and "new reed bed". By new reed bed we mean stands where there are no dead stems erect and new live stems are reproduced (Figure 2). By old reed bed we mean stands where dead stems are erect and new live stems are emerging amongst the dead stems. Three targets were chosen for time series measurements. Targets 1 and 2 represent old reed bed and target 3 represents new reed bed. In order to study the temporal variability of reed beds during the growth period, a field campaign was carried out where the spectra of the three targets were measured at nine time instances throughout the phenological cycle (see the measurement dates indicated in Figure 3). The measurement intervals were not exactly even due to adverse weather conditions.
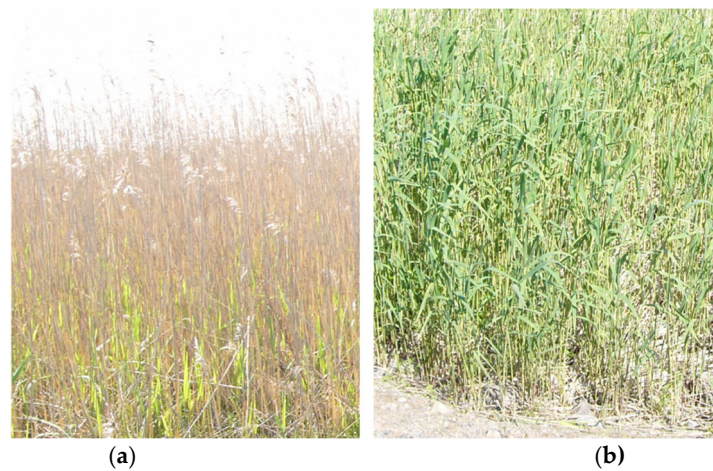
Figure 2. Old reed bed of target 2 (**a**) and new reed bed of target 3 (**b**). The photographs are taken on 12 June 2012.
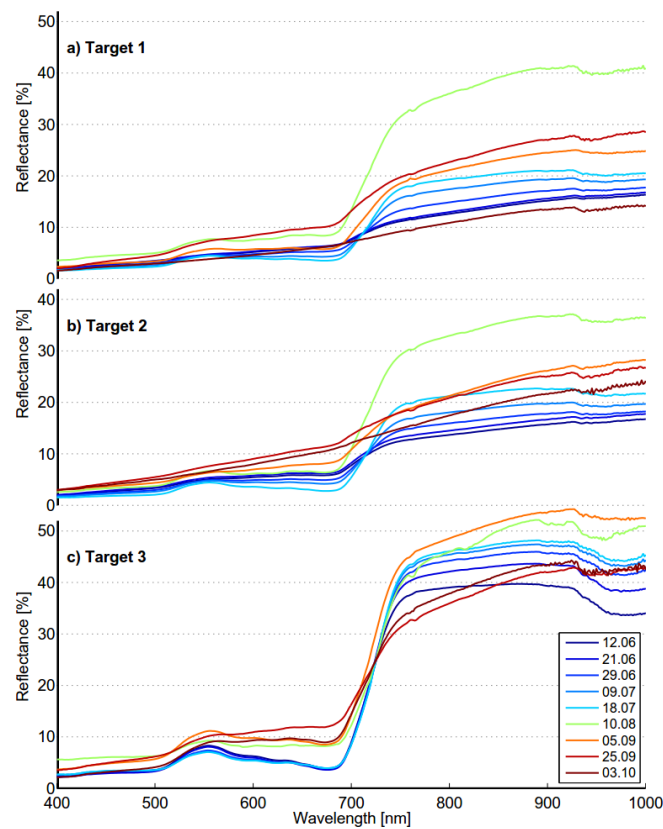
Figure 3. The measured spectra of targets 1, 2 and 3 during the growth period. The measurement dates are shown in the legend. (**a**) Target 1; (**b**) Target 2; (**c**) Target 3.

Several factors such as height, density, soil type, nutrition and wetness may contribute to the spectral variability of reed beds [26]. Spatial variability was studied at two scales: within a small local neighborhood as well as all over the Olkiluoto Island. The measurements used to evaluate local variability were made at site Pier located at the south coast of Olkiluoto (Figure 1). The site was chosen because visually homogenous reed bed was found there and the pier provided a good platform for measurement setup. Measurements were taken along 40 meters long line parallel to the pier. The distance between the targets was 5 meters, roughly corresponding to the spatial resolution commonly

used in airborne hyperspectral data acquisition. Out of the 8 targets, one target was discarded due to excessive interference in measured spectra. The measured reed bed was visually homogenous and the characteristics of targets such as height, water depth and density were similar. The spectral field measurements were performed on 27 July 2012. In addition, 4 randomly selected meadow targets representing green vegetation in the neighborhood of the Pier site were measured in the immediate vicinity of the reed beds.

In summer 2012, an extensive field survey of wetland vegetation was carried out in Olkiluoto. As a part of that field campaign, reed bed spectra were measured at four different sites: Flutanperä, Munakari, Kornamaa and Satama (see Figure 1). Three targets were measured at each site. The distance between the targets within a site ranges from 20 to 30 meters. These measurements provided information on the spatial variability of reed beds at different locations of the Olkiluoto Island. The spectral field measurements were performed on 14 and 15 August 2012. The height and density of reed beds at each target were measured as well (Table 2). The measurements were done using a half-meter frame. Reed stems are enclosed inside the square frame and all stems inside are cut near the base. Live and dead stems are then counted and measured separately.

Table 2. The average density (pcs/m^2) and height (cm) of live and dead stems at Olkiluoto sites. Each value is the average of three measurement points.

	Density Live	Height Live	Density Dead	Height Dead
Flutanperä	65.33	201.3	10.67	72.22
Munakari	32.00	240.4	12.00	136.2
Kornamaa	53.33	186.3	4.000	97.00
Satama	56.00	197.3	33.33	146.6

2.4. Airborne Hyperspectral Data

The HYPE08 flight campaign was carried out in July 2008. The total number of recorded flight lines was 27, of which 23 flight lines were recorded on 4 July 2008 and 4 flight lines 13 July 2008. The acquisition of Olkiluoto Island took place on 4 July 2008. The cloud cover on both days was absent providing homogenous solar irradiation from ground surface. The flight altitude during the acquisition was 1.9 km leading to ground resolution of 2.5 m × 2.5 m per pixel. The acquisition was done using Piper Pa23-250 aircraft carrying an AISA dual imaging spectrometer. The AISA dual spectrometer collects reflected solar radiation in 481 bands from 399 to 2452 nm wavelength. This includes the visible, near infrared and shortwave infrared regions of the electromagnetic spectrum. The spectral resolution is 3.3 nm at VNIR range and 12 nm at SWIR range.

2.5. Methods

The Euclidean distance between two vectors **X** and **Y** with N_b bands and is defined as:

$$d_e = \sqrt{\sum_{i=1}^{N_b} (x_i - y_i)^2} \tag{1}$$

and the SAM measure is defined in [27] as:

$$\alpha = cos^{-1} \frac{\sum \mathbf{XY}}{\sqrt{\sum (\mathbf{X})^2 \sum (\mathbf{Y})^2}} \tag{2}$$

where α is the angle formed between reference spectrum, **X** is the image spectrum and **Y** is the reference spectrum.

Calculation of between and within-class variability for classes $\{X_k\}$, $k = 1 \ldots n_x$ and $\{Y_k\}$, $k = 1 \ldots n_y$, where n_x and n_y denote the number of spectra in the respective classes, is performed as

follows. Let μ_x and μ_y denote the mean spectra of classes $\{X_k\}$ and $\{Y_k\}$, respectively, and let μ denote the mean over all spectra. The between-class variability S_b can then be expressed as

$$S_b = \frac{1}{2}\left[\left(\mu_x - \mu\right)^T \left(\mu_x - \mu\right) + \left(\mu_y - \mu\right)^T \left(\mu_y - \mu\right)\right] \tag{3}$$

and the within-class variability S_{w_x} for class $\{X_k\}$ can be expressed as:

$$S_{w_x} = \frac{1}{n_x}\sum\nolimits_{k=1}^{n_x} \left(X_k - \mu_x\right)^T \left(X_k - \mu_x\right). \tag{4}$$

The Jeffries–Matusita distance (JM) is defined in [28] as:

$$\propto = \frac{1}{8}\left(\mu_i - \mu_j\right)^T \left(\frac{c_i + c_j}{2}\right)^{-1}\left(\mu_i - \mu_j\right) + \frac{1}{2}\ln\left(\frac{\left|\left(c_i + c_j\right)/2\right|}{\sqrt{|c_i| \times |c_j|}}\right) \tag{5}$$

$$JM_{ij} = \sqrt{2(1 - e^{-\propto})} \tag{6}$$

where i and j = the two classes being compared. c_i = the covariance matrix of signature i. μ_i = the mean vector of signature i. ln = the natural logarithmic function. $|c_i|$ = the determinant of c_i.

Continuum removal is sometimes used to isolate and analyze features in reflectance spectra. Continuum removal is a normalization technique that allows comparison of individual absorption features from a common baseline. Continuum is a convex hull over the top of the spectrum, using straight-line segments that connect local spectral maxima [29]. Continuum is removed by dividing the reflectance value *R* at each wavelength by the reflectance level of the continuum R_c. The first and last spectral data values are on the hull and therefore the values of the first and last bands in the continuum removed spectra are equal to 1 while all the other values remain between 0 and 1. Continuum removed spectra were calculated using the ENVI software package [30].

3. Results

3.1. Temporal Variability of Reed Bed Spectrum

Temporal variability of reed bed reflectance spectrum is illustrated in Figure 3. Seasonal variability of the reflectance spectrum of target 1 is remarkable (Figure 3). At the beginning of the growth period the spectrum is smooth although there is a gentle slope at the red edge region. Reflectance increases steadily as the wavelength increases. At the end of June the characteristic features of green vegetation, *i.e.*, the gentle local maximum near 560 nm and the slope at the red edge region, become visible in the spectrum. In July these features become more distinct; the slope at the red edge becomes steeper and the maximum near 560 nm becomes stronger. In August the shape of the spectrum shows the form commonly associated with healthy and vigorous vegetation. The red edge is steeper and the reflectance is generally higher than earlier in the season. In addition, there is a weak local maximum near 640 nm. In late September, signs of senescence are visible in the spectrum; the red edge becomes gentler and the local maximum near 560 nm has disappeared. At the beginning of October, the spectrum is smooth without distinctive features. The seasonal spectra of target 2 show similar trends as those of target 1.

The seasonal spectral variability is significantly smaller in target 3 compared to targets 1 and 2 (Figure 3). The red edge is clearly visible in all measured spectra. The local maximum near 560 nm can be seen except in those measurements made in the autumn season. The spectral features of healthy vegetation are most distinctive in the spectrum measured on 5 September 2012, although the spectrum measured on 10 August 2012 is quite similar. The symptoms of senescence in late season are not as clear as in the spectra of targets 2 and 3; the red edge is still clearly visible.

3.2. Discrimination of Reed Beds from Reference Spectrum at Different Phases of the Phenological Cycle

In order to evaluate the feasibility of discriminating reed beds from other vegetation, field studies were performed and remote sensing data were analyzed in the neighborhoods of the reed beds in Olkiluoto Island. The datasets were analyzed by layering them using the ArcMap software. Datasets included very high resolution true and false color aerial photographs (2007 and 2009), hyperspectral data (2008) and reed bed maps (2007). Reed bed maps were produced by following the reed bed border on foot or by boat and tracking the route using a portable DGPS device. The reed bed borders were studied by switching the layers while following the reed bed map in ArcMap. The studies indicated that even though it is fairly easy to separate reed beds from other surfaces in the neighborhood such as water and rocks, the real difficulty lies in the discrimination between reed and other green vegetation. In order to determine the optimal time window for discriminating reed beds from surrounding vegetation, the reflectance spectrum of haircap moss *(Polytrichum juniperinum)* was selected from the spectral library as a reference. Haircap moss is commonly found near reed beds in Olkiluoto and its color is almost consistent during the observation period (Figure 4). The spectral library was collected in Olkiluoto on 20 and 26 July 2012.
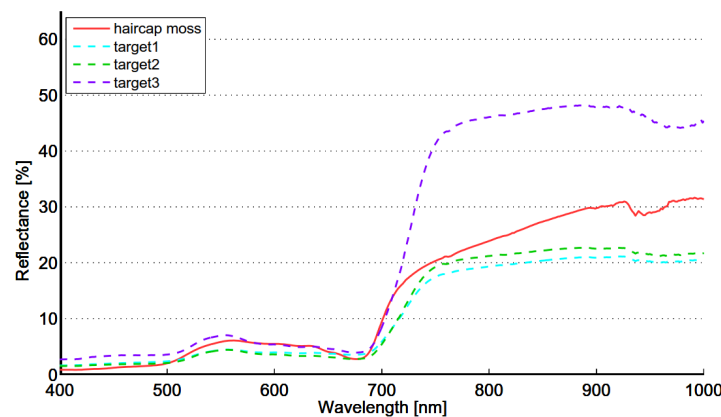
Figure 4. The reference spectrum of haircap moss and the spectra of targets 1–3 measured on 18 July 2012.

In order to measure the separability of target and reference spectra, Euclidean Distance (ED), Jeffries–Matusita distance (JM) and Spectral Angle Mapper (SAM) value were calculated between all targets and the moss spectra (Tables 3–5 respectively) As can be expected on the basis of the spectra shown in Figure 3, the seasonal variability of the ED values is remarkable. The overall trend of the ED values is quite similar for targets 1 and 2, except on 3 October 2012 when there is a significant difference. The best separability of old reed bed from moss is obtained on 12 June 2012. The best separability of new reed bed is obtained on 5 September 2012. As in the case of ED values, the seasonal variability of the SAM values is remarkable. The overall trend of the SAM values is quite similar for targets 1 and 2. The best separability of old reed bed is obtained on 3 October 2012 while the best separability of new reed bed is obtained on 12 June 2012. The seasonal trends were quite similar when Jeffries–Matusita distance (JM) were used compared to those given by ED measure.

Table 3. The Euclidean Distance (ED) values between the reference spectrum and target spectra during the growth period.

ED	12.06	21.06	29.06	09.07	18.07	10.08	05.09	25.09	03.10
target1/moss	177.1	171.9	152.1	124.6	104.9	156.4	64.2	57.1	202.1
target2/moss	167.3	155.6	141.6	118.1	87.1	104.8	54.3	79.8	108.7
target3/moss	156.6	199.8	227.6	244.8	254.2	284.6	322.1	177.7	185.2

Table 4. The Spectral Angle Mapper (SAM) values between the reference spectrum and target spectra during the growth period.

Radians	12.06	21.06	29.06	09.07	18.07	10.08	05.09	25.09	03.10
target1/moss	0.1824	0.1825	0.1282	0.096	0.0935	0.0791	0.0901	0.1500	0.2007
target2/moss	0.1733	0.1737	0.1219	0.0991	0.1038	0.0777	0.1195	0.2000	0.2157
target3/moss	0.1546	0.1408	0.1355	0.1337	0.1330	0.0941	0.0839	0.1062	0.0732

Table 5. The Jeffries-Matusita (JM)-distance values between the reference spectrum and target spectra during the growth period.

| JM-Dist.	12.06	21.06	29.06	09.07	18.07	10.08	05.09	25.09	03.10
target1	0.394	0.371	0.268	0.157	0.096	0.099	0.041	0.027	0.513
target2	0.350	0.302	0.226	0.139	0.053	0.048	0.029	0.066	0.139
target3	0.089	0.142	0.176	0.197	0.209	0.247	0.293	0.122	0.132

The results show that optimal date for best separability is largely dependent on the used separability measure and the phase of phenological cycle (Table 6). The optimal dates were the same when ED or JM-distance was used as separability measure.

Table 6. The optimal date to separate reed beds from other vegetation.

Measure/Reed Bed Type	Old	New
Euclidean distance	12.06	05.09
Spectral angle mapper	03.10	12.06
JM-distance	12.06	05.09

3.3. Local Spatial Variability of Reed Bed Spectra and Separation from Meadow

The mean and standard deviation of the reed bed and meadow class reflectance spectra are shown in Figure 5. The mean reed bed and meadow spectra are rather similar both in shape and reflectance level. The most noticeable common features are the slope at the red edge and local reflectance maximum near 560 nm. The most remarkable difference in reflectance level occurs in the blue region of visible light. The standard deviation of meadow class is higher than that of the reed bed above wavelengths of 500 nm.
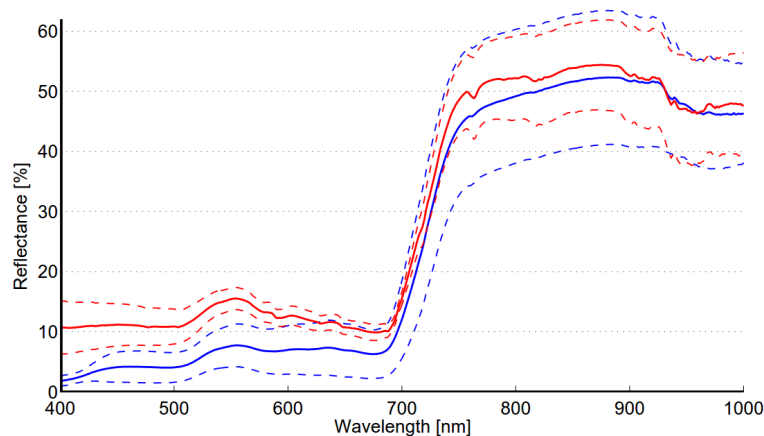
Figure 5. Mean and standard deviation of the reflectance spectra of meadow (blue) and reed bed (red) classes. The standard deviation is presented using dashed lines.

In order to study the feasibility of discriminating between the reed bed and the meadow class, ED, SAM and JM-distance values were calculated between the mean spectra of the classes and the spectra of each target (both reed bed and meadow) separately (Tables 7–9 respectively). When ED measure was used, four reed spectra and one meadow spectrum were closer to the spectra of other class than its own. The use of JM-distance showed slightly poorer results, five reed spectra and one meadow spectrum were closer to the spectra of the other class. The use of SAM measure produced different results, only one of the meadow targets (M4) was closer to the reed class to the meadow class.

Table 7. The Euclidean distance (ED) values between the individual targets and the mean spectra of the two classes. R1–R2 and R4–R8 represent reed bed targets and M1–M4 represents meadow targets.

| ED	R1	R2	R4	R5	R6	R7	R8	M1	M2	M3	M4
Reed	242.4	15.0	116.6	75.0	108.0	144.9	108.0	131.0	119.7	243.7	136.9
Meadows	216.9	67.7	111.7	117.3	109.3	137.7	99.7	125.7	71.6	225.8	153.6

Table 8. The SAM values between the individual targets and the mean spectra of the two classes. R1–R2 and R4–R8 represent reed bed targets and M1–M4 represents meadow targets.

R	R1	R2	R4	R5	R6	R7	R8	M1	M2	M3	M4
Reed	0.0692	0.0233	0.0298	0.0889	0.0086	0.0153	0.0447	0.1508	0.1343	0.0738	0.072
Meadows	0.0208	0.0985	0.0843	0.1693	0.0929	0.0821	0.0778	0.0804	0.0631	0.0723	0.0500

Table 9. The JM-distance values between the individual targets and the mean spectra of the two classes. R1–R2 and R4–R8 represent reed bed targets and M1–M4 represents meadow targets.

α	R1	R2	R4	R5	R6	R7	R8	M1	M2	M3	M4
Reed	0.1082	0.0018	0.0289	0.0112	0.0243	0.0426	0.0251	0.0301	0.0384	0.1003	0.0450
Meadow	0.0673	0.0128	0.0162	0.0315	0.0164	0.0260	0.0126	0.0276	0.0104	0.0665	0.0629

The spectral features of the reed bed and meadow targets were also studied using the continuum removal (CR) method (Figure 6). The method allows comparison of individual absorption features from a common baseline. The main features of the continuum removed reed bed class spectra are located in the red edge region (680 to 750 nm) and near 560 nm. The steepness and position of the red edge are quite similar for all the reed targets. The depth of the feature near 560 nm is similar for all targets except R1, where it is deeper. It can be seen that high within-class variability is largely due to target R1. The feature at 760 nm is related to oxygen in the atmosphere. The origin of the feature near 840 nm is unknown, it cannot be found from other spectra measured at other reed bed sites in Olkiluoto. A small common feature is found near 950 nm. The main features of meadow class CR spectra are the same as for the reed bed class. Higher within-class variability of the meadow class is distinct and the variability is clearly higher in the visible region below red-edge. Two CR spectra, those of targets 1 and 4 clearly differ from typical CR spectra of green vegetation. Target 1 has a strong feature near 440 nm, whereas target 4 has a gentle local maximum near 640 nm. These are most likely due to changes in floral cover of the target.
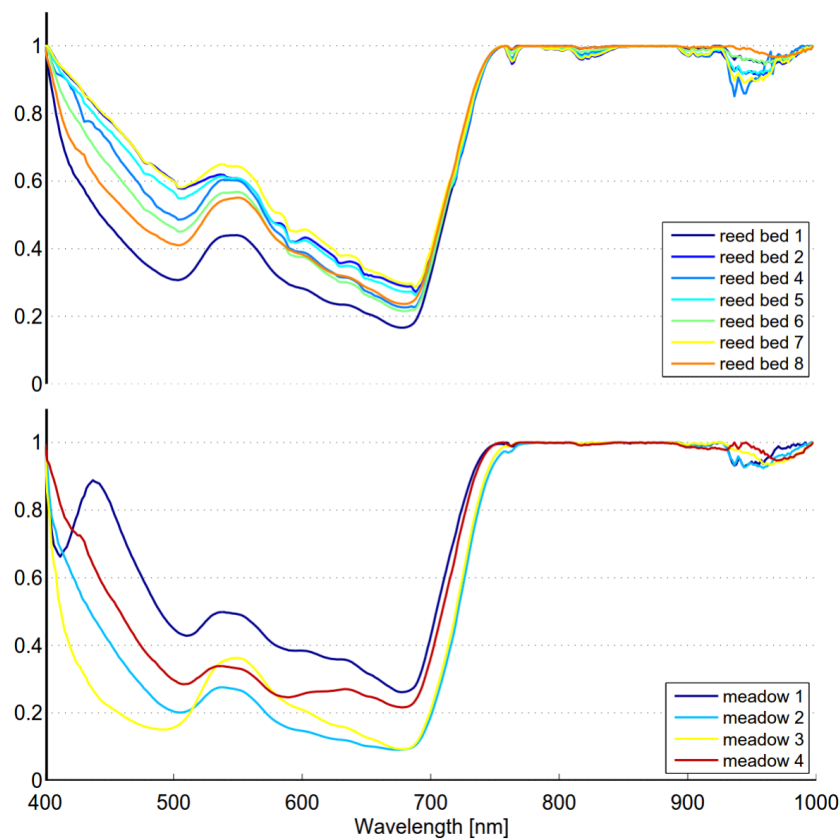
Figure 6. Continuum removed spectra of reed bed and meadow classes.

Within-class variability calculated for the reed and meadow classes are shown in Table 10. The within-class variability of the reed class was somewhat lower (15.95) compared to that of the meadow class (24.62).

**Table 10.** Within-class variability S_w of reed and meadow classes.

Class	S_w
Reed bed	15.95
Meadow	24.62
Savannah trees *	5.574
Grass field **	8.857

* Published figure in reference [31]. ** Calculated using field measurements made in summer 2010 near Olkiluoto.

3.4. Spatial Variability of Reed Bed Spectra in Olkiluoto Island

In Figure 7, reed bed reflectance spectra at the four test sites at the Olkiluoto Island are shown. The shape of the measured reed spectra is quite similar in the visible region of the spectrum; however, differences in the near infrared region were remarkable. The measured spectra were quite convergent at sites Munakari and Kornamaa, while the spectra at Flutanpera and Satama differed from those.

Between-class variability was calculated between each pair of the reed bed sites (Table 11). Each site was considered to form a separate class. The results show that between-class variability ranges from 3.85 to 114.02 the variability between Munakari and Kornamaa being the lowest. The variability between Flutanpera and those two sites is significantly higher and especially high with respect to Satama. When the JM-distance was used the results were highly consistent with those calculated using ED measure (Table 12.).
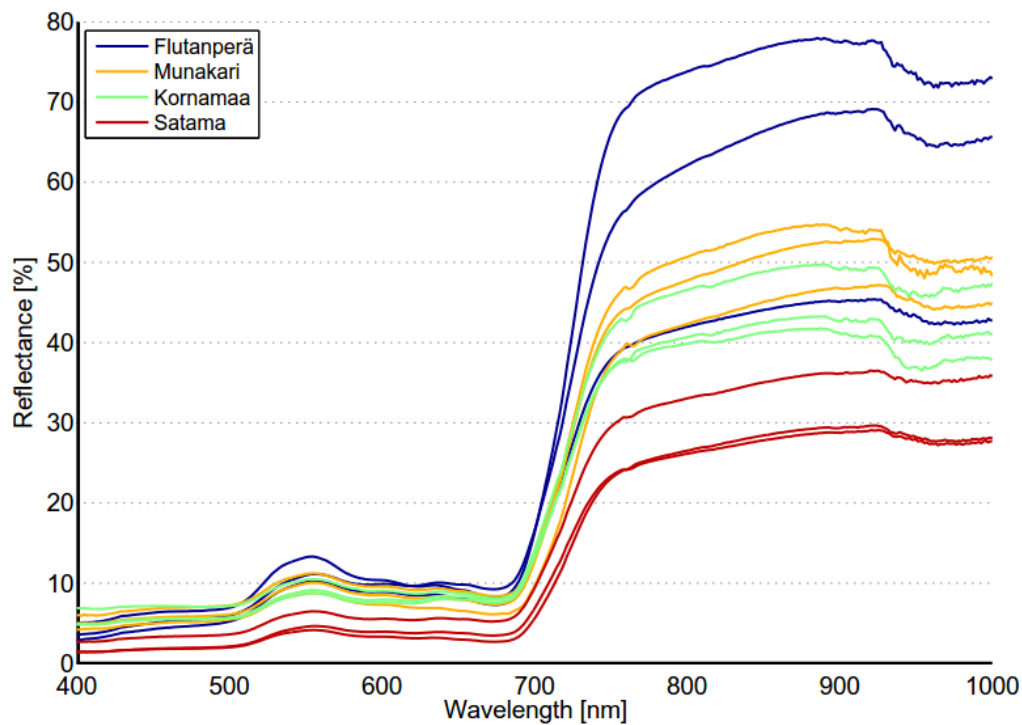
Figure 7. The reed bed reflectance spectra at the four test sites in Olkiluoto Island.

Table 11. The calculated between-class variability between reed sites.

	Flutanperä	Munakari	Kornamaa	Satama
Flutanperä		17.97	37.58	114.02
Munakari	17.97		3.85	42.01
Kornamaa	37.58	3.85		22.06
Satama	114.02	42.01	22.06	

Table 12. The calculated JM-distances between reed sites.

	Flutanperä	Munakari	Kornamaa	Satama
Flutanperä		0.0615	0.1328	0.3718
Munakari	0.0615		0.0160	0.1850
Kornamaa	0.1328	0.0160		0.1106
Satama	0.3718	0.01850	0.1106	

In order to study the spectral variability of reed beds at Olkiluoto and Hilskansaari, the within-class variability for both locations was calculated. Since all measurements in Olkiluoto were made in July and August, measurements at other times were excluded from the Hilskansaari data. Variability in Hilskansaari was calculated using nine samples, while 19 samples were used in the case of Olkiluoto. The within-class variability of the reed bed spectra at the two sites was similar: 69.81 for Hilskansaari and 64.40 for Olkiluoto. The between-class variability of these two sites was 33.20, meaning that within-class variability is more significant.
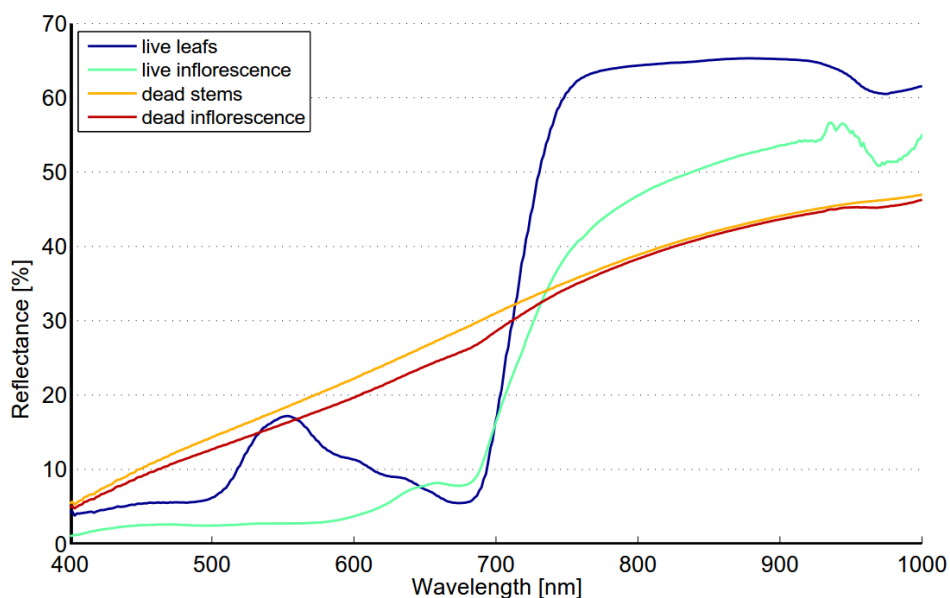
3.5. Partial Spectra of Reed Beds

In dense reed bed the spectrum is a mixture of several partial spectra such as live leafs, live inflorescence, dead stems and dead inflorescence (Figure 8). Each component of reed has specific

spectral features while the dead components are featureless (Figure 9). The spectrum of live leafs has typical features of healthy and vigorous green vegetation. Live inflorescence has gentle local maximum near 650 nm and the slope is less steep compared to live leaf.


Figure 8. Samples of measured reed components: (**a**) live leafs; (**b**) live inflorescence; (**c**) dead stems; and (**d**) dead inflorescence.

Figure 9. The partial spectra of reed bed.

3.6. Reed Bed Discrimination Using Airborne Hyperspectral Data

In order to study the effects of within-class variability in Olkiluoto on actual mapping results of reed beds, mapping of site Kornamaa was tested using an airborne hyperspectral data collected in summer 2008 and using SAM classification method. The classification results using the mean spectrum of Kornamaa are shown in Figure 10. The reed map produced in 2007 was used as ground truth (described in Section 3.2). The test area was classified into two classes; reed bed and other. Five different target spectra were used in SAM-classification: the mean spectra of sites Kornamaa, Munakari, Flutanperä and Satama as well as the mean reed bed spectrum of Olkiluoto. The results of agreement accuracy were modest albeit the overall accuracy values were good (Table 13.). The best accuracy was obtained when the mean spectrum of Kornamaa was used followed by the mean spectrum of Olkiluoto.
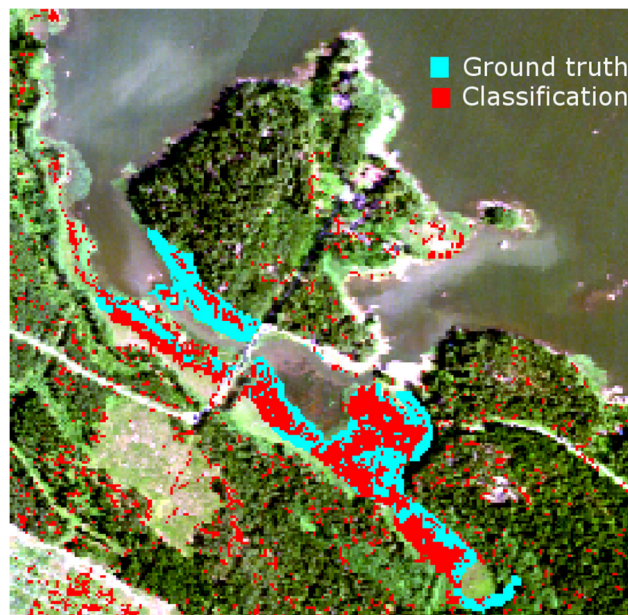
Figure 10. The classification results using the mean spectrum of Kornamaa.

Table 13. Classification accuracy of reed beds at site Kornamaa.

Target Spectra	Agreement Accurary	Overall Accuracy
Kornamaa	48.0%	93.1%
Munakari	31.3%	90.8%
Flutanperä	31.8%	90.2%
Satama	30.6%	89.2%
Olkiluoto	37.1%	90.9%

4. Discussion

Several seasonal time-series spectra of *Phragmites* have been published in the literature. Seasonal spectra are dependent on local conditions, but spectral features reflecting phenological stages should be found in time-series spectra anywhere. The seasonal spectra of targets 1 and 2 are quite consistent with those published by Ouyang *et al.* [19]. The shape of the spectra is quite similar at the beginning and the end of the season as well as in the "full vigor" state. The growth period is naturally somewhat shorter in Finland than in Dongtan, China. The seasonal spectra of target 3 differ from those in [19] at the beginning and end of the season. The seasonal spectra of targets 1 and 2 show similar trends as those found in time-series spectra of *Phragmites* measured in New Jersey Meadowlands [20]. When seasonal spectra were compared to those published by Gilmore *et al.* [26], the situation was quite the opposite: the published spectra were very similar to those of target 3 in our study. The results show that the optimal time for data acquisition is dependent on classification method to be used. For distance based classifier optimal time for old reed bed is in the middle of June when it is the beginning of September for new reed bed. Optimal times are different when shape based classifier is used; beginning of October for old reed bed and the middle of June for new reed bed. The separability of old reed bed is almost as high in the middle of June as in October. Acquisition in the middle of June could give good results for both reed bed types.

The seasonal spectral changes of targets 1, 2 and 3 are largely determined by two variables: density of the reed bed and the ratio of dead and live biomass. Density defines if the soil or water is visible. Dark soil and water have low reflectance, which lowers the mixed spectra. Dead biomass has low and flat spectrum, whereas live biomass has distinct features of green vegetation. In the beginning of season old reed beds have only a small fraction on live biomass and the soil is partly visible because

of low density. The spectrum is low and flat and therefore separable from moss. In the beginning of October old reed beds are full of dead biomass, resulting similar flat spectrum and high separability from green vegetation. The spectra of moss show signs of moderate chlorophyll content, modest local maximum near 560 nm and gentle red-edge. Target 3 is in "full vigor" state on 5 September 2012, the reflectance in green and NIR region is at the season's highest level and therefore the separability from moss is optimal.

The within-class variability of reed is somewhat lower than that of the meadow class (see Table 8). This can be expected as the meadow class contains several species, *i.e.*, grasses, weeds and flowers. The well-kept grass field was visually very homogenous; however, the spectral variability obtained for this class is higher than could be expected. This is most likely due the structural changes in grass. Results indicate that a single target (R1) significantly contributes to the within-class variability of the reed class. Debba *et al.* [31] studied the spectral within-class variability of different savannah trees. The average variability of seven tree species was lower than that of reed in this study. The published reflectance spectra of tree species showed that the within-class variability of some species (*Combretum apiculatum*, *Terminalia sericia*) was at the same level as obtained here for reed, although the average variability over all species was lower. Based on the analysis of the mean and standard deviation of the spectra obtained for the reed and meadow classes (see Figure 5) it is fair to argue that the two classes are extremely difficult to discriminate due to high within-class variability of both classes as well as spectral similarity of the classes. Several published studies have proposed fusion of hyperspectral and LiDAR data in wetlands mapping applications [16]. LiDAR can complement the spectral information of optical imagery and thus improve classification results. As the height of reed beds clearly differs from that of meadows, such approach could be highly beneficial. In addition, using textural features together with spectral information has been shown to enhance the classification accuracy of remotely sensed data [32].

Spectral variability of reed beds within the Olkiluoto Island is significant (see Figure 7). Zomer *et al.* [33] studied the reflectance spectra of dominant wetland species. The measured results of common reed (*Phragmites Australis*) showed similar shape and high variability as in Figure 7. This suggests that high spectral variability could be common characteristics for reed beds. In order to study spectral variability between reed sites, each site was assigned to a separate class and between-class variability was calculated for each pair of sites. Surprisingly the between-class variability of sites Munakari and Kornamaa (3.85) was lower than local spatial inter-class variability of reed bed at site Pier (15.95). The between-class variability of these two sites was also lower than the variability between spectrally similar Savannah trees [31]. The highest variability was measured between sites Flutanperä and Satama. This is likely due to remarkable reflectance differences in the NIR region shown in Figure 7. This can be explained by the characteristics of reed beds presented in Table 2. The density and height of dead reed stems is clearly higher at Satama than at Flutanperä. The effects of spectral variability to reed bed discrimination within Olkiluoto Island were studied using airborne hyperspectral data. The accuracy of classification was measured using mean spectra of reed bed sites as a target spectra. Overall accuracy was good, mainly because the other class was much larger than reed bed class, *i.e.*, the relative amount of commission errors stays low. The results of agreement accuracy were modest. This is most likely due to two factors: unfavorable time to separate reed beds from other vegetation and variety of reed bed types present, *i.e.*, old, new and dry reed beds. Conventional remote sensing schemes use one reference spectrum for each species. The results suggest that the use of multiple-endmember approach might be beneficial, agreement accuracy increases when dedicated spectrum is used for reed bed site instead of using one spectrum for the whole island.

The spectrum of reed bed is largely determined by the density of reed stems and the ratio of live and dead biomass. The reed bed spectra may also include background contributions from water, soil, understory vegetation and shade depending on the density and structure of reed stems. Live leafs have typical spectrum of healthy green vegetation, *i.e.*, steep red edge and reflectance peak near 560 nm while the spectrum of dead stems is flat and the reflectance level is low (Figure 9). The reflectance of a

dead stem is higher in the NIR region when compared to autumn spectra of targets 1 and 2. This is most likely due to shadows between stems or visible soil/water or both. The spectrum of type "old reed bed" varies depending on the ratio of live and dead stems. Field studies made in August 2012 showed that there is considerable variability in the ratio of live and dead stems. The fraction of dead stems varied from 0 to 83%. The most obvious reason for high spectral variability within Olkiluoto Island is the changes in the ratio of live and dead stems.

5. Conclusions

The temporal and spatial variability of reed bed spectra was evaluated in this study. The temporal variability of reed bed spectra was found to be significant. The main challenge related to temporal variability is that there are two different types of reed beds having different seasonal spectra. The optimal time of data acquisition depends on the reed bed type. When this is combined with the fact that usually the phenological state of the other vegetation has to be considered as well, careful timing of the data acquisition is needed. The spectral within-class variability of both reed bed and meadow in local neighborhood was found to be large when compared to references. Both classes have similar mean spectra, however, all the targets except R1 had lower spectral angle to the mean spectrum of the corresponding class than that of the other class. This gives a positive indication for successful reed bed mapping. The results on within-class spectral variability of reed bed at four test sites within the Olkiluoto Island showed that while the reed spectra from the sites of Kornamaa and Munakari were close to each other, the spectra measured at Satama and Flutanperä differed significantly. This is at least partly due to the variation in the density and height of live and dead reed stems among the four sites. It can be concluded that if features such as reed characteristics, temporal variation and surrounding habitats are known and can be controlled, mapping of reed beds is feasible based on their spectral properties; otherwise LiDAR data or textural features would be needed.

In this study, the optimal times to separate reed beds from other vegetation was determined. Depending on the reed bed types present and classification method to be used, it might be beneficial to use multi-temporal classification, *i.e.*, use several dataset collected at different times. High spectral within-species variability measured advocates the use of multiple-endmember methods. The test using airborne hyperspectral data further supports this conclusion. Scaling from spectral field measurements to airborne/satellite data brings with it new challenges. Poor spatial resolution can lead to significant amount of mixed pixels confusing the classification process. Modest signal-to-noise ratio of satellite sensors can further increase this confusion. The spectral resolution of spaceborne multispectral sensors might be too low to differentiate to subtle differences between reed beds and other wetland vegetation. The study using spectral field measurements showed poor separability between reed beds and meadows when distance and statistical measures where used although better results were obtained using a SAM-measure. The errors in geometric, radiometric and atmospheric correction related to air- and spaceborne sensors can deteriorate this subtle separability. This study provides a sound basis for future research of reed bed discrimination using air- and spaceborne data.

Author Contributions: Jyrki Tuominen was the principal author of the paper. Tarmo Lipping contributed to the study design and the preparation of the manuscript.

Conflicts of Interest: The authors declare no conflict of interest.

References

1. Altartouri, A.; Nurminen, L.; Jolma, A. Modeling the role of the close-range effect and environmental variables in the occurrence and spread of Phragmites australis in four sites on the Finnish coast of the Gulf of Finland and the Archipelago Sea. *Ecol. Evol.* **2014**, *4*, 987–1005. [CrossRef] [PubMed]

2.   Kern, J.; Idler, C. Treatment of domestic and agricultural wastewater by reed bed systems. *Ecol. Eng.* **1999**, *12*, 13–25. [CrossRef]

3.   Köbbing, J.F.; Thevs, N.; Zerbe, S. The utilisation of reed (*Phragmites australis*): A review. *Mires Peat* **2013**, *13*, 1–14.

4.   Hansson, P.A.; Fredriksson, H. Use of summer harvested common reed (*Phragmites australis*) as nutrient source for organic crop production in Sweden. *Agric. Ecosyst. Environ.* **2004**, *102*, 365–375. [CrossRef]

5.   Fyfe, S.K. Spatial and temporal variation in spectral reflectance: Are seagrass species spectrally distinct? *Limnol. Oceanogr.* **2003**, *48*, 464–479. [CrossRef]

6.   Cho, M.A.; Debba, P.; Mathieu, R.; Naidoo, L.; Van Aardt, J.; Asner, G.P. Improving discrimination of savanna tree species through a multiple-endmember spectral angle mapper approach: Canopy-level analysis. *IEEE Trans. Geosci. Remote Sens.* **2010**, *48*, 4133–4142. [CrossRef]

7.   Price, J.C. How unique are spectral signatures? *Remote Sens. Environ.* **1994**, *49*, 181–186. [CrossRef]

8.   Clark, M.; Roberts, D.; Clark, D. Hyperspectral discrimination of tropical rain forest tree species at leaf to crown scales. *Remote Sens. Environ.* **2005**, *96*, 375–398. [CrossRef]

9.   Schmidt, K.S.; Skidmore, A.K. Spectral discrimination of vegetation types in a coastal wetland. *Remote Sens. Environ.* **2003**, *85*, 92–108. [CrossRef]

10. Thenkabail, P.S. Optimal hyperspectral narrowbands for discriminating agricultural crops. *Int. J. Remote Sens.* **2001**, *20*, 257–291. [CrossRef]

11. Vahtmäe, E.; Kutser, T.; Martin, G.; Kotta, J. Feasibility of hyperspectral remote sensing for mapping benthic macroalgal cover in turbid coastal waters—A Baltic Sea case study. *Remote Sens. Environ.* **2006**, *101*, 342–351. [CrossRef]

12. Ramsey, E.; Rangoonwala, A. Hyperspectral remote sensing of wetland vegetation. In *Hyperspectral Remote Sensing of Vegetation*; Taylor & Francis: Abingdon, UK, 2011; pp. 487–511.

13. Adam, E.; Mutanga, O.; Rugege, D. Multispectral and hyperspectral remote sensing for identification and mapping of wetland vegetation: A review. *Wetl. Ecol. Manag.* **2010**, *18*, 281–296. [CrossRef]

14. Pengra, B.W.; Johnston, C.A.; Loveland, T.R. Mapping an invasive plant, Phragmites australis, in coastal wetlands using the EO-1 Hyperion hyperspectral sensor. *Remote Sens. Environ.* **2007**, *108*, 74–81. [CrossRef]

15. Lopez, R.; Edmonds, C.; Neale, A.; Slonecker, T.; Jones, B.; Heggem, T.; Lyon, J.; Jaworski, E.; Garofalo, D.; Williams, D. Accuracy assesments of airborne hyperspectral data for mapping opportunistic plant species in freshwater coastal wetlands. In *Remote Sensing and GIS Accuracy Assessment*; Taylor & Francis: Abingdon, UK, 2007; pp. 318–339.

16. Onojeghuo, A.O.; Blackburn, G.A. Optimising the use of hyperspectral and LiDAR data for mapping reedbed habitats. *Remote Sens. Environ.* **2011**, *115*, 2025–2034. [CrossRef]

17. Stratoulias, D.; Balzter, H.; Zlinszky, A.; Tóth, V.R. Assessment of ecophysiology of lake shore reed vegetation based on chlorophyll fluorescence, field spectroscopy and hyperspectral airborne imagery. *Remote Sens. Environ.* **2015**, *157*, 72–84. [CrossRef]

18. Goetz, A.F.H. Three decades of hyperspectral remote sensing of the Earth: A personal view. *Remote Sens. Environ.* **2009**, *113*, S5–S16. [CrossRef]

19. Ouyang, Z.T.; Gao, Y.; Xie, X.; Guo, H.Q.; Zhang, T.T.; Zhao, B. Spectral discrimination of the invasive plant spartina alterniflora at multiple phenological stages in a Saltmarsh Wetland. *PLoS ONE* **2013**, *8*, 1–12. [CrossRef] [PubMed]

20. Artigas, F.J.; Yang, J.S. Hyperspectral remote sensing of marsh species and plant vigour gradient in the New Jersey Meadowlands. *Int. J. Remote Sens.* **2005**, *26*, 5209–5220. [CrossRef]

21. Van der Meer, F. The effectiveness of spectral similarity measures for the analysis of hyperspectral imagery. *Int. J. Appl. Earth Obs. Geoinformation* **2006**, *8*, 3–17. [CrossRef]

22. Haapanen, R.; Lahdenperä, A.M. *The Inventory of the Terrestrial Part of Land-To-Sea Transects on Olkiluoto Island in 2008 and the Investigations of Reedbeds Surrounding Olkiluoto Island Carried out in 2007–2008*; Posiva Ltd.: Eurajoki, Finland, 2011.

23. Kangasniemi, V.; Helin, J. *Studies on the Aquatic Environment at Olkiluoto and Reference Area: 1. Olkiluoto, Reference Lakes and Eurajoki and Lapijoki Rivers in 2009–2010*; Posiva Ltd.: Eurajoki, Finland, 2014.

24. Pohjola, J.; Turunen, J.; Lipping, T.; Ikonen, A.T.K. Computers and geosciences landscape development modeling based on statistical framework. *Comput. Geosci.* **2014**, *62*, 43–52. [CrossRef]

25. Lambertini, C.; Gustafsson, M.H.G.; Frydenberg, J.; Speranza, M.; Brix, H. Genetic diversity patterns in Phragmites australis at the population, regional and continental scales. *Aquat. Bot.* **2008**, *88*, 160–170. [CrossRef]

26. Gilmore, M.S.; Wilson, E.H.; Barrett, N.; Civco, D.L.; Prisloe, S.; Hurd, J.D.; Chadwick, C. Integrating multi-temporal spectral and structural information to map wetland vegetation in a lower Connecticut River tidal marsh. *Remote Sens. Environ.* **2008**, *112*, 4048–4060. [CrossRef]

27. Kruse, F.A.; Lefkoff, A.B.; Boardman, J.W.; Heidebrecht, K.B.; Shapiro, A.T.; Barloon, P.J.; Goetz, A.F.H. The spectral image proccessing system (SIPS)—Interactive visualization and analysis of imaging spectrometer data. *Remote Sens. Environ.* **1993**, *44*, 145–163. [CrossRef]

28. Swain, P.H.; Davis, S. *Remote Sensing: The Quantatitative Approach*; McGraw Hill Book Company: New York, NY, USA, 1978.

29. Kokaly, R.F. Investigating a physical basis for spectroscopic estimates of leaf nitrogen concentration. *Remote Sens. Environ.* **2001**, *75*, 153–161. [CrossRef]

30. Canty, M.J. *Image Analysis, Classification, and Change Detection in Remote Sensing: With Algorithms for ENVI/IDL*; CRC Press: Boca Raton, FL, USA, 2010.

31. Debba, P.; Cho, M.A.; Mathieu, R. Within- and between-class variability of spectrally similar tree species. In Proceedings of the 2009 IEEE International Geoscience and Remote Sensing Symposium, Cape Town, South Africa, 12–17 July 2009; Volume 4, pp. 272–275.

32. Onojeghuo, A.O.; Blackburn, G.A. Mapping reedbed habitats using texture-based classification of QuickBird imagery. *Int. J. Remote Sens.* **2011**, *32*, 8123–8138. [CrossRef]

33. Zomer, R.J.; Trabucco, A.; Ustin, S.L. Building spectral libraries for wetlands land cover classification and hyperspectral remote sensing. *J. Environ. Manag.* **2009**, *90*, 2170–2177. [CrossRef] [PubMed]

Chapter 10

Publication P4

Tuominen, J. and Lipping, T. (2012). Assessment of hyperspectral classification methods for benthic cover type mapping. In *Proceedings of IEEE International Geoscience and Remote Sensing Symposium*, Munich, Germany

ASSESSMENT OF HYPERSPECTRAL CLASSIFICATION METHODS FOR BENTHIC COVER TYPE MAPPING

Jyrki Tuominen, Tarmo Lipping

Tampere University of Technology, Pohjoisranta 11, Pori, Finland

ABSTRACT

Though several research papers exploring the possibilities of benthic cover type classification have been published, little emphasis has been given to comparison of the performance of the various spectral classification methods. In this study four different classification methods were tested with and without water column correction. The comparison of the methods was done using a simulated data set. The data set was generated using spectral in situ measurements. The results showed significant differences in mapping accuracy among the tested classification methods. The best overall mapping accuracy (75.0%) without water column correction was achieved using SCM classification while the ED classification produced best results (84.5%) when the correction was applied.

Index Terms— hyperspectral, classification, benthic mapping, water column

1. INTRODUCTION

Sustainable management of coastal environments requires regular collection of accurate information on recognized ecosystem health indicators. Benthic algal cover and trends in changes of algal cover can be used as indicators of biological state in coastal areas [1]. Such indicators are valuable tools when the protection and preservation of marine environments is planned. Mapping of benthic cover types based on remote sensing data has been carried out successfully in optically clear, shallow coastal and reef waters [2]. Research papers addressing benthic cover mapping have typically explored modeling methods and water column correction techniques. The suitability of different classification methods has not gained much attention. The Spectral Angle Mapper (SAM) method has been proposed in several papers [3]. Casal et al. have demonstrated that in some cases of benthic mapping Maximum Likelihood Classifier (MLC) has some advantages over SAM [4]. The objective of our study was to evaluate the suitability of different classifiers for benthic cover type mapping. In this study we utilized simulated data which was generated using empirical spectral and water quality measurements.

2. DATA AND METHODS

2.1. In situ measurements of benthic reflectance

The study area is located at the coast of the city of Pori in South-West Finland. Reflectance spectra of benthic cover types were measured using handheld GER1500 spectroradiometer. Benthic cover types for this study were selected based on the initial submerged survey in the study site. Specimens of the typical green (*Fucus vesiculosus)*, brown *(Ectocarpus siliculosus*) and red (*Ceramium tenuicorne*) benthic macroalgae were selected. In addition to benthic vegetation, three typical bottom covers, i.e., sand, clay and reddish pebble were measured. The measured spectra of studied benthic cover types is shown in Fig 1.
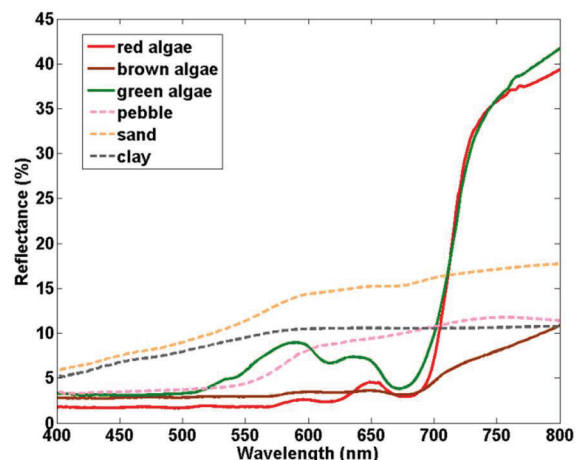

Fig 1. Reflectance spectra of studied benthic cover types.

2.2. In situ measurements of water quality

Spectral water quality parameters were measured at the four different sites on 26th of May 2011. Two spectral parameters were measured at each site; the optically deep water reflectance R_{∞} and the water attenuation coefficient K. The water attenuation coefficient K was measured using white reference plate. It has been shown by Maritorena et al. [5]

that the diffuse reflectance of shallow waters just below the water surface can be calculated using the following equation:

$$R(0-,z) = R_\infty + (R_b - R_\infty)\exp(-2Kz) \qquad (1)$$

where z is the water depth, R_b is bottom reflectance, R_∞ is reflectance of optically deep water, and K is diffuse attenuation coefficient of the water. Coefficient K can be calculated by using equation 1.

2.3. Generation of synthetic data

In order to study the mapping accuracy of each classification method, a synthetic data set was generated. The data set contains 800 simulated spectra for each cover type representing different depth and water quality conditions. The whole data set contains a total of 4800 simulated spectra. The depth varies between 0.01 and 2.0 meters. Four different water type classes are considered: Q1, Q2, Q3 and Q4, where Q1 represents the least turbid and Q4 the most turbid water. Classes are based on empirical spectral water quality measurements. The data set is modeled using Equation 1. The simulated spectrum R is calculated using deep water reflectance R_∞ and attenuation coefficient K corresponding to water type which is simulated. In fig 2. three simulated spectra of green algae are shown as well as the measured spectrum without water column. The simulated water type is Q1 and the water depth varies from 20 to 60 cm.
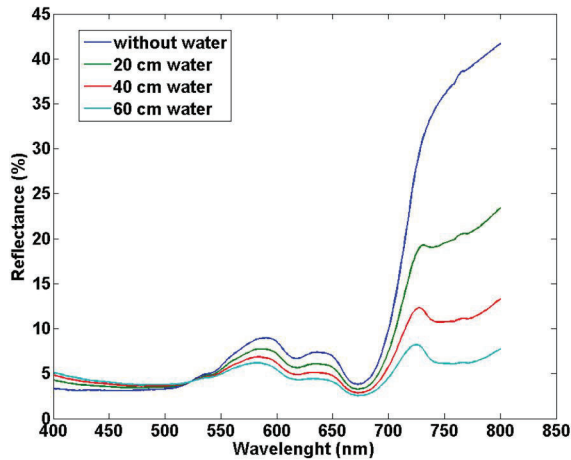

Fig 2. Simulated reflectance spectra representing the spectrum of green algae through water column.

2.4. Water column correction

The major problem involved with remote sensing of submerged cover types is that the water column affects the signal received at the sensor depending on the water depth

and water quality. In the water column correction approach, methods accounting for the effects of water depth and turbidity variation are employed. The most well-known correction technique is Lynzenga's method that creates a single depth-invariant band from each pair of visible spectral bands [9]. However, the method assumes that the water column is uniform over the scene and the signatures of optically deep water pixels are needed, which often prevents its use. The fundamental problem in water column correction is that the depth and attenuation properties of water are often unknown. Mishra et al. have proposed a method where the depth and water properties are derived from hyperspectral data itself [10]. However, the calibration of the method requires extensive *in situ* measurements. In this study classification using simple water column correction method was tested. The method is based on an assumption that there is 1 meter type Q1 water above the bottom i.e. the water depth is half of the studied depth range. A new reference spectrum for each benthic cover type is calculated using equation 1. which are then used in classification instead of original measured spectra. The advantage of the used method is that it only needs one water quality measurement.

2.5. Classification methods

In this study four classification methods were tested:

1. Euclidean Distance (ED) classifier
2. Spectral Angle Mapper (SAM) classifier
3. Spectral Correlation Mapper (SCM) classifier
4. Spectral Information Divergence (SID) classifier

ED method was chosen as a classical reference to more sophisticated methods. SAM is well established classification method for hyperspectral data commonly used in benthic cover mapping. SCM is an improved version of the SAM classifier with the distinction that it can measure negative correlation whereas SAM can't. SID classifier represents an information theoretic approach to hyperspectral classification. SID compares the similarity between two pixels by measuring the probabilistic discrepancy between two corresponding spectral signatures.

Euclidean distance measure is defined by

$$ED(s_r, s_i) = \|s_r - s_i\| \equiv [\sum_{l=1}^{L}(s_{rl} - s_{il})^2]^{0.5} \qquad (2)$$

where s_r is the reference spectrum and s_i is the image spectrum. SAM measure is defined in [6] as:

$$\propto = cos^{-1}\frac{\sum XY}{\sqrt{\sum(X)^2 \sum(Y)^2}} \qquad (3)$$

where ∝ is the angle formed between reference spectrum and image spectrum, X is the image spectrum and Y is the reference spectrum. The SCM measure is defined in [7] as:

$$R = \frac{\sum (X - \bar{X})(Y - \bar{Y})}{\sqrt{\sum (X - \bar{X})^2 (Y - \bar{Y})^2}} \qquad (4)$$

where $\bar{X}$ and $\bar{Y}$ are the means of corresponding spectrum vectors. The SID measure is defined in [8] as:

$$SID(r_i, r_j) = D(r_i || r_j) + D(r_j || r_i) \qquad (5)$$

where

$$D(r_j || r_i) = \sum_{l=1}^{L} q_l D_l(r_j || r_i) = \sum_{l=1}^{L} q_l (I_l(r_i) - I_l(r_j)) \qquad (6)$$

and

$$D(r_i || r_j) = \sum_{l=1}^{L} p_l D_l(r_i || r_j) = \sum_{l=1}^{L} p_l (I_l(r_j) - I_l(r_i)) \qquad (7)$$

derived from the probabilities vectors $p = (p_1, p_2, ..., p_L)^T$ and $q = (q_1, q_2, ..., q_L)^T$ for the spectral signatures of vectors, s_i and s_j, where $p_k = s_{ik} / \sum_{i=1}^{L} s_{il}$ and $q_k = s_{jk} / \sum_{i=1}^{L} s_{jl}$ and $I_l(r_j) = -\log q_l$ and similarly $I_l(r_i) = -\log p_l$.

3. RESULTS

Classification of synthetic data was followed by the assessment of mapping accuracy. Accuracy for each class together with the overall accuracy of tested classification methods without water column correction is presented in Table 1. The depth range under study was 0.0-2.0 m.

The best mapping accuracy was obtained using the SCM classifier. There was very little difference between the SAM and the SID methods. The classification of sand class produced very poor results for all tested methods. The mapping accuracy for each class together with the overall accuracy of tested classification methods using water column correction is presented in Table 2. In this case the best accuracy was obtained using the ED classification. All classification methods except SCM seem to benefit from water column correction.

4. CONCLUSIONS

The overall conclusion of this study is that the selection of classification method can have significant effect on the mapping accuracy. The use of the water column correction and the selection of correction method can determine which classification method should be used. Therefore several classification methods should always be tested to ensure best possible results. Karpouzli et al. concluded that the

results of studies where single measurements of 'average' attenuation have been used to depth-correct remotely sensed imagery should be interpreted with a high degree of caution [11]. Yet, the results of this study showed that mapping accuracy can be improved even when a simple correction technique using only one water quality measurement is employed.

5. REFERENCES

[1] J.A. Juanes, X.Guinda, A.Puente and J.A.Revilla, "Macroalgae, a suitable indicator of the ecological status of coastal rocky communities in the NE Atlantic," *Ecological Indicators* ,vol.8, pp.351-359, 2008.

[2] A.G. Dekker, V.E. Brando, J.M. Anstee, N. Pinnel, T. Kutser, E.J. Hoogenboom et al., Imaging spectrometry of water. In F. D van der Meer, & S.M. de Jong (Eds.), *Imaging spectrometry: Basic principles and prospective applications*, Kluwer Academic Publishers, Dordrecht, 2001.

[3] T.Kutser, I.Miller and D.Jupp, "Mapping coral reef benthic substrates using hyperspectral space-borne images and spectral libraries*," Estuarine, Coastal and Shelf Science*, vol.70, pp.449-460, 2006.

[4] G.Casal, T.Kutser, J.A.Dominguez-Gomez, N.Sanches-Carnero and J.Freire," Mapping benthic macroalgal communities in the coastal zone using CHRIS-PROBA mode 2 images," *Estuarine, Coastal and Shelf Science*, vol.94, pp.281-290, 2011.

[5] S.Maritorena, A.Morel and B.Gentili," Diffuse reflectance of oceanic shallow waters: Influence of water depth and bottom albedo," *Limnology and Oceanography*, vol.37, pp.1689-1703, 1994.

[6] F.A.Kruse, A.B Lefkoff, J.W. Boardman, K.B Heidebrecht, A.T.Shapiro, P.J. Barloon and A.F.H Goetz," The spectral image processing system (SIPS)—interactive visualization and analysis of imaging spectrometer data," *Remote Sensing of Environment*, vol.44, pp.145–163, 1993.

[7] O.A.Jr. Carvalho, and P.R. Meneses," Spectral Correlation Mapper (SCM): An improvement on the Spectral Angle Mapper (SAM)," Summaries of the 9th Airborne Earth Science Workshop, Pasadena, California, 2000, JPLPublication 00-18.

[8] C.I.Chang," An Information-Theoretic Approach to Spectral Variability, Similarity, and Discrimination for Hyperspectral Image Analysis," *IEEE Transactions on Information Theory*, vol.46, pp.1927-1932, 2000.

[9] D.R.Lyzenga," Remote sensing of bottom reflectance and water attenuation parameters in shallow water using aircraft and Landsat data," *International Journal of Remote Sensing*, vol.2, pp.71-82, 1981.

[10] D.R.Mishra, S.Narumalani, D.Rundquist, M.Lawson and R.Perk," Enhancing the detection and classification of coral reef and associated benthic habitats: A hyperspectral remote sensing approach*," Journal of Geophysical research*, vol.112, C08014, 2007.

[11]E.Karpouzli, T.Malthus, C.Place, A.M. Chui, M.I.Garcia and J.Mair," Underwater light characterization for correction of remotely sensed images," *International Journal of Remote Sensing*, vol.24, pp.2683-2702, 2003.

Table 1. The mapping accuracy of the classification methods without water column correction.

water	method	red algae	brown algae	green algae	pebble	sand	clay	Overall
Q1	ED	30.5	35.9	28.5	26.6	18.0	38.4	47.9
	SAM	35.5	17.5	31.9	20.0	13.9	32.9	41.4
	SCM	100	75.5	80.3	59.0	16.0	44.4	75.0
	SID	27.5	16.8	29.4	20.0	14.8	33.0	39.9
Q2	ED	25.5	32.2	24.0	24.1	15.0	32.4	43.2
	SAM	29.5	13.9	27.7	17.0	11.0	30.7	37.2
	SCM	100	64.0	75.8	45.0	12.9	40.8	70.3
	SID	23.0	13.3	25.6	17.0	12.8	30.2	35.9
Q3	ED	22.0	29.3	20.5	21.9	13.0	30.1	40.0
	SAM	25.0	12.1	24.4	14.5	9.7	28.3	34.2
	SCM	100	56.5	93.0	33.5	10.5	34.8	66.8
	SID	19.5	11.7	23.0	15.0	11.0	27.9	33.2
Q4	ED	20.0	28.05	18.5	21.1	12.0	29.2	38.4
	SAM	21.5	10.7	21.9	13.0	8.0	26.7	31.8
	SCM	100.0	43.5	80.0	24.5	8.7	30.0	59.6
	SID	17.0	12.1	21.0	15.6	9.8	26.1	31.3

Table 2. The mapping accuracy when water column correction is applied.

water	method	red algae	brown algae	green algae	pebble	sand	clay	Overall
Q1	ED	82.5	85.1	80.0	83.3	55.6	57.4	84.5
	SAM	63.2	76.2	51.5	57.4	32.9	48.6	69.9
	SCM	100.0	60.0	74.0	61.7	31.2	46.4	75.0
	SID	64.8	79.8	55.0	59.0	34.7	47.3	71.3
Q2	ED	69.5	68.7	67.0	68.2	48.8	56.0	77.1
	SAM	53.6	47.5	42.1	48.9	29.5	39.2	59.9
	SCM	100	40.5	75.5	51.5	27.7	37.8	69.0
	SID	54.2	49.7	46.0	50.2	30.8	38.6	61.2
Q3	ED	60.5	58.0	58.1	62.6	43.9	55.0	72.1
	SAM	46.5	31.6	37.9	42.9	27.4	35.4	53.3
	SCM	100	26.5	76.0	43.4	25.0	33.9	64.7
	SID	46.7	33.6	41.4	43.5	28.1	34.6	54.2
Q4	ED	54.5	54.6	52.0	58.9	40.9	51.6	68.7
	SAM	41.4	23.5	33.9	38.4	24.4	32.4	48.5
	SCM	91.0	9.0	61.6	37.0	22.0	31.5	57.2
	SID	40.9	24.8	38.2	38.5	26.4	31.7	49.2

Chapter 11

Publication P5

Tuominen, J. and Lipping, T. (2011). Atmospheric correction of hyperspectral data using combined empirical and model based method. In *Proceedings of 7th EARSeL Imaging Spectroscopy Workshop*, Edinburgh, Scotland

ATMOSPHERIC CORRECTION OF HYPERSPECTRAL DATA USING COMBINED EMPIRICAL AND MODEL BASED METHOD

J. Tuominen[a][*] T. Lipping[a]

[a] Tampere University of Technology,Signal Processing, Pohjoisranta 11, 28100 Pori, Finland - (jyrki.tuominen, tarmo.lipping)@tut.fi

KEY WORDS: Hyperspectral, Atmospheric Correction, ATCOR, Empirical Line, Remote Sensing

ABSTRACT:

Atmospheric correction is a difficult procedure due to the complex nature of the atmosphere and yet it should be done with utmost care because it largely determines the usability of the final data. Atmospheric correction is usually done using either empirical or model based method. In this paper a combined method proposed. The proposed method has two phases. In the first phase hyperspectral radiance data is corrected using the model-based ATCOR 4 software. In the second phase the modelled reflectance data is corrected using Empirical-Line (EL) method. The accuracy of the method was tested using Pseudo Invariant Feature (PIF) targets. The average RMSE error of the PIF targets was 6.8% when the reflectance was derived using ATCOR 4 software. The average RMSE error of the PIF targets was 1.8% when the reflectance was derived using the combined method proposed in this paper. The proposed method produced better results especially in the wavelength regions 950-1100nm and 2300-2500nm.

1. INTRODUCTION

The objective of atmospheric correction is to retrieve the surface reflectance (that characterizes the surface properties) from remotely sensed imagery by removing the atmospheric effects. In atmospheric correction, the radiance values are converted into reflectance data, measuring the fraction of radiation reflected from the surface. Atmospheric correction is a difficult procedure due to the complex nature of the atmosphere; the correction procedure usually must be done individually for each flight line.

Atmospheric correction should be done with utmost care because it largely determines the usability of the final data. The application of most algorithms and indices requires well calibrated reflectance data. Accurate change detection cannot be accomplished without atmospheric correction because otherwise it is impossible to determine whether the change occurred in the continuously varying atmosphere conditions or in the target under study.

Several methods for the atmospheric correction have been proposed in the literature. They can be divided into two categories: (1) empirical and (2) model-based methods. The empirical methods rely on the scene information and do not use any physical model as the model-based methods do. The scene information means the information that is embedded in the image, i.e., the radiance at certain location. There are empirical-based methods that rely on the raw scene data without ground reference information whereas some methods rely on the raw scene data together with ground reference information. There are two common approaches that do not use the ground reference information, the Internal Apparent Relative Reflectance (IARR) method (Kruse et al., 1985) and the Flat Field (FF) method (Roberts et al., 1986). In both methods, the spectral data of each pixel is divided by a reference spectrum. In the FF method the reference spectrum is from a homogenous bright target and in the IARR method an average scene spectrum is used as the reference spectrum. The drawback of these methods is that they are prone to artefacts and strongly dependent on the landscape of the target (Ben-Dor et al., 2004).

Most recent addition to empirical methods that do not use ground reference information is the Quick Atmospheric Correction (QUAC) method. The QUAC is based on the empirical finding that the average reflectance of a collection of diverse material spectra, such as the end-member spectra in a scene, is essentially scene-independent (Bernstain et al.,

2005). The use of QUAC has some restrictions, e.g., there must be a certain minimum amount of land area in the scene. The most widely used empirical method is the Empirical Line (EL) approach (Conel et al., 1987). The EL approach requires field measurements of reflectance spectra for at least one bright target and one dark target. The imaging spectrometer data over the surface targets are linearly regressed against the field-measured reflectance spectra to derive the gain and offset curves. The curves are then applied to the whole image for the derivation of surface reflectances for the entire scene. This method produces spectra that are most comparable to reflectance spectra measured in the field. However, if changes occur in the atmospheric conditions outside the area for which ground data is available, which is often the case the spectral reflectance data will contain atmospheric features.

Model-based correction approaches use methods in which the radiance at the sensor is modelled using radiative transfer models and the data from detailed atmospheric and sun information archives (e.g., MODTRAN, HITRAN2000). In this procedure, field measurements are not required and only the basic information such as the site location and elevation, flight altitude, sensor model, local visibility and acquisition times are required. Several model-based methods dedicated to retrieving reflectance information from hyperspectral data have been developed, such as ATREM (Gao et al., 1993), ATCOR (Richter, 1996), FLAASH (Adler-Golden et al., 1998), HATCH (Qu et al., 2000) and ACORN (Kruse, 2004). All the methods are quite similar in their basics and operation. ATCOR, FLAASH and ACORN are based on the use of MODTRAN 4 radiative transfer code.

The use of combined methods in which model and empirical methods are used together have been proposed in few papers. Clark et al. (1993) suggested the use of hybrid EL and model based method which produced better results than EL or model based methods alone. Ben-Dor et al. (2004) showed that combined EL and model based method produces good results when tested using synthetic imaging spectroscopy data. Despite the promising research results combined methods are very rarely used in the processing of hyperspectral data. The purpose of this study was to determine whether combined methods offers any advantages compared to model based methods.

2. DATA AND METHODS

2.1 Test area

The location of the test area is in west coast of Finland covering the city of Rauma and partially the county of Eurajoki. The geographic location is shown in Fig.1. Landscape of the area is quite complex containing rural, urban and marine areas. All land areas are located near the sea. The

size of the test area is 750 km2. A detailed map of the test area demonstrating the flight lines is shown in Fig.2.

Figure 1. The geographic location of the test site

Figure 2. A map demonstrating the flight lines over the test area.

2.2 Test data

This study utilized data from AISA Dual airborne hyperspectral scanner recorded at 4th of July 2008. During the acquisition the cloud cover was nonexistent. The AISA dual spectrometer collects reflected solar radiation in 481 bands covering the wavelengths from 399 to 2452 nm. This includes the visible, near infrared and short-wave infrared regions of the electromagnetic spectrum. The ground resolution of one pixel

was 2.5*2.5 meters. The acquisition of the test area lasted over 5 hours.

2.3 Method

The proposed method has two phases. In the first phase hyperspectral radiance data is corrected using model-based ATCOR 4 software. In the second phase the modelled reflectance data is corrected using Empirical-Line (EL) method. The method is illustrated in Fig.3.
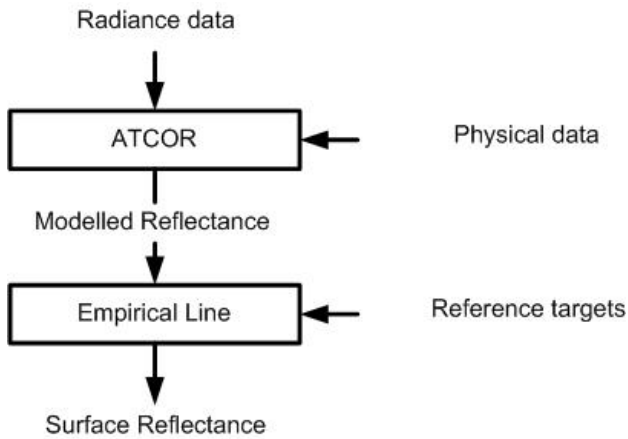

Figure 3. Description of the combined correction method.

An integral part of ATCOR 4 is a large database containing the results of radiative transfer calculations based on the MODTRAN5 code. While ATCOR 4 uses MODTRAN code to calculate the database of atmospheric look-up tables (LUT), the correctness of the LUT's is the responsibility of ATCOR 4. The use of ATCOR 4 is quite straightforward. Program takes the radiance data and physical parameters as the input and returns modelled reflectance data.

The EL method requires field measurements of reflectance spectra. Targets can be specially made reference targets or natural homogenous areas on the ground. The imaging spectrometer data over the surface targets are linearly regressed against the field-measured reflectance spectra in order to calculate the gain and offset values for each wavelength channel. The gain and offset values are then applied to the whole image for the derivation of surface reflectance for the entire scene. In general EL method is used to transform radiance data in to surface reflectance but in this combined correction method the modelled reflectance was transformed in to surface reflectance. In this study two specially made tarpaulins sized 15*15m was used as REF targets. Tarpaulins were laid in to the ground during the over flight. The reflectance spectra of both tarpaulins was measured during the over flight. The principle of empirical line correction in combined method is shown in Fig.4.
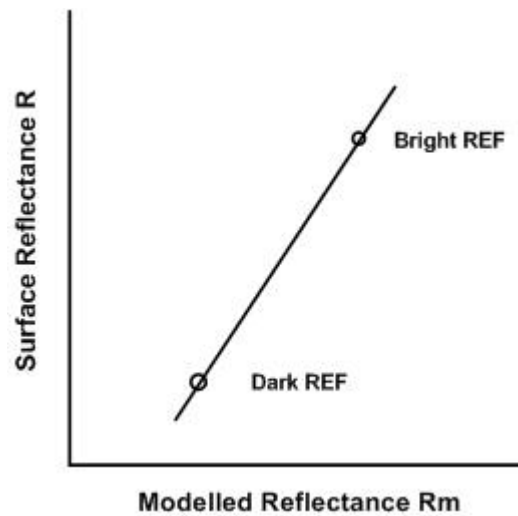

Figure 4. The principle of empirical line in combined correction method.

3. RESULTS

The proposed method was tested using 6 different Pseudo Invariant Feature (PIF) targets. PIF targets are natural homogenous areas on the ground surface. The spectra of each PIF target was measured during the over flight using ASD FieldSpec FR portable field spectrometer. The corrected and ground truth spectra of 3 different PIF targets are shown in Fig 5, Fig 6. and Fig 7. It can be seen that combined method (ATCOR+EL) produces better results compared to model-based ATCOR. The proposed method produced better results especially in the wavelength regions 950-1100nm and 2300-2500nm. The RMSE errors were calculated for each PIF target. The average RMSE error of the PIF targets was 6.8% when the reflectance was derived using ATCOR 4 software. The average RMSE error of the PIF targets was 1.8% when the reflectance was derived using the combined method proposed in this paper.
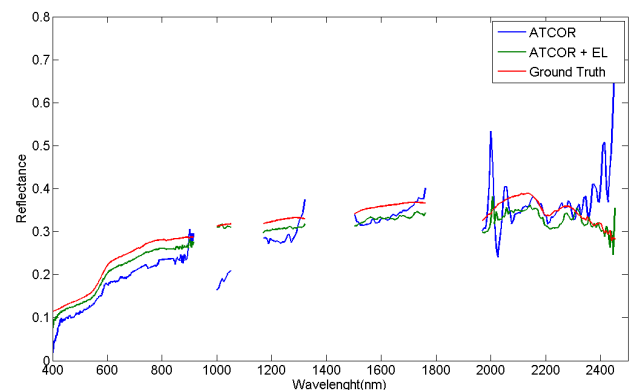
Figure 5. The corrected and ground truth spectra of PIF1
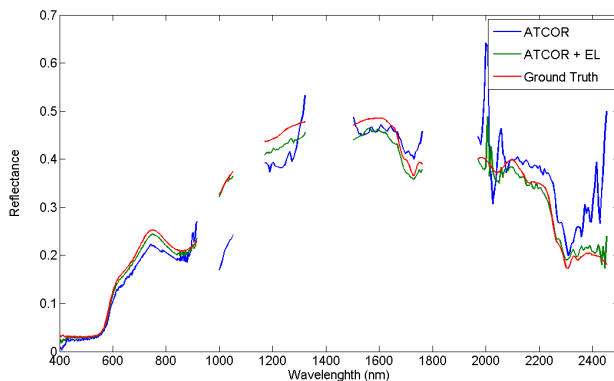(reddish sand field)

Figure 6. The corrected and ground truth spectra of PIF2
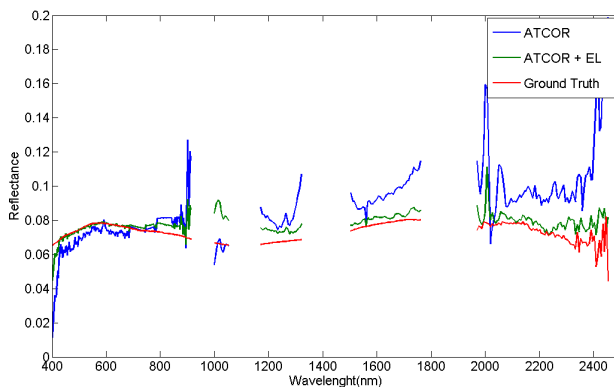(synthetic stadium pavement)

Figure 7. The corrected and ground truth spectra of PIF3 (dark
gravel)

4. CONCLUSIONS

A method combining both model- and empirical methods is presented in this paper. Test results indicated that proposed method can produce better results that model based ATCOR alone. The test data presented a complex marine dominated atmosphere. Model based correction methods can fail with this kind of atmosphere. The overall conclusion of this paper is that more accurate results can be produced using combined correction methods compared to model based methods used alone. Even in situations when there is limited number of spectral ground truth measurements, the proposed method can improve atmospheric correction accuracy over the whole acquisition area.

5. REFERENCES

Adler-Golden, S., Berk, A., Bernstein, L. S., & Richtsmeier, S. (1998). FlAASH, A MODTRAN4 atmospheric correction package for hyperspectral data retrievals and simulations. Summaries of the seventh JPLairborne earth science workshop. JPL-Pub., vol. 97-21 (pp. 1 – 9). Pasadena, CA: JPL Pub.

Ben-Dor, E., Kindel, B. & Goetz, A.F.H. 2004. Quality assessment of several methods to recover surface reflectance using synthetic imaging spectroscopy data. *Remote Sensing of Environment*, 90:389-404.

Bernstein, L. S., Adler-Golden, S.M., Sundberg, R.L., Levine, R.Y., Perkins, T.Y, Berk, A., Ratkowski, A.J., Felde, G. & Hoke, M.L. 2005. Validation of the QUick atmospheric Correction (QUAC) algorithm for VNIR-SWIR multi- and hyperspectral imagery. SPIE Proceedings, Algorithms and Technologies for Multispectral, Hyperspectral,and Ultraspectral Imagery XI. Vol. 5806.

Clark, R. N., Swayze, G., Heidebrecht, K. B., Goetz, A. F. H., & Green, R.O. (1993). Comparison of methods for calibrating AVIRIS data to ground reflectance. Proceedings of the fourth annual JPL airborne geoscience workshop, October 25–29, 1993, vol. I (pp. 35–36). Pasadena, CA: JPL Pub.

Conel, J. E., Green, R. O., Vane, G., Bruegge, C. J., Alley, R. E., & Curtiss, B. J. 1987. Airborne imaging spectrometer-2: Radiometric spectral characteristics and comparison of ways to compensate for the atmosphere. Proceedings of SPIE, 834: 140– 157.

Gao, B. -C., Heidebrecht, K. B., & Goetz, A. F. H. 1993. Derivation of scaled surface reflectance from AVIRIS data. *Remote Sensing of Environment*, 44:145–163.

Kruse, F. A., Raines, G. I., & Watson, K. 1985. Analytical techniques for extracting geologic information from multichannel airborne spectroradiometer and airborne imaging spectrometer data. Proceedings of the 4th thematic conference on remote sensing for exploration geology. Ann Arbor, MI.

Kruse, F. A. 2004. Comparison of ATREM, ACORN, and FLAASH atmospheric corrections using low-altitude AVIRIS data of Boulder, CO. Summaries of 13th JPL Airborne Geoscience Workshop, Jet Propulsion Lab, Pasadena, CA.

Qu, Z., Goetz, A. F. H., & Heidbrecht, K. B. 2000. High accuracy atmosphere correction for hyperspectral data (HATCH). Proceedings of the 9th JPL airborne earth science workshop. JPL-Pub., vol. 00-18 (pp. 373– 381). Pasadena, CA

Richter, R. 1996. A spatially adaptive fast atmosphere correction algorithm. *International Journal of Remote Sensing*, 11: 159– 166.

Roberts, D. A., Yamaguchi, Y., & Lyon, R. J. P. 1986. Comparison of various techniques for calibration of AIS data. Proceedings of the 2nd AIS workshop. JPL Publication, vol. 86-35. Pasadena, CA.